LBL-14231 c.2

Lawrence Berkeley Laboratory

UNIVERSITY OF CALIFORNIA

ENERGY & ENVIRONMENT DIVISION

RECEIVED
LAWRENCE
BERKELEY LABORATORY

JUL 15 1982

LIBRARY AND
DOCUMENTS SECTION

THE KINETICS OF LEACHING OF ORGANIC CARBON FROM IN SITU SPENT SHALE

William Gordon Hall
(Ph.D. thesis)

May 1982

TWO-WEEK LOAN COPY

This is a Library Circulating Copy which may be borrowed for two weeks. For a personal retention copy, call Tech. Info. Division, Ext. 6782.

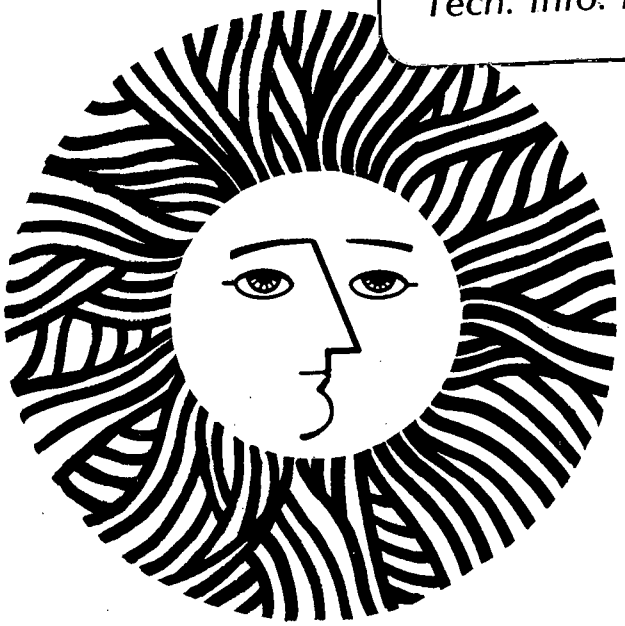

LBL-14231 c.2

Prepared for the U.S. Department of Energy under Contract DE-AC03-76SF00098

DISCLAIMER

This document was prepared as an account of work sponsored by the United States Government. While this document is believed to contain correct information, neither the United States Government nor any agency thereof, nor the Regents of the University of California, nor any of their employees, makes any warranty, express or implied, or assumes any legal responsibility for the accuracy, completeness, or usefulness of any information, apparatus, product, or process disclosed, or represents that its use would not infringe privately owned rights. Reference herein to any specific commercial product, process, or service by its trade name, trademark, manufacturer, or otherwise, does not necessarily constitute or imply its endorsement, recommendation, or favoring by the United States Government or any agency thereof, or the Regents of the University of California. The views and opinions of authors expressed herein do not necessarily state or reflect those of the United States Government or any agency thereof or the Regents of the University of California.

LBL-14231

THE KINETICS OF LEACHING OF ORGANIC CARBON FROM IN SITU SPENT SHALE

William Gordon Hall

Lawrence Berkeley Laboratory
University of California
Berkeley, California 94720

This work was supported by the Assistant Secretary for Environment, Office of Environmental Compliance and Overview, Environmental Control Technology Division and the Assistant Secretary for Fossil Energy, Deputy Assistant Secretary for Oil, Gas and Shale Technology, Office of Oil Shale of the U.S. Department of Energy under Contract No. DE-AC03-76SF00098.

INDEX

ABSTRACT.....vii

LIST OF FIGURES.....ix

LIST OF TABLES.....xii

ACKNOWLEDGEMENTS.....xvi

CHAPTER I - INTRODUCTION.....1

OIL SHALE RETORTING PROCESSES 1

Surface Retorting.....2

In-situ Retorting.....2

WATER POLLUTION POTENTIAL OF SPENT SHALE 3

Control of Leaching from Abandoned VMIS Retorts 4

IMPACT OF ABANDONED VMIS RETORTS ON WATER QUALITY.....5

Factors Complicating Impact Analyses.....5

STUDY OBJECTIVES.....8

CHAPTER II - LITERATURE SEARCH.....10

LEACHATE CHARACTERIZATION STUDIES.....10

Inorganic Characterization of Oil Shale Leachates.....10

Summary of Inorganic Leachate Characterization Studies....17

Organic Characterization of Leachates.....17

LEACHING AND TRANSPORT MECHANISMS.....18

Diffusive Mechanisms.....19

Dispersive Transport Mechanisms.....20

INVESTIGATIONS INTO OIL SHALE LEACHING MECHANISMS.....22

DIFFUSIVE AND DISPERSIVE MECHANISM RESEARCH IN ALLIED FIELDS...29

CHAPTER III - EXPERIMENTAL PROCEDURES.....32

PHYSICAL CHARACTERISTICS OF SPENT SHALE.....32

Handling and Classification of Spent Shale.....32

Characterization of Shale.....35

CHEMICAL CHARACTERISTICS OF SPENT SHALE.....42

WATER ANALYSES.....45

pH and Conductivity.....45

TOC.....45

Sampling and Analytical Procedures.....47

Reliability of Data.....48

WATER SUPPLY AND LEACHATE CHARACTERISTICS.....49

Composition of TDS Leached from Spent Shale,.....51

Leachate Trace Organics.....54

Correlation of EC and TDS.....56

BATCH INVESTIGATIONS.....59

Equilibrium Relationships.....59

Rates of Increase of Leachate Solutes.....60

SMALL COLUMN STUDIES.....67

Columns.....69

Water Supply and Pumps.....70

System Operation.....70

Quiescent Leaching.....72

Sampling Procedures.....72

Results.....74

LARGE COLUMNS.....79

Columns.....79

Water Supply and Pumping.....81

Column Operation.....82

Sampling Procedures.....83

Results.....83

CHAPTER IV - LEACHING AND TRANSPORT MODEL.....86

PHYSICAL MODEL.....86

Physical Characteristics of the Fixed Bed.....86

Mass Transfer Mechanisms.....87

TOC Break-through Curve.....88

TOC Distribution in Solid Phase.....91

Physical Model of Leaching in Fixed Bed.....92

MATHEMATICAL MODELLING.....94

MATHEMATICAL MODEL OF STAGE II.....96

Solution by Numerical Inversion.....101

Verification of Solution.....102

MATHEMATICAL MODEL OF STAGE III.....107

Physical Model of Stage III.....107

Mathematical Model of Stage III.....107

Mass Transfer Coefficient.....109

CHAPTER V - MODEL VERIFICATION AND ANALYSES OF RESULTS.....112

STAGE II MODEL VERIFICATION.....112

Calculation of Diffusion Coefficients.....113

Sensitivity of Analyses to Experimental Variables.....124

Dispersion.....127

Analysis of Calculated Diffusion Coefficients.....132

STAGE III MODEL VERIFICATION.....136

ANALYSIS OF LEACHING IN LARGE COLUMNS.....139

CHAPTER VI - SUMMARY, CONCLUSIONS AND RECOMMENDATIONS.....150

STUDY OBJECTIVES.....150

SUMMARY OF STUDY.....150

FULFILLMENT OF OBJECTIVES.....152

RECOMMENDATIONS.....155

Model Framework.....156

Multi-disciplinary Approach.....157

APPENDIX A

COLUMN LEACHING DATA.....A-1

Small Column Data.....A-2

Large Column Data.....A-29

APPENDIX B

STAGE II MODEL DERIVATION.....B-1

APPENDIX C

LAPINV COMPUTER PROGRAM.....C-1

SOLUTIONS OF EQUATION IV-9 FOR SELECTED VALUES OF ALPHAX.....C-5

APPENDIX D

BIBLIOGRAPHY.....D-1

THE KINETICS OF LEACHING OF ORGANIC CARBON FROM IN SITU SPENT SHALE

William Gordon Hall

Lawrence Berkeley Laboratory
University of California
Berkeley, California 94720

ABSTRACT

Spent oil shale from the Laramie Energy Technology Center 10-ton simulated in situ retort was leached in a series of batch and column experiments. The packed columns, (11.4 and 30 cm in dia), were filled with water and allowed to reach equilibrium before leaching flows were commenced. Batch leachate and column break-through concentration data are presented, characterized by electrical conductivity (EC), total organic carbon (TOC), and pH. Column (TOC) break-through data typically dropped to less than 10 percent of initial levels within three to four leachate pore volumes and thereafter decreased very slowly.

A three-stage model of the break-through curve was proposed in which solute moves from the solid surface into the fluid contained in the micro-pore structure of the particle during Stage I, and then diffuses to the external liquid phase in Stage II. Solute from sites within the mineral matrix is transported to the micro- and macro-pores by Stage III mechanisms. Stage II mechanisms disappear within a few pore volumes while Stage III continues for an extended period depending on the mass of solute initially present.

Mathematical models of Stages II and III were developed and verified. Solutions of the Stage II model, obtained by numerical inversion of Laplace transforms, were adjusted to observed column TOC data and diffusion coefficients then being calculated. The proximity of the calculated coefficients to 10^{-5} cm^2 sec, a mean diffusivity for weak concentrations of organics in water, was taken as evidence of model validity. The Stage II model predictions were found to be particularly sensitive to particle and bed porosity measurements, and to axial dispersion in the column. Fluid density and temperature gradients were also shown to have a significant effect on experimental results.

The Stage III model predicted leachate concentrations of less than 1 mg/L in the tail of the break-through curve. A reasonable verification of this model against observed data was obtained considering the reliability of TOC analytical techniques in this low range.

LIST OF FIGURES

Figure II-1 Schematic section through porous media in a fixed bed....21

Figure III-1 Spent shale particles, (-1/2 to +1/8) inch size range....37

Figure III-2 Spent shale particles, (-1 to +1/2) inch size range....38

Figure III-3 Spent shale showing carbon zone demarcation....39

Figure III-4 Histograms of shale particle diameter and height for a shale size range of (-1 to +1/2) inch....43

Figure III-5 Histograms of shale particle diameter and height for a shale size range of (-1/2 to +1/8) inch....44

Figure III-6 Relation between leachate TOC and solid-liquid ratio at equilibrium in shaking batch studies at 22 ^{o}C....62

Figure III-7 Equilibrium isotherm for ground spent shale and distilled water at 22 ^{o}C....62

Figure III-8 Schematic of small column leaching apparatus....68

Figure III-9 Schematic of large column leaching apparatus....80

Figure IV-1 Schematic column break-through curve showing contributions of stage mechanisms....90

Figure IV-2 Model of Spent Shale Particle....93

Figure IV-3 Leachate solute concentration as a function of ALPHAX and TIME/ALPHAX....103

Figure IV-4 Comparison of J-function with the LAPINV inversion of Equation IV-10....111

Figure IV-5 TOC concentration versus time for quiescent leaching studies in small columns....111

Figure V-1 Break-through curve and normalized observed TOC concentrations plotted versus pore volumes of passage. Run D-1, 25 cm bed depth, and 0.15 internal porosity....115

Figure V-2 Break-through curve and normalized observed TOC concentrations plotted versus pore volumes of passage. Run D-2, 55 cm bed depth,

and 0.15 internal porosity.....115

Figure V-3 Break-through curve and normalized observed TOC concentrations plotted versus pore volumes of passage. Run D-4, 25 cm bed depth, and 0.15 internal porosity.....116

Figure V-4 Break-through curve and normalized observed TOC concentrations plotted versus pore volumes of passage. Run D-4, 85 cm bed depth, and 0.15 internal porosity.....116

Figure V-5 Break-through curve and normalized observed TOC concentrations plotted versus pore volumes of passage. Run D-5, 85 cm bed depth, and 0.15 internal porosity.....117

Figure V-6 Break-through curve and normalized observed TOC concentrations plotted versus pore volumes of passage. Run D-6, 70 cm bed depth, and 0.15 internal porosity.....117

Figure V-7 Break-through curve and normalized observed TOC concentrations plotted versus pore volumes of passage. Run D-7, 55 cm bed depth, and 0.15 internal porosity.....118

Figure V-8 Break-through curve and normalized observed TOC concentrations plotted versus pore volumes of passage. Run D-7, 70 cm bed depth, and 0.20 internal porosity.....118

Figure V-9 Break-through curve and normalized observed TOC concentrations plotted versus pore volumes of passage. Run D-8, 25 cm bed depth, and 0.15 internal porosity.....119

Figure V-10 Break-through curve and normalized observed TOC concentrations plotted versus pore volumes of passage. Run D-8, 70 cm bed depth, and 0.20 internal porosity.....119

Figure V-11 Break-through curve and normalized observed TOC concentrations plotted versus pore volumes of passage. Run D-8, 85 cm bed depth, and 0.15 internal porosity.....120

Figure V-12 Arithmetic plot of dimensionless break-through curves for ALPHAX parameters of 0.5, 1.0, 5.0, and 10.0.....126

Figure V-13 A comparison of dispersive mechanisms with observed TOC data and the Stage II model for Run D-8 at 85 cm. Internal porosity = 0.15.....129

Figure V-14 Break-through curves and normalized observed TOC concentrations plotted versus pore volumes of passage. Run D-8, 85 cm bed depth and 0.20 internal porosity.....135

Figure V-15 Break-through curves and normalized observed TOC concentrations plotted versus pore volumes of passage. Run D-8, 85 cm bed depth and 0.20 internal porosity.....135

Figure V-16 Break-through curve and normalized observed TOC concentrations plotted versus pore volumes of passage. Run LC-1, 58 cm bed depth, and 0.15 internal porosity.....140

Figure V-17 Break-through curve and normalized observed TOC concentrations plotted versus pore volumes of passage. Run LC-1, 134 cm bed depth, and 0.15 internal porosity.....140

Figure V-18 Break-through curve and normalized observed TOC concentrations plotted versus pore volumes of passage. Run LC-2, 68 cm bed depth, and 0.15 internal porosity.....141

Figure V-19 Break-through curve and normalized observed TOC concentrations plotted versus pore volumes of passage. Run LC-2, 145 cm bed depth, and 0.15 internal porosity.....141

Figure V-20 Break-through curve and normalized observed TOC concentrations plotted versus pore volumes of passage. Run LC-3, 68 cm bed depth, and 0.15 internal porosity.....142

Figure V-21 Break-through curve and normalized observed TOC concentrations plotted versus pore volumes of passage. Run LC-3, 145 cm bed depth, and 0.15 internal porosity.....142

LIST OF TABLES

Table II-1 Conductivities, pH and Major Ion Concentrations, Leachate from Core E2, Occidental In-situ Retort 3E.....15

Table II-2 < 2 mm Spent Shale Leached with 0.01 M $CaCl_2$ LETC 10-ton Retort.....16

Table III-1 Operating Conditions, LETC 10-ton Retort - Run S-55.....33

Table III-2 Spent Shale Quantity.....34

Table III-3 Size Classification of Spent Shale as Received at Richmond, CA.....36

Table III-4 Size and Bulk Density of Sieved Spent Shale.....40

Table III-5 Analysis of Richmond Tap Water Used in Large Column Studies 50

Table III-6 Spent Shale Leachates, Physical Properties.....52

Table III-7 Spent Shale Leachates, Major Inorganic Ion Analysis, After Acidification with Phosphoric Acid.....53

Table III-8 Estimated Contribution of Inorganic Ions to Leachate by Spent Shale.....55

Table III-9 Trace Organic Analysis, 30 Day Quiescent Leaching Sample from Large Column Containing (-1/2 to +1/8) Shale.....56

Table III-10 Relation of EC with TDS in Leachate Collected from Non-steady Batch Experiment.....57

Table III-11 Equilibrium Achieved in Agitated Batch Studies with Pulverized Spent Shale (< 0.35mm mesh size) at 22 °C.....61

Table III-12 Increase of Solute EC with Time, Pulverized Spent Shale in Agitated Flasks.....63

Table III-13 Comparison of Spent Shale Solutes Black, Tan and Grey Types 2.8mm to 1.4mm Mesh Size Range.....64

Table III-14 Long Term Leaching, Leached Spent Shale Derived from Column Studies.....65

Table III-15 Increase in Solute EC with Time for a Single Piece of Shale Suspended in Agitated Water....66

Table III-16 Quiescent Leaching in Columns Subsequent to Column Runs....73

Table III-17 Small Column Experiments, Summary of Operational Parameters....75

Table III-18 Large Column Experiments, Summary of Operational Parameters....85

Table V-1 Small Column Diffusion Coefficients, Internal Porosity of 0.15....121

Table V-2 Small Column Diffusion Coefficients, Internal Porosity of 0.20....121

Table V-3 Small Column Diffusion Coefficients, Summary for Internal Porosity of 0.10....122

Table V-4 Large Columns, Summary of Parameters used for Calculation of Break-through Curves....143

Table V-5 Maximum Velocity in Macro-pores Due to Density Gradients....146

APPENDIX A

Table A-1 Small Column U-1, Electrical Conductivity of Leachate....A-2

Table A-2 Small Column U-1, Total Organic Carbon in Leachate....A-3

Table A-3 Small Column U-2, pH of Leachate....A-4

Table A-4 Small Column U-2, Electrical Conductivity of Leachate....A-5

Table A-5 Small Column U-2, Total Organic Carbon in Leachate....A-6

Table A-7 Small Column D-1, Electrical Conductivity of Leachate....A-8

Table A-8 Small Column D-1, Total Organic Carbon in Leachate....A-9

Table A-9 Small Column D-2, pH of Leachate....A-10

Table A-10 Small Column D-2, Electrical Conductivity of Leachate....A-11

Table A-11 Small Column D-2, Total Organic Carbon in Leachate....A-12

Table A-12 Small Column D-3 pH of Leachate....A-13

Table A-13 Small Column D-3, Electrical Conductivity of Leachate....A-14

Table A-14 Small Column D-3, Total Organic Carbon in Leachate....A-15

Table A-15 Small Column D-4, pH of Leachate....A-16

Table A-16 Small Column D-4, Electrical Conductivity of Leachate....A-17

Table A-17 Small Column D-4, Total Organic Carbon in Leachate....A-18

Table A-18 Small Column D-5, pH of Leachate....A-19

Table A-19 Small Column D-5, Electrical Conductivity of Leachate....A-20

Table A-20 Small Column D-5, Total Organic Carbon in Leachate....A-21

Table A-21 Small Column D-6, Electrical Conductivity of Leachate....A-22

Table A-22 Small Column D-6, Total Organic Carbon in Leachate....A-23

Table A-23 Small Column D-7, Electrical Conductivity of Leachate....A-24

Table A-24 Small Column D-7, Total Organic Carbon in Leachate....A-25

Table A-25 Small Column D-8, pH of Leachate....A-26

Table A-26 Small Column D-8, Electrical Conductivity of Leachate....A-27

Table A-27 Small Column D-8, Total Organic Carbon in Leachate....A-28

Table A-28 Large Column LC-1, Leachate pH....A-29

Table A-29 Large Column LC-1, Leachate Electrical Conductivity A-30

Table A-30 Large Column LC-1, TOC Data.....A-31

Table A-31 Large Column LC-2, Leachate pH.....A-32

Table A-32 Large Column LC-2, Leachate Electrical Conductivity.....A-33

Table A-33 Large Column LC-2, TOC Data.....A-34

Table A-34 Large Column LC-3, Leachate pH.....A-35

Table A-35 Large Column LC-3, Leachate Electrical Conductivity.....A-36

Table A-36 Large Column LC-3, TOC Data.....A-36

ACKNOWLEDGEMENTS

The author wishes to acknowledge the support and encouragement of my family, friends, and teachers and staff at the University of California.

Special thanks are due to:

Professor Robert E. Selleck

Professor Jerome F. Thomas

Dr. T. N. Narasimhan

Professor Alan Foss

Dr. Phyllis Fox

Dr. Sergio Leao

Dr. Richard Valentine

Professors Selleck, Thomas and Narasimhan have been my teachers and also served on my oral and dissertation committees. Professor Foss was a member of my dissertation committee. Phyllis Fox, Project Manager of the Oil Shale Project, Energy and Environment Division, Lawrence Berkeley Laboratory, was instrumental in obtaining financial support for my graduate studies. Sergio Leao and Rich Valentine were my fellow students who helped by both listening and offering advice.

This work was supported by the Assistant Secretary for Environment, Office of Environmental Compliance and Overview, Environmental Control Technology Division and the Assistant Secretary for Fossil Energy, Deputy Assistant Secretary for Oil, Gas and Shale Technology, Office of Oil Shale of the U.S. Department of Energy under Contract No. DE-AC03-76SF00098.

CHAPTER I

INTRODUCTION

Oil shale is a marlstone, a clay-carbonate rock, which contains appreciable amounts of kerogen, a high molecular weight organic compound. The kerogen is a potential source of oil which can help meet national energy needs.

The deposit was formed in the geologic past in sedimentary formations on lake bottoms. With progressive burial, algae and other organic content were converted to kerogen.

Oil shale is found in the United States in the tri-state area of Colorado, Wyoming, and Utah. Several exploratory developments are presently under way in the Piceance Creek Basin in north-western Colorado to exploit the resource. The potential impact of these developments on regional water quality was a primary motivation for this study.

SHALE OIL RETORTING PROCESSES

Both surface and underground techniques have been proposed for the production of oil from raw oil shale. These are discussed in detail in articles contained in the Proceedings of the Oil Shale Symposia, published annually by the Colorado School of Mines at Golden (Colorado School of Mines, 1964-1981). Heating of the raw shale to 950 ^{o}F or more thermally converts the kerogen to hydrocarbon vapors and liquids, and carbon. The vapors and liquids are then collected for processing and subsequent marketing.

Surface Retorting

Surface retorting may be used as the sole means of oil shale processing or it may be used in conjunction with underground retorting. In either case, raw shale is mined and conveyed to the surface facilities for retorting. Paraho Direct and TOSCO II are two examples of surface retorting methods that have been proposed and studied in detail. The Paraho Direct retort is a vertical kiln in which raw shale moves downward through a combustion zone. Heat from this zone converts the organic kerogen into vapors which are recovered. A high molecular weight carbon remains in the mineral matrix and becomes the fuel for combustion. Spent shale, the combustion residue, is removed from the bottom of the retort and hauled to nearby disposal sites.

The TOSCO process uses heated ceramic balls to contact crushed raw shale in a rotating kiln. The resulting hydrocarbon vapors are removed from the kiln and condensed. After passage through the kiln the balls and the spent shale are separated, the balls are reheated, and the spent shale sent to disposal piles.

In-Situ Retorting

Underground or in-situ shale oil retorting operations are an alternative to aboveground processes. The in-situ retort is prepared by fracturing the raw shale bed by external means and then retorting the rock in place. One of the many methods, which have been proposed and studied in detail, is the Vertical Modified In-Situ (VMIS) process. A VMIS development consists of large numbers of underground chambers filled with fractured shale. These chambers are located in

oil shale beds several hundred meters below the surface and may be 30 to 50 meters square in plan by 200 or more meters high. Each chamber is separated from its neighbors by vertical walls of bed material. The actual dimensions of the retorts, wall thickness, and extent of development depend on site conditions and the process variations favored by the developer.

An individual retort is constructed by using conventional mining techniques to remove about 20 or 30 percent of the raw shale within the boundaries of the proposed retort. The raw shale is conveyed to the surface for disposal or for retorting in surface facilities. The void space remaining after removal of the raw shale is then distributed throughout the retort by drilling and blasting. The result is an underground chamber filled with fractured shale. The oil shale at the top of the chamber is set on fire and the combustion zone driven down through the bed by injected air. Steam or recycled retorting gases may also be injected to aid combustion. Kerogen conversion occurs in the pyrolysis zone immediately below the flame front. The retorted liquids and gases are driven to the bottom of the retort for collection and conveyance to the surface. The carbon remains in the mineral matrix and becomes the fuel for combustion. When the flame front nears the bottom of the retort the fire is allowed to die and the retort abandoned.

WATER POLLUTION POTENTIAL OF SPENT SHALE

Large volumes of spent oil shale are generated by both surface and in-situ processes. About one ton of rock is co-produced along with each 25 gallons of oil. Spent shales from surface activities

are conveyed to nearby disposal piles while in-situ spent shales remain underground. The pollution potential is considerable. Leachate from spent shale, formed when rain, snow melt, or groundwater contact the retorted material, may seriously degrade surface and groundwater supplies. Extensive protective measures may be necessary. Surface protective facilities might include use of liners under disposal piles to restrict vertical movement of leachate into the underlying soil and containment structures to collect runoff from pile surfaces.

Control of Leaching from Abandoned VMIS Retorts

Isolation, modification of retort operating conditions, and intentional leaching have been proposed to control leaching from abandoned in-situ retorts (Fox et al.,1980). Isolation techniques prevent or minimize groundwater contact with the spent shale. The construction of grout curtains around the retort and filling voids with grout decrease permeability. Since water is restrained from entering the retort, soluble material will remain fixed within the solid shale. Locating retorts above groundwater tables is also an isolation technique.

Modification of retort operating conditions has been suggested because investigators have reported that leachability of shale depends on retort operating conditions such as temperature, rate of flame advance, and composition of injected gases (Fox et al., 1980).

Intentional leaching is a technique in which most of the soluble substances are removed from spent shale by first injecting water into

the retort and then recovering the resulting leachate. The leachate is treated at the surface to remove dissolved solids and then re-injected. The process is continued until the concentrations of the solutes of interest in the leachate are low enough not to create problems in the aquifers. The proposed technique is based on observations that effluent concentrations from columns drop rapidly to low levels after the passage of only a few pore volumes of water (Amy, 1980), (Kuo et al., 1979).

IMPACT OF ABANDONED VMIS RETORTS ON WATER QUALITY

The potential impact of an abandoned VMIS retort on quality of regional water supplies is impossible to predict given the present state of knowledge. The difficulties may be illustrated by considering a hypothetical VMIS retort complex at the time of abandonment. Dewatering activities have lowered the groundwater table in the vicinity so that retorting could be undertaken in the dry state. Air injection and combustion have ceased, dewatering pumps have been shut off, and the groundwater begins to reinvade the dewatered unsaturated zone. The returning water eventually reaches the retorts and contacts the spent shale. Soluble material is transferred from the solid phase to the liquid. Ultimately, there is a net flow of fluid through the retort carrying quantities of dissolved solids into the groundwater aquifers.

Factors Complicating Impact Analysis

Factors which complicate the analysis of impact on water quality from an abandoned in-situ retort are:

1. Non-homogeneity of the material within the retort.

2. Elevated temperatures of the spent shale at the start of leaching.

3. Non-uniform and generally unpredictable leachate flow patterns.

4. Unknown quality of influent leaching fluid.

5. Poorly defined rate-limiting leaching mechanisms.

6. Poorly defined solute transport mechanisms in the aquifers.

Non-homogeneity of Retorted Shale. Material within an abandoned retort is extremely heterogeneous. Retorting by-products are distributed throughout on shale surfaces and within particles. The spent shale varies in size and shape, chemical composition, and solubility. Differences are due to natural variations in the raw shale beds, retort preparation, and operating techniques.

Elevated Temperatures. The temperature of spent shale within the retort may be well above the boiling point of water at the time when the groundwater arrives. Early leaching may thus occur at elevated temperatures in the presence of solid, liquid, and gaseous phases. Leaching mechanisms will be difficult to define except in the most general manner.

Non-uniform Leachate Flow Patterns. The flow pattern of the re-invading groundwater depends on the geo-hydrology of the surrounding aquifer system, as well as conditions within the in-situ chamber.

Reliable calculations of flow patterns therefore depend on an adequate knowledge of regional aquifer parameters. In most cases, data of this sort are inadequate (Merhan et al., 1981). Additional complications are encountered once the water reaches the retort. Leachate flow within the pores will not be uniform. Both liquid and gaseous phases will be present. Variations in particle and porosity size and distribution due to the nature of the techniques used in retort preparation will encourage channelizing and short circuiting. Temperature and density gradients formed within the fluid phase will tend to establish counter-currents. Mechanical dispersion in the pore system will also become a significant factor.

Quality of Influent Leaching Fluid. The quality of the effluent leaving the retort depends on the quality of the entering water. Influent concentrations, in turn, depend on the flow regime established in the aquifer after dewatering operations are terminated. The penetration of relatively impervious layers of bed rock by the highly pervious VMIS chambers may permit flows from previously isolated saline areas to enter the aquifer system. Leachates from one retort may also be directed into another retort.

Leaching Mechanisms. Basic mechanisms involved in the transport of a solute from a site in the solid phase to the fluid phase moving through the pores between the particles are generally understood and have been well described in the literature. On the other hand, mechanisms for solute transport in spent shale are not well defined. A primary reason for this is the non-homogeneity of the material. Many of the previous leaching studies that have been reported in the

literature have been directed toward characterizing a leachate produced in laboratory column or batch studies. The data produced are useful in understanding the composition of the leachate produced under the given conditions from a specific shale; however, the results cannot be extended to other shales or other leaching conditions with any degree of certainty because leaching mechanisms are not defined.

Transport Mechanisms. Solute may precipitate, decay, or react with other chemical compounds as it is conveyed through the fractured raw shale aquifers. The modelling of flow through fracture systems is in itself a difficult and complex problem.

STUDY OBJECTIVES

One of the basic reasons for the inability to determine the impact of abandoned VMIS retorts on water quality is a lack of knowledge of the leaching mechanisms involved in the transfer of a solute from the solid shale to the leaching fluid.

The objective of the present study is to investigate the kinetics of leaching of soluble substances from in-situ spent shales by water. Specifically the following is undertaken:

1. Evaluate mass-transfer mechanisms involved in the leaching of in-situ spent shale by water and determine which are rate-limiting.

2. Evaluate changes in mass transfer coefficients with respect to changes in bed media, approach velocity and bed porosity.

3. Develop a mathematical model of the variation of concentration of organic compounds with time and depth in a spent shale bed.

The following assumptions are made to simplify the analyses:

1. Inorganic and organic species concentrations in the leachates will be characterized by electrical conductivity and total organic carbon, respectively.

2. Column and batch leaching experiments will be conducted at ambient temperatures.

CHAPTER II

LITERATURE SEARCH

Research on leaching of inorganic and organic substances from spent oil shale can be classed roughly into two groups: leachate characterization, and leaching and transport mechanisms. A majority of oil shale leaching studies has been directed toward the characterization of leachates[1]; leaching and transport mechanisms, however, have received relatively little consideration.

LEACHATE CHARACTERIZATION STUDIES

Inorganic Characterization of In-Situ Spent Oil Shale Leachates

Inorganic characterization studies of leachates from in-situ spent oil shale have been made by Jackson et al. (1975), Parker et al. (1980), Kuo et al. (1979), Wildung et al. (1977, 1978), Krause et al. (1980), McWhorter (1980, 1981) and Peterson et al. (1981). Studies of leachates from spent shales derived from cores taken from the Occidental Oil in-situ retort were conducted at three laboratories, University of Colorado, Los Alamos Scientific Laboratory (LASL), and Battelle Pacific Northwest Laboratories (PNL), (Oil Shale Task Force, 1980).

1. Fox (1982) has prepared a review and evaluation of the literature on leaching of oil shale including raw, and surface and in-situ spent shales. The author of this dissertation had the opportunity to read a preliminary draft of the report just prior to the completion of the present study. The Fox report is comprehensive and detailed and should be a primary reference for oil shale leaching investigations.

Kuo et al., Park et al., and Peterson et al. used Occidental Oil Company in-situ retort material, as did investigators at PNL and the University of Colorado. Jackson et al., and Wildung et al. investigated shale from the 10-ton simulated in-situ retort at the Laramie Energy Research Center (LETC) in Wyoming. Parker et al., Park et al., and Kuo et al. investigated leachates from cores produced in laboratory scale retorts. Krause et al. investigated the inorganic quality of leachates of spent shales from Geokinetics in-situ retorts.

The studies conducted by Kuo et al., Park et al., Peterson et al., and Wildung et al. are summarized below.

Kuo et al. Kuo et al. (1979) leached cores obtained from Occidental Retort 3E. The spent shale showed leaching properties similar to those of raw shales for elements Ca, SO_4, Na, and B. The pH levels of core leachates were less than 9.5. They also conducted a series of experiments with laboratory-produced spent shale samples covering a retorting range of 540° to 900°C. Raw shale grades ranged from 10 to 37 gal per ton and particle sizes varied from 0.3 to 4.0 cm. Stirred batch tests were conducted at room temperature in de-ionized water with water-to-shale ratios varying from 7 to 75 mL/g. Spent shale was also leached with de-ionized water in continuous flow columns 7.5 cm in diameter by 1.2 m long.

Results and conclusions from these latter experiments included the following:

1. For shales retorted above 650 °C, concentrations of most ions fell to negligible levels after the passage of 5 void volumes of water. This was attributed to a two-stage removal mechanism. Solute was first removed from the particle surfaces. After the surface was depleted, additional material came from within the solid phase.

2. Calcium and hydroxyl ions were found in relatively high concentrations in early leachates. Calcium levels increased for the first few void volumes and did not reach low levels for as many as 20 volumes. The pH remained above 11 for as many as 50 volumes.

3. Ion concentrations in leachates produced from shales retorted at lower temperatures fell off more slowly than did those produced from higher temperature material.

4. Leachate concentrations fell off most rapidly for runs conducted with the larger particles and with shale retorted at higher temperature. The effects could not be separated because retorting of larger particles tended to result in higher retort temperatures.

Park et al. Park et al. (1979) investigated the mineralogy of spent shale from the Occidental in-situ retort with particular emphasis on identifying the major minerals present and the effects of retorting conditions on each phase. The spent shale mineralogy was found to depend on the original mineralogy of the raw oil shale and retorting conditions such as temperature, time at temperature and

retorting gas composition. High temperatures, long reaction times, and steam environment should result in the formation of relatively insoluble silicates. Park et al. also investigated effects of retorting conditions on quality of leachate from spent shale produced in a small laboratory retort..

Peterson et al. Peterson et al., (1981) performed extensive studies of the mineralogy, trace element content, and leaching characteristics of three cores retrieved from Occidental Oil Retort 3E. Core samples were examined for major, minor and trace elements content. Leachates from the core samples were also analysed for trace elements.

The identities of the mineral species found were correlated with retorting conditions encountered within the retort. Silicate species that form under high temperatures or long heating durations were prevalent in the upper 60 percent of the retort. There was a general absence of these silicate species in the lower portions. Several minerals normally found in raw shale were also found in the lower regions. The lack of silicates and the presence of the raw shale minerals in the lower regions indicates that the retorting conditions were probably not so severe as those that occurred in the upper levels.

Carbonate compounds were distributed throughout the retort. Carbonates are normally decomposed below temperatures at which silicates are formed and one would expect that carbonates and silicates would not co-exist. The authors hypothesized that the carbonates in the upper part, predominantly aragonite ($CaCO_3$), were created during

post-burn activities when water was introduced into the retort for cooling purposes. The aragonite crystals were deposited from leachates containing soluble calcium and carbon dioxide.

Leachate compositions generally reflected retorting conditions experienced by the spent shale. Concentrations of major cations in leachates from shales containing the high temperature silicate species tended to be lower than leachates from shales without silicates. A corresponding reduction in conductivity was also noted. The authors observed, however, that solubilities of some environmentally sensitive trace elements, i.e., As, B, F, and V, were not necessarily mitigated by the formation of the high temperature silicate species.

Maximum, minimum, and mean values of pH, conductivity, and major ion concentrations found in leachates from core R3E2 are tabulated in Table II-1. These data represent 19 samples distributed over a retort depth of 106 feet. Leachates were produced by 48-hour static shaker leaches of -100-mesh material having solid-liquid-container volume ratios of 1:5:10. Solutions, separated from the solids by centrifugation, were filtered through 0.45 micron Millipore filters.

The studies done by Peterson et al. may be summarized by the following:

1. Zones characterized by different mineral species were produced in the retort depending on processing temperatures, rates and other conditions.

Table II - 1

Conductivities, pH and Major Ion Concentrations
Leachate from Core R3E2
Occidental In-situ Retort 3E

Item	Units	Range	Mean
pH		8.78-11.60	10.06
Conductivity	mmhos/cm	0.88-2.78	1.78
B	mg/L	0.29-6.55	2.14
Ca	mg/L	3.5-566	167
F	mg/L	0.3-21	6.3
K	mg/L	53-220	154
Na	mg/L	92-308	173
Si	mg/L	5.4-46	23

2. Material in the retort ranged from shales containing partially decomposed carbonates to shales containing partially or wholly silicated species.

3. The solubility of most major cations was reduced to low levels and conductivity was also reduced when high-temperature silicate product phases are formed during processing.

4. Some trace elements, i.e., As, B, F, Mo, Ni, and V, may not be immobilized by the formation of high-temperature silicates.

Wildung et al. Wildung et al., (1977, 1978) leached in-situ shale from the 10-ton LETC retort with a 0.01 M $CaCl_2$ solution. The spent shale was < 2 mm in size and was packed in a glass column, 4.05 cm in diameter by 34 cm long. Leaching flow was 0.168 mL/min in an upward direction. Effluent was collected in 15 mL fractions and analysed for major ions, trace elements, and organic and total carbon. Selected cation and carbon concentrations are shown in Table II-2. The data for Na, K and carbon exhibit rapid drops with time. Ca, on the other hand, increases toward a quasi-equilibrium condition.

Table II-2

< 2 mm Spent Shale Leached with 0.01 M $CaCl_2$
LETC 10-ton Retort

Sample	Pore Vol	Na mg/L	K mg/L	Ca mg/L	Organic Carbon mg/L	Total Carbon mg/L
1	0.015	23925	2980	565	1430	1460
3	0.056	8140	1240	728	349	360
5	0.114	1980	501	670	120	124
10	0.282	200	91	816	20	22
15	0.442	180	55	902	10	11
50	1.57	171	55	1338	4	8
99	3.10	207	52	1127	5	5

Reference- Wildung et al. (1977)

Summary of Inorganic Leachate Characterization Studies

It is difficult to review the above characterization studies on a common basis. The compositions of the mineral species content of the raw and retorted shales are not available, and the retorting conditions experienced by the various spent shales are not known. Leachate quality also depends on such factors as solid-liquid contact time, leaching fluid composition, temperature, particle size and porosity. Information on these factors has not been reported on a uniform basis by the investigators.

Fox (Dec. 1980) has compared in-situ leachate data compiled by Amy (1978), Jackson et al. (1975), Kuo et al. (1979), and Parker et al. (1977). Constituent concentrations, expressed as mass leached per 100 grams of shale, were grouped according to the maximum observed value as follows:

1. Less than 10 mg/100g - Al, B, Cl, Cr, F, Fe, Li, Mo, Mg, NO_3, Pb, Sr, Zn.

2. Between 10 and 100 mg/100g - HCO_3, K, OH, Si.

3. Greater than 100 mg/100g - Ca, CO_3, Na, SO_4.

This grouping is subject to the qualifications imposed for lack of information about material composition and retorting conditions but it does serve to identify the major ions typically found in in-situ spent shale leachate to be Ca, Na, SO_4, and CO_3.

Organic Characterization of Leachates

Organic characterization studies of leachates from spent shales have generally been limited to the measurement of total organic carbon (Jackson et al., 1975), (Wildung et al., 1977, 1978).

TOC analyses are simple compared to the techniques required to identify and quantify individual organic species. Some investigators have conducted more detailed analyses. Wildung et al. (1977) investigated organics and organic-metal complexes in leachates from lysimeters containing retorted shales originating from the Paraho retort. Amy (1978) conducted fractionation studies of leachates from simulated in-situ spent shales and found approximately equal amounts of acidic, neutral, and basic materials present.

LEACHING AND TRANSPORT MECHANISMS

Leaching and transport of solutes within the pores of a fixed bed can be described by the classic advection-dispersion equation:

$$\frac{\partial C}{\partial t} = E \frac{\partial^2 C}{\partial Z^2} - U_p \frac{\partial C}{\partial Z} - R_r - \frac{1}{m} \frac{\partial q}{\partial t} \qquad \text{(II-1)}$$

in which:

C = Concentration of solute in liquid phase

t = Time

Z = Distance in direction of flow

E = Dispersion coefficient

U_p = Interstitial fluid velocity

R_r = Chemical reaction rate

m = Ratio of macro-pore to micro-pore volumes

q = Uniform concentration of solute in solid phase

The terms on the right side of the equation represent dispersive transport, convective transport, chemical reaction, and internal mass transfer. A source term may be added if necessary.

The transport of solute between phases can be described by Fick's law of diffusion:

$$\frac{\partial q}{\partial t} = D_m \nabla^2 q \qquad \text{(II-2)}$$

in which:

D_m = Diffusion coefficient

∇^2 = Laplacian operator for the applicable coordinate system.

These two equations were the bases for several of the research investigations into leaching mechanisms discussed later in this chapter.

Diffusive Mechanisms

Diffusive solute transport is conventionally described by transport mechanisms driven by concentration gradients (Sherwood et al., 1975), (Bird et al., 1960), (Perry et al., 1973). Consider a

particle located in a fixed bed of similar particles as shown on Figure II-1. The bed porosity is proportioned into micro- or internal porosity and macro- or external porosity. Micro-porosity lies totally within the particle boundaries and macro-porosity occurs only in the space between the particles. An element of solute moves from a site within the solid phase to the solvent flowing through the macro-pores by mechanisms of solid diffusion, surface diffusion, interface transfer, and ordinary or Knudsen diffusion in the liquid phase. Rates of solute transport are expressed in terms of diffusion coefficients or diffusivities.

Dispersive Transport Mechanisms

Axial and radial dispersive mechanisms mix and spread solute through the macro-pore system. These dispersions are a combination of molecular diffusion driven by local concentration gradients and mechanical or hydrodynamic dispersion caused by variations in direction and magnitude of local pore velocities. The dispersion causes the solute to be distributed within continually increasing bed volumes in the direction of net flow. Relationships between dispersion, molecular diffusion and particle Reynolds number have been established from correlations of experimental data (Sherwood et al., 1975).

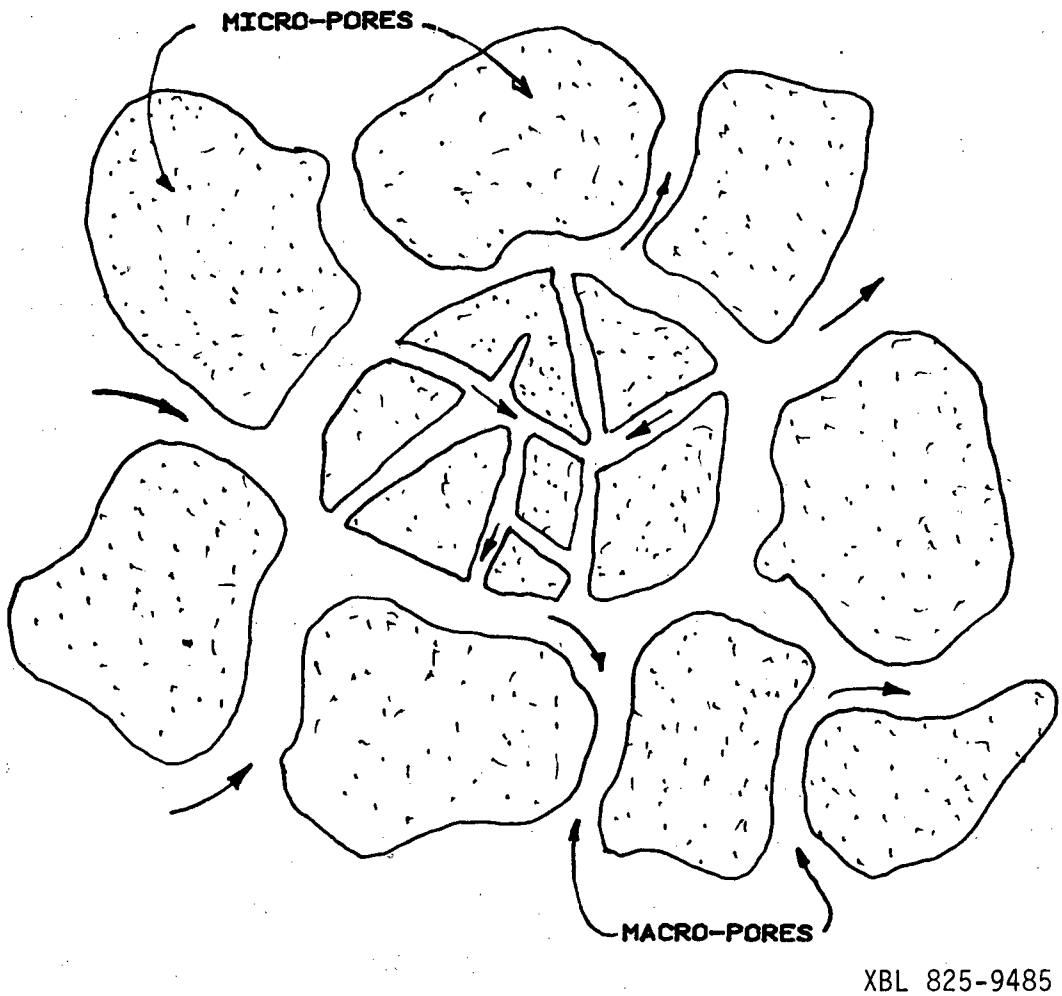

Figure II-1. Schematic section through porous media in a fixed bed.

INVESTIGATIONS INTO OIL SHALE LEACHING MECHANISMS

Amy (1978,1980), Kuo et al. (1979), McWhorter (1980, 1981), and Rameriz (1981) have conducted investigations into the mechanisms of leaching of solutes from oil shale. Only the portions of work pertinent to leaching mechanisms are summarized herein:

Amy

Amy (1978, 1980) conducted continuous flow column and equilibrium batch experiments on four types of spent shale from the Lawrence Livermore Laboratory 125-kg simulated in-situ retort. Two of the shales, type 1 and type 2, were retorted in an oxygen environment and in an inert gas atmosphere, respectively. The study objective was to define the mechanisms by which organic matter is leached from spent shale by groundwater.

Columns, 2.5 cm in diameter by 15 or 30 cm long, were filled and compacted with spent shales having a particle size range of 0.14-0.64 cm. Distilled water at 20 ^{o}C was pumped through the pores at a rate of 0.6 mL/min for 96 hours. Time-averaged composite samples were analysed for total organic carbon, conductivity and pH.

Equilibrium isotherms describing the relationship between the solute concentration in the solid and the equilibrium concentration of the solute in the liquid were also developed from batch tests.

Amy presented a model of leaching in a packed bed based on Equation II-1 with dispersive and reactive terms neglected as follows:

$$\left(\frac{\partial q}{\partial t}\right)_Z = \frac{F}{\rho_B A}\left(\frac{\partial C}{\partial Z}\right)_t + \frac{1}{\rho_B}\left(\frac{\partial C}{\partial t}\right)_Z \qquad \text{(II-3)}$$

in which:

q = TOC concentrations in the solid phase

t = Time

Z = Distance in the direction of flow.

F = Water flow rate

A = Cross-sectional area of column

C = TOC concentration in liquid phase

ρ_B = Bulk density of shale

Amy assumed that the rates of leaching of TOC from the solid phase could be expressed by the following mass transfer equations:

External Mass Transfer

$$\left(\frac{\partial q}{\partial t}\right)_Z = K_E(C - C^*) \qquad \text{(II-4)}$$

Surface Reaction

$$\left(\frac{\partial q}{\partial t}\right)_Z = K_{BA}(q_\infty - q) \qquad \text{(II-5)}$$

Internal Mass Transfer

$$\left(\frac{\partial q}{\partial t}\right)_Z = K_G(q^* - q) \qquad \text{(II-6)}$$

in which:

K_E = External Mass Transfer Coefficient

C^* = Equilibrium leachate TOC concentration

C = Measured leachate TOC concentration

K_{BA} = Surface reaction rate coefficient

q_∞ = Maximum potential of solid phase TOC on shale surface

q = Actual solid-phase TOC on shale particle

K_G = Internal mass transfer rate coefficient

q^* = Equilibrium solid phase TOC concentration

Equation II-3 was solved together with each of the equations II-4, II-5, and II-6 to determine which of the three mechanisms were limiting for the two types of shale investigated.

Amy hypothesized that internal mass transfer is the rate controlling mechanism for the combustion retorted shale. He deemed this likely because the relatively high internal porosity associated with combustion retorted shales implied an extensive internal network of pores that solute must travel.

None of the rate models accurately described the rate of leaching over the entire range of time for type 2, the inert gas retorted material. Some evidence, although not conclusive, indicated that internal mass transfer or surface reaction mechanisms may have been rate limiting during time periods after 10 hours of leaching.

External mass transfer appeared to be rate limiting during the first 10 hours. Amy suggested that this may have been due to the early high TOC concentration in the leachate which served as an external resistance to mass transfer.

Kuo et al.

Kuo et al. (1979) derived a simple mass transfer model for leaching of inorganic ions from spent shale columns. The model predicted effluent concentrations with time for the spent shale used in the experiments.

The model was described but not presented. It was based on a shrinking core model for individual particles and presumed that pore diffusion is the rate controlling process. The column was taken as a series of well-stirred tanks. Solutions were obtained by numerical analysis of difference equations. Pore diffusivity was determined from both single particle leaching data and by fitting the column leaching data to the numerical model. Coefficients with values between 10^{-7} and 10^{-8} cm^2/sec were obtained.

McWhorter

McWhorter (1981) reported on studies of the role that the bi-modal property of shale fragments played in the leaching of raw oil shale.

In previous studies the author had saturated two columns of fresh raw shale and one column of weathered raw oil shale with de-ionized water (McWhorter, 1980). De-ionized water was then passed

through the columns at a constant rate and the conductivities of the resultant effluent measured. In general the EC of the effluent started to drop just prior to the passage of one pore volume, and then showed a gradual decrease over the next several pore volumes producing an asymmetrical breakthrough curve.

Following the initial run, the columns were allowed to gravity drain for about 6 weeks, re-saturated with de-ionized water and the experiment repeated. Initial EC concentrations in the columns containing fresh raw shale approached those observed in the first cycle. After the passage of one pore volume, the EC again dropped in a similar manner to the first run. Effluent conductivities in the second cycle for a given pore volume passage were about half to two-thirds of those in the initial runs.

The naturally weathered shale did not recover in the same manner as did the fresh shale. Initial EC concentrations were an order of magnitude less than those observed during the first part of the experiment. Effluent EC did however show a gradual decrease with increasing time.

Tentative conclusions reached by the author were:

1. Simple linear desorption was not the rate limiting mechanism.

2. Non-equilibrium chemistry within the macro-space did not provide an adequate explanation of the asymmetry of the breakthrough curve.

3. The diffusion of dissolved species within the micro-pores may contribute to the asymmetry of the breakthrough curve but is not, by itself, an explanation.

4. The diffusion process may also have an indirect effect on the rate of reaction within the micro-space by limiting mass transport to and from the reaction sites.

McWhorter proposes a mathematical advective-dispersive model of the leaching process based on Equation II-1.

$$D \frac{\partial^2 C}{\partial X^2} - V \frac{\partial C}{\partial X} = \frac{\partial C}{\partial t} - \frac{\partial s}{\partial t} \qquad \text{(II-7)}$$

in which:

D = Hydrodynamic dispersion coefficient

C = Tracer concentration

V = Mean pore velocity

t = Time

X = Space coordinate

S = Source term

The source term S represents a rate of solute mass addition to the macro-space by the particle. It depends on, among other factors, the size, shape, size distribution, porosity and tortuosity of the particles. McWhorter used an analogy based on diffusion flux from a

sphere resulting from a unit step change in surface concentrations to define the source term for a wide distribution of particle shapes and sizes. This source term was substituted into the advective-dispersive equation and a solution obtained by Laplace transform techniques was given in operational form. A closed form solution was not obtained.

Ramirez

Ramirez (1981) has proposed a mathematical model of the leaching and transport mechanisms of spent shale. The model consists of two equations, one applicable to the main channels in the porous media and the other to dead space. Scanning electron microscope studies identified the possibility of significant dead space volume in addition to main channel flow regions. The equations are:

$$f \frac{\partial C_m}{\partial t} + V \frac{\partial C_m}{\partial Z} = Df \frac{\partial^2 C}{\partial Z^2} - K(C_m - C_d) - \frac{A_m}{\phi} \frac{d\Gamma_m}{dt} \qquad \text{(II-8)}$$

and

$$(1 - f) \frac{\partial C_d}{\partial t} = K(C_m - C_d) - \frac{A_d}{\phi} \frac{d\Gamma_d}{dt} \qquad \text{(II-9)}$$

in which:

C_m = Main channel leachate composition

C_d = Dead space leachate composition

f = Flowing fraction

V = Liquid phase velocity in media

D = Dispersion coefficient

K = Mass transfer coefficient

A_m = Main channel leaching area per volume

ϕ = Porosity of spent shale

Γ_m = Amount of pollutant leached in main channel

A_d = Dead space leaching area per volume

Γ_d = Amount of leached solute in dead space

The Γ_m and Γ_d terms will be defined by equilibrium isotherms.

DIFFUSIVE AND DISPERSIVE MECHANISM RESEARCH IN ALLIED FIELDS

Research conducted in allied fields such as chemical engineering, soil science, and geo-physics are valuable sources of information on the the basic phenomena encountered in oil shale leaching.

Passioura et al.

Passioura (1971) and Passioura and Rose (1971) developed and tested a model of hydrodynamic dispersion in aggregated soil media in which pores are partioned into large and small sizes. Viscous flow occurs only in the large or macro-pores and solute movement takes place in the micro-pores only by diffusion. The micro-pores act as reservoirs for solute storage. The net effect of the storage is to extend the tail of the break-through curves.

Rosen

Rosen (1952, 1954) studied the kinetics of diffusion into spherical particles in a fixed bed system. He presented a solution to the general problem of transient behavior in a linear fixed bed system. The rate of adsorption is determined by the combined effects of liquid film resistance and diffusion within a particle in a fixed bed containing homogeneous spherical particles of uniform radius. A fluid phase flows through the bed with a constant linear velocity.

Two primary assumptions were made to linearize the system and thus facilitate the solution; (1) Solid diffusion and liquid film resistance coefficients are independent of concentration and position and (2) the equilibrium isotherm between phases is linear. Two solutions were presented: an exact solution based on numerical integration of an infinite integral and an approximate solution based on a saddle point integration of a Laplace transform inversion integral. The dependent variable in the Rosen solution is the solute concentration C in the leaching fluid. This term is a function of the bed length and time following a step increase in influent concentrations from zero to C_o at time zero. Independent variables included were particle radius, coefficient of solid diffusion, equilibrium isotherm slope, ratio of void volume to particle unit volume, solute concentration in the solid phase, surface film resistance, pore velocity of the liquid phase, and time and distance of leachate travel. Graphical and tabular solutions were given for dimensionless time, distance, and film resistance parameters.

Rasmunson and Neretnieks

Rasmunson and Neretnieks (1981) developed and solved a model of migration of radionuclides in the fissures of bed rock based on equations II-1 and II-2. The rock was regarded as a double porosity media consisting of porous blocks surrounded by fissures. Viscous flow takes place only in the fissures. The solution considered diffusion of a solute into the porous blocks, linear sorption, and longitudinal dispersion.

For the case of no dispersion and a non-decaying species the solution is identical to that found by Rosen for diffusion into porous spheres.

CHAPTER III

EXPERIMENTAL PROCEDURES

PHYSICAL CHARACTERISTICS OF SPENT SHALE

Batch and column experiments were conducted on spent shale produced in Run S-55 of the Laramie Energy Technology Center (LETC) 10-ton simulated in-situ retort. The LETC retort, located in Laramie, Wyoming, is operated in the following manner. After the retort has been carefully packed with random-sized raw shale, the top layer is ignited. The resulting flame front is then driven down through the shale bed by air injected at the top. The kerogen contained in the shale is converted to oil, gas, and carbon in the hot, oxygen-free zone immediately below the burning mass. The advancing flame front feeds on the carbon remaining after the kerogen conversion and the oil and gases are forced to the bottom and removed. After the combustion zone reaches the bottom, the air injection is stopped and the shale allowed to cool. A summary of the operating conditions for Run S-55 is shown on Table III-1.

Handling and Classification of Spent Shale

Run S-55 of the LETC 10-ton retort was completed in the last week of June 1978. The entire charge of spent shale was made available to the Oil Shale Project at Lawrence Berkeley Laboratory (LBL). The following is a brief description of the steps taken to unload the retort and to pack, ship, and classify the material. This is significant because the original "as retorted" condition of the shale pieces is affected by abrasion and impact incurred during handling and shipping.

Table III-1

Operating Conditions
LETC 10-ton Retort - Run S-55

Shale source	Anvil Points, CO
Shale grade	26 gal per ton
Particle size range	fines to 24 in.
Run type	67% air/33% steam
O_2 content of retort gas	13.8%
Steam injection rate	920 scfh
Superficial gas velocity	2.8 scfh/ft^2
Maximum temperature	1200 ^oF
Retorting rate	1.53 in/hr
Average heating value of gas	67 BTU/ft^3
Yield % Fischer Assay	46.6 vol.%

The spent shale was first dropped through a hatch located in the retort bottom into a tared dump truck. The truck was driven several miles to a scale, and the weight of the shale determined. The load was then returned to LETC, dumped on a concrete slab, and loaded into plastic-lined, 55-gallon drums with an end-loader. Twenty-seven drums, weighing some 5500 kgs, were shipped by truck to LBL facilities in Richmond, Calif.

At Richmond, the shale was classified with motorized vibrating screens having openings of 1, 1/2, and 1/8 inches. Pieces of shale greater than 3 inches were removed by hand. The number of barrels

accumulated of each size is shown on Table III-2. Shale size is expressed inside brackets as a range, the negative term is the screen opening that passes the particle and the positive term is the opening that retains the particle. Dimensions are in inches unless otherwise noted. Two drums of (-1/8) inch shale were saved, and the remainder of this fine material was discarded. Two barrels of the "as shipped" material were retained for reference.

Table III-2

Spent Shale Quantity

Size (in)	Number of Drums
(-1/8)	2
(-1/2 to + 1/8)	2.5
(-1 to + 1/2)	4.5
(-3 to + 1)	11
(+3)	5
Unclassified	2

In general, most experiments were conducted with spent shale taken from barrels containing classified material in the (-1 to +1/8) inch range. Samples for batch and column leaching were taken randomly from drums containing the desired size and composited. These composites were then divided into portions suitable for use in the individual batch and small column studies.

Characterization of Shale

A randomly selected drum of "as shipped" S-55 shale was screened by hand to characterize the material. The results of the size classification are shown on Table III-3. The nature of the spent shale was heterogeneous, with the pieces ranging from shiny black to grey and tan in color and from heavy and dense to light and porous in density. A sample of shale from the (-1 to +1/2) range contained about 50 percent black particles, 33 percent tan, and 17 percent grey. The shape of the pieces were generally flat and angular. The retorting weakened the internal bonding of the minerals; and the stresses induced during heating, cooling and handling caused the shale to split along natural bedding planes. Photographs of typical shale particles in two size ranges, (-1/2 to +1/8) and (-1 to + 1/2), are presented in Figures III-1 and III-2, respectively.

Pieces larger than 4 inches were generally uniformly grey or tan on the exterior. Many of the larger pieces, however, exhibited a unique shading pattern. A black center sector, corresponding roughly to the general outline of the particle, was surrounded by a band of light grey extending out to the edges. These pieces were split in the handling process with the interiors being exposed. The black zone contained carbon derived from the conversion of the kerogen. The carbon has been removed by oxidation in the grey zone. The sharp line of demarcation between zones is the limit of the penetration of the oxygen into the solid. Examples are shown on Figure III-3.

Table III-3

Size Classification of Spent Shale
as Received at Richmond, CA

Size (in)	Percent Weight*
Passing #8 screen**	15
(-1/2 to +#8)	22
(-1 to +1/2)	20
(-2 1/2 to +1)	23
(-4 to +2 1/2)	12
(-6 to +4)	4
(+6)	4

* Total weight of sample 178 kg.

** Mesh opening 2.36 mm

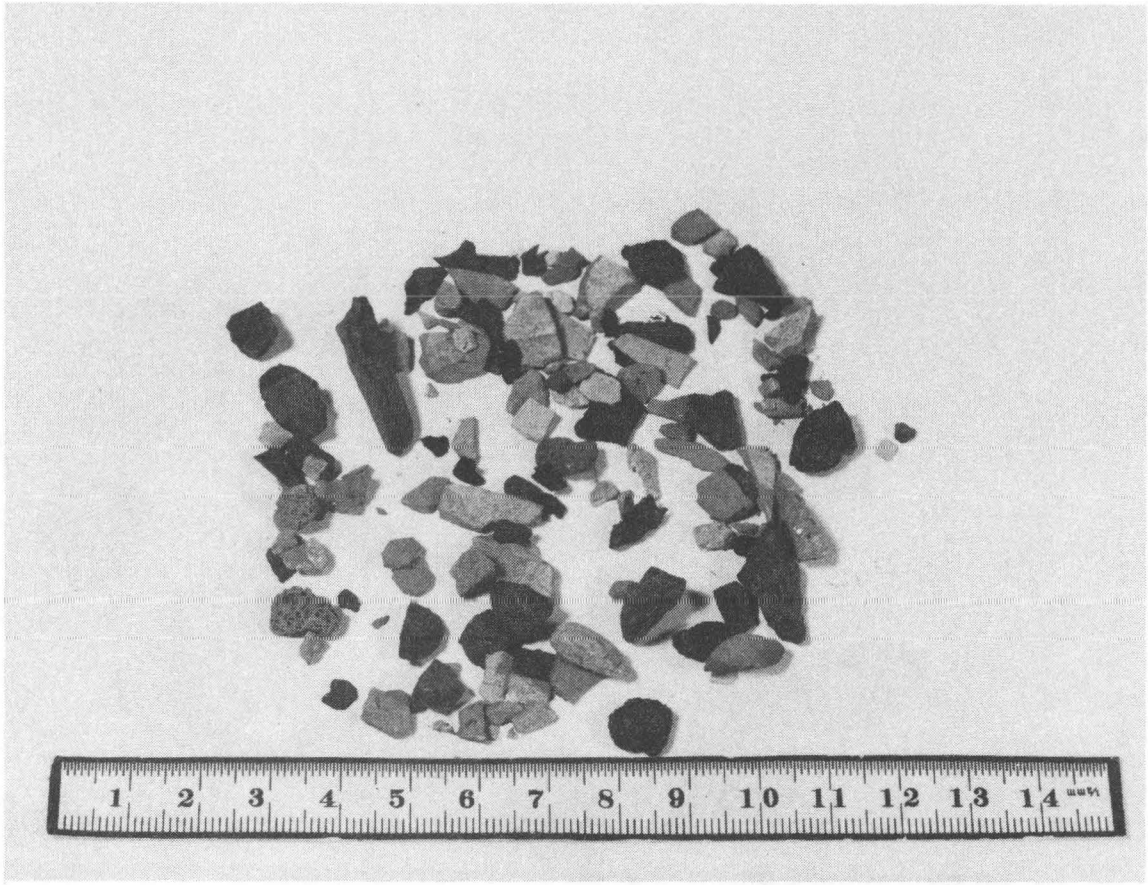

XBB 818-8169

Figure III-1. Spent shale particles, (-1/2 to +1/8) inch size range.

XBB 818-8167

Figure III-2. Spent shale particles (-1 to +1/2) inch size range.

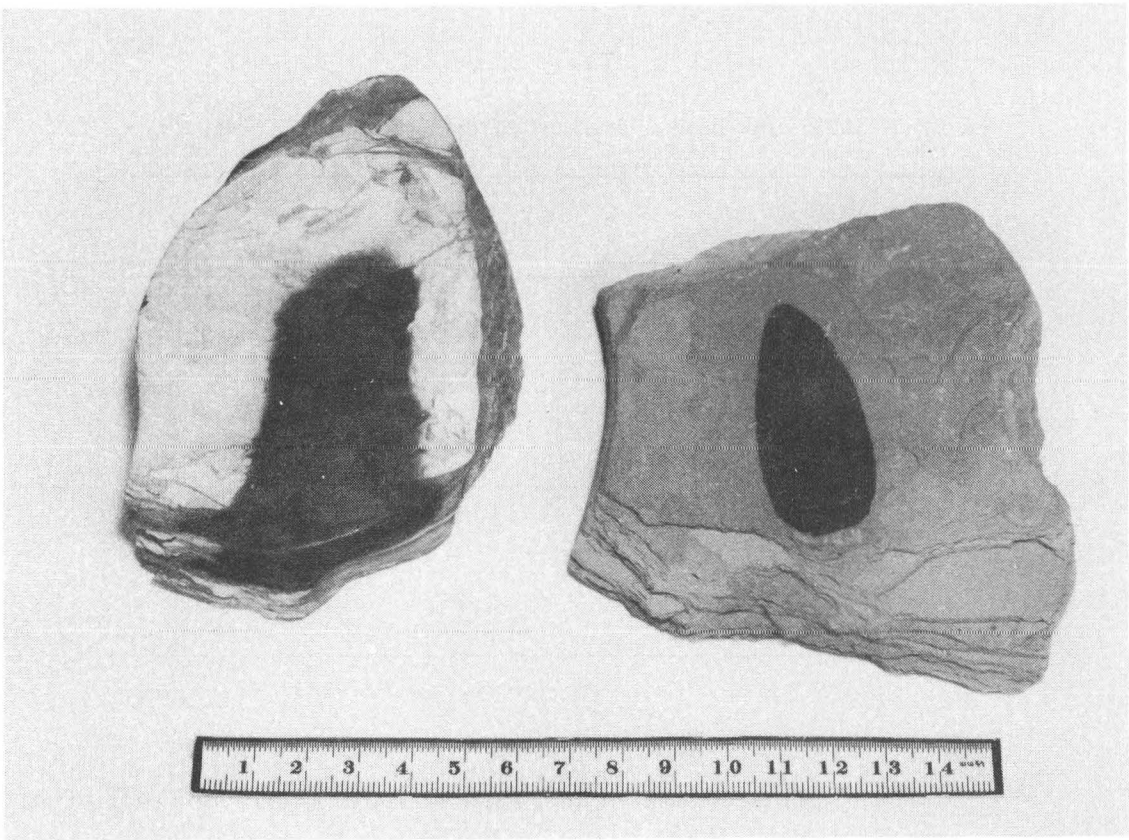

XBB 818-8168

Figure III-3. Spent shale showing carbon zone demarcation.

Bulk Density. The bulk density of the shale was determined from weights and volumes obtained by packing pieces of the shale into small columns. The bed was compacted by impact in the same manner used for preparing the actual leaching experiments. Average bulk densities computed in this manner are tabulated on Table III-4.

Table III-4

Size and Bulk Density of Sieved Spent Shale

	Range in Sieve Mesh (in.)	
	(-1 to +1/2)	(-1/2 to +1/8)
Bulk Density - g/cm^3	0.94	0.88
Mean particle size		
Diameter - cm	2.2	0.7
Height - cm	0.7	0.2

Porosity. Pore volume measurements were made for each individual column. After the column was filled with shale and compacted, a known volume of water was introduced into the bed and the corresponding rise noted. Well packed small columns of (-1/2 to +1/8) shale were found to have total porosities of about 62 percent of the column volume. Tables III-17 and 18 contain tabulations of observed total porosities.

The total porosity estimated by this method contains two types of voids: external, which occur between the particles, and internal,

which are located within the boundaries of the solids. Both types may contain water. Internal porosity can be a significant factor since the spent shale particles have an appreciable porosity resulting from the retorting process. Pieces containing internal void ratios of up to 50 percent of the total particle volume were identified by a pressurized mercury test.

The relative contributions of the two types of porosities to the total was estimated by calculating the sphericity of a typical shale particle. This factor, which relates the surface area of a given particle to that of a sphere of the same volume, can in turn be related empirically to external pore volume in a fixed bed (Foust 1960). According to this method, the external porosity in a packed bed of (-1 to +1/8) shale should lie between 45 and 50 percent of the total bed volume. A column having a total porosity of 60 percent and an external porosity of 45 percent would have an internal pore volume of 15 percent of the total bed volume or 37.5 percent of the particle volume. Porosities of this magnitude are not unreasonable assuming that some thermal decomposition of mineral carbonates occured during retorting (Tisot, 1967). Total porosities encountered in columns and estimated external pore volumes based on an assumption of a 15 percent bed internal porosity are tabulated in Tables III-17 and 18.

Solid Density. The solid density is the bulk density divided by the volume of the solid particles as determined in the column porosity test. A shale sample having a bulk density of 0.88 g/cm^3 and a measured total porosity of 60 percent has a solid density of 2.2

g/cm^3. This is an average value. Individual pieces of spent shale were found to have densities as high as 2.6 g/cm^3.

Particle Size. For modeling purposes the shale pieces were assumed to be cylinders having average diameters and heights obtained by the following method (Foust 1960). A quantity of shale was selected from a larger volume by quartering to obtain a suitable sample. The pieces were then spread out on a sheet of graph paper and a direction of measurement chosen along one axis of the paper. The greatest distance across each particle was recorded. The mean of these dimensions was presumed to be the diameter of a cylinder characterizing this range of shale. The cylinder height was obtained by measuring the heights of the particles and averaging. Average heights and diameters are tabulated on Table III-4. Histograms of dimensions determined in this manner are shown on Figures III-4 and III-5 for the (-1 to +1/2) and (-1/2 to +1/8) size ranges, respectively. Note that there are particles falling outside the selected ranges. This was because many pieces are oblong and either pass or are retained by the sieve depending on the direction of approach to the mesh opening.

CHEMICAL CHARACTERISTICS OF SPENT SHALE

The total organic carbon (TOC) content of the spent shale was determined with wet oxidation in accord with the procedures of Jackson (1958). A representative sample of the shale was taken from the (-1 to +1/8) sieve size range, crushed in a jaw crusher and pulverized in a mortar to pass a #45 (0.354 mm mesh) screen. The pulverized shale was soaked overnight in sulfurous acid to remove the

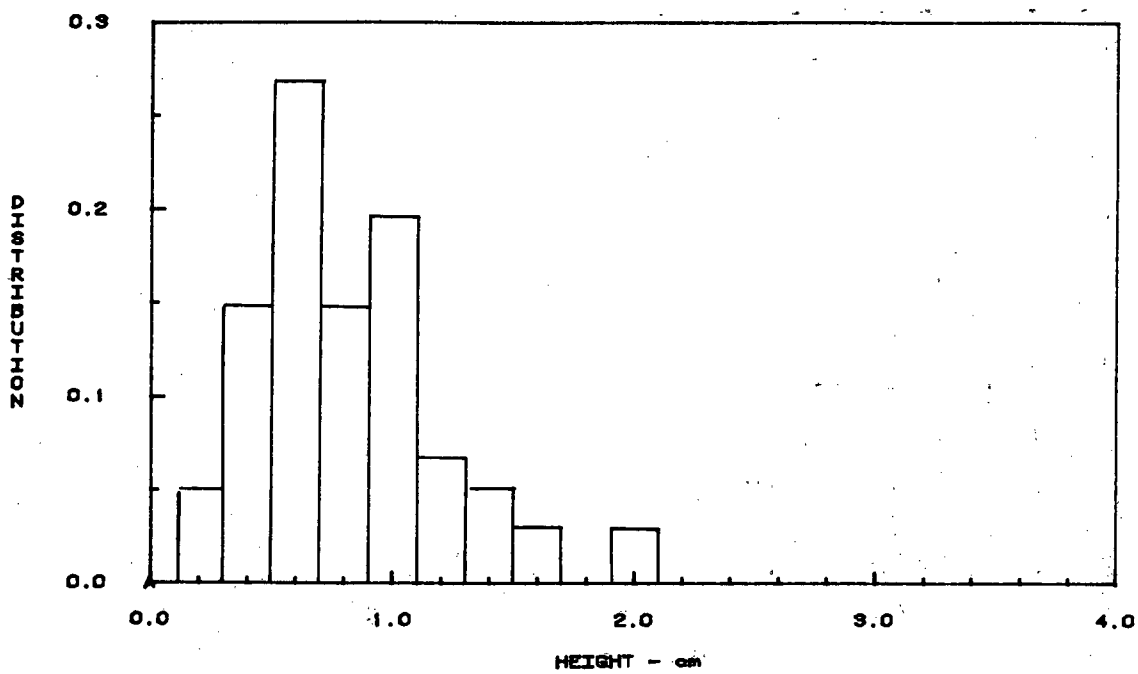

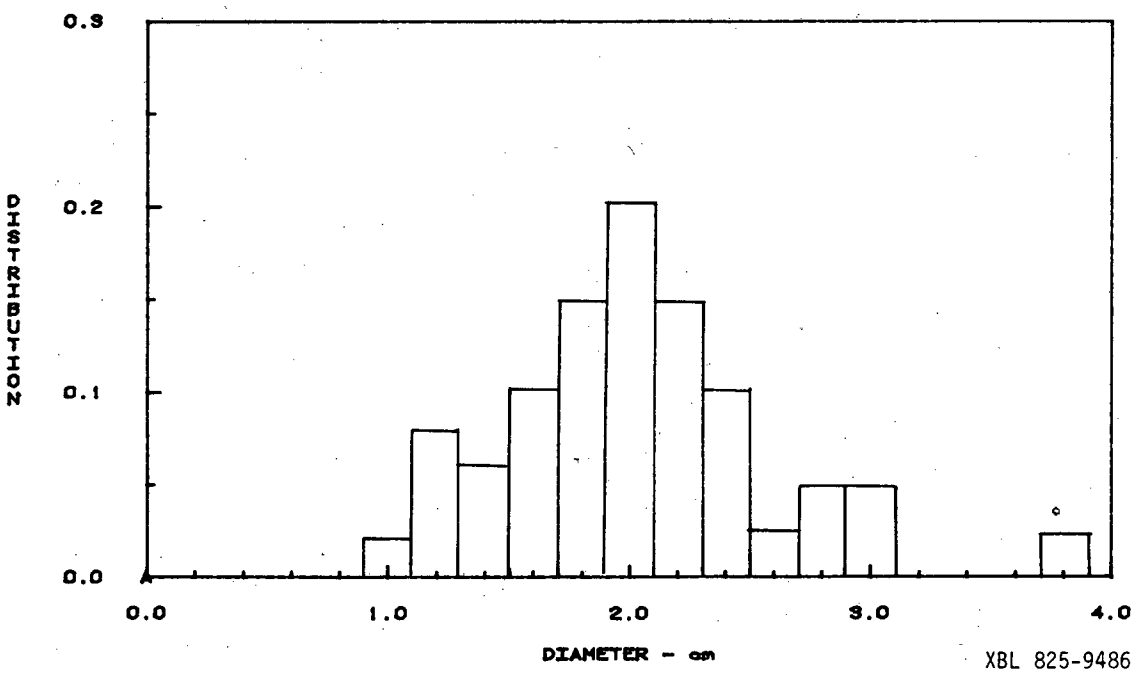

Figure III-4. Histograms of shale particle diameter and height for a shale size range of (-1 to +1/2) inch .

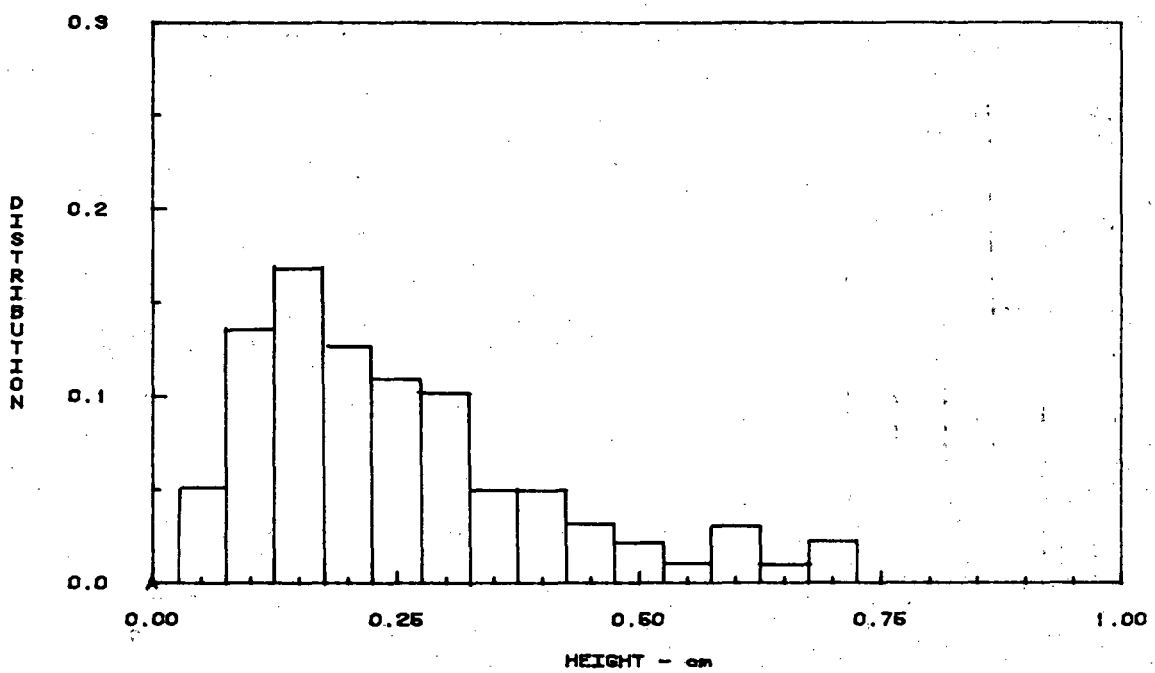

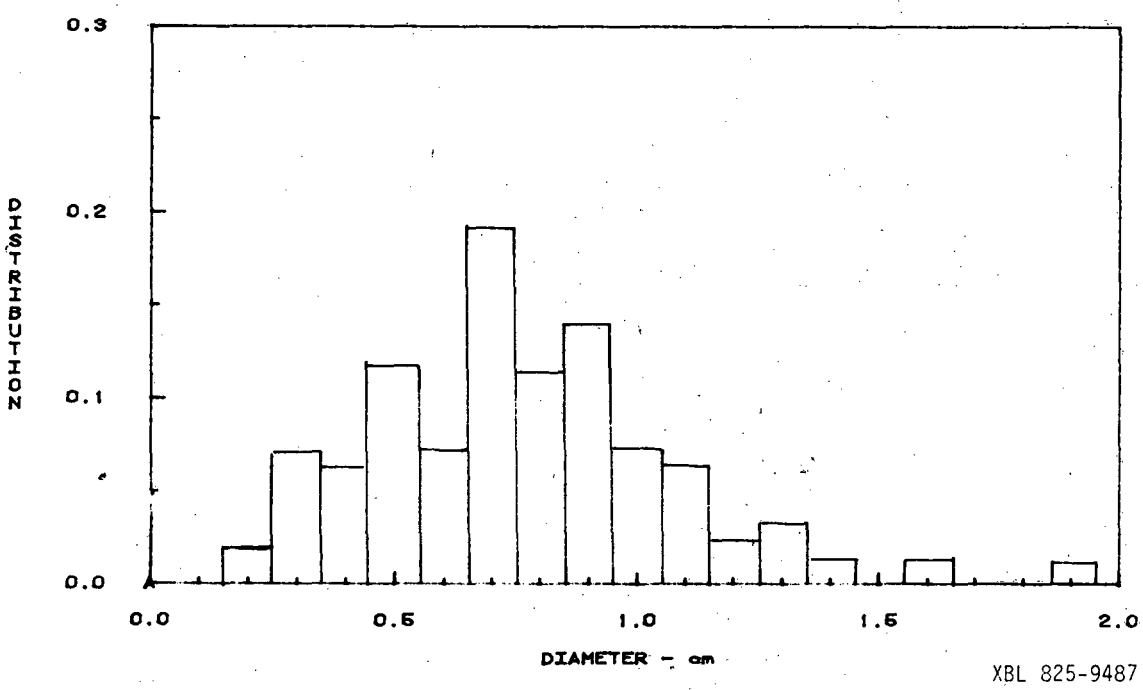

XBL 825-9487

Figure III-5. Histograms of shale particle diameter and height for a shale size range of (-1/2 to +1/8) inch.

inorganic carbonates. The residue was then digested in a hot bath of chromic, sulfuric and phosphoric acids. The evolving carbon dioxide was captured in a 0.5 N solution of sodium hydroxide. After completion of the acid digestion step, the NaOH was titrated with 0.5 N HCl to determine the amount of CO_2 captured. This procedure was repeated four times to obtain TOC contents of 1.86, 1.56, 1.44, and 1.80 percent of the dry weight of the shale. A mean value of 1.7 percent was taken to be the representative TOC content of the spent shale.

WATER ANALYSES

Leachate samples taken during the course of these investigations were routinely analysed for pH, electrical conductivity (EC), and total organic carbon (TOC).

pH and Conductivity

pH readings were made on a Beckman Model 4500 pH meter and a Sensorex probe calibrated against an Orion probe and fresh pH 10 buffer. Electrical conductivity was measured with a Yellow Springs Instrument Model 31 meter and a Model 3403 probe calibrated with a standard potassium chloride solution. Most EC measurements were made in an open cell mode in which 3 mL of solution was poured into a chamber at the end of the probe.

TOC

Total organic carbon analyses were made on two Beckman carbon analysers (Models 915-A and 915-B). The operation of the two models is similar. An injected sample is heated in a furnace in the

presence of oxygen and a catalyst to convert the carbon content to carbon dioxide. The amount of CO_2 produced is then determined with an infra-red detector and shown as a peak on a chart recorder. Two furnaces are incorporated in the instrument. One, maintained at 960 ^{o}C, measures total carbon and the other, operated at 150 ^{o}C, measures inorganic carbon.

Conventional analytical methods for measuring carbon were followed as outlined in Standard Methods (1975). At the start of each session, the instrument was calibrated. Small volumes, either 50 or 100 micro-liters, of standard carbon solutions containing 2.5, 5, 10, 20, 40, and 80 mg/L total carbon, were injected into the analyser and the resulting peak heights recorded. The standards were freshly made for each session by diluting a potassium biphthalate stock solution with carbon-free water. A calibration curve, relating chart peak height to sample carbon concentration, was then constructed. Samples of leachates were then injected into the instrument and the carbon content determined from the peak heights and the calibration curve.

A common method of TOC analyses is to determine both total and inorganic carbon and then take the difference to obtain TOC. The large number of leachate samples discouraged the use of this procedure. An alternate method was followed in which the inorganic carbon was converted to carbon dioxide by acidification with hydrochloric acid to a pH of 2. The CO_2 was then purged with nitrogen gas. The remaining carbon was considered to be all organic. The TOC concentration was determined directly by a single injection into the total carbon channel of the analyser.

Tests demonstrated that a purging period of 5 minutes was sufficient to remove most of the CO_2 derived from the inorganic carbon after acidification. Acidification and sparging has at least one drawback in that volatile organic carbon may be removed from the leachate by the sparging gas; consequently, the total organic carbon measured by the sparging method is defined as non-purgable TOC.

The inorganic constituents in the injected samples caused some difficulty in the operation of the carbon analyser. Salts, remaining after sample evaporation, tended to coat the interiors of the analyser tubes and cells and distort the analyser output. A halogen filter was installed in the analyser to control salt deposition but was not completely effective. Disassembly and cleaning of analyser tubing and cells was required after approximately every 200 samples.

Sampling and Analytical Procedures

Liquid leachate samples were collected in 2-dram (9 mL) glass vials with screw tops. All samples were kept sealed and stored in the refrigerator until the analyses were completed. Samples collected from batch leaching studies commonly contained a large amount of suspended solids. In these cases, leachates were first filtered through a 0.45 micron filter before conducting the TOC analyses. Early samples taken from the column studies also contained some suspended material, but later samples were usually clear with no visible evidence of either suspended or collodial material. Tests conducted on filtered and clear unfiltered leachate samples column studies indicated no significant difference in TOC measured. For this reason samples containing small amounts of suspended solids were

allowed to set until the solids settled to the bottom of the vial. The supernate was then decanted into a clean vial. Fresh acid cleaned vials were used for all samples.

The pH of the leachate samples commonly exceeded 10.5, a condition which favors the fast absorption of CO_2 from the atmosphere. This reduces the sample pH and encourages the formation of chemical precipitates in the presence of Ca and Mg ions. For this reason, EC and pH were determined as quickly as possible after sample collection. The pH was then lowered to 2 to discourage precipitate formation and to remove the inorganic carbonates.

Reliability of Data

Replicate electrical conductivity measurements of selected leachate samples indicated a precision of plus or minus 3 percent. The precision of pH measurements was affected by the high pH of the leachates. The tendency of the leachate to absorb CO_2 from the atmosphere made it difficult to conduct replicate measurements in small samples. In addition, the accuracy of pH probes at elevated levels was questionable. Special probes are available for these applications: however, they are affected by dissolved substances such as silica and are difficult to maintain properly. Measurement precision for pH levels above 10.5 was considered to be plus or minus 0.05 units.

In general, TOC concentrations reported herein are the means of at least two separate injections from a sample. In case consecutive injections resulted in significantly different recorder peaks,

additional injections from the same sample were made, and the incorrect recorder peaks eliminated. Gross errors caused by injection of particulates or improper technique were thereby minimized.

TOC concentrations equal to or greater than 5 mg/L are estimated to have a coefficient of variation, (standard deviation / mean), of 10 percent. At TOC levels of 2.5 and 1.0 mg/L the estimated coefficients of variation were greater, being 20 and 30 percent, respectively.

TOC error estimates given above should be viewed with caution. They are based on multiple injections from the same sample and would probably be reasonable for liquids containing simple organic compounds such as the potassium biphthalate used for standards. There is no assurance that the complex mixtures of organics and inorganics in the samples will combust within the analyser in the same manner as the reference standard does.

WATER SUPPLY AND LEACHATE CHARACTERISTICS

Distilled water was used to conduct batch and small column studies in the laboratory. Richmond City tap water was supplied to the large columns located outdoors at the Richmond Field Station. Water supplies were checked frequently for contamination. Typical EC and TOC concentration levels found in fresh distilled water were 2 mmhos/cm and << 1 mg/L, respectively. The conductivity of the Richmond tap water was about 0.1 mmho/cm and the TOC levels varied between 2 and < 1 mg/L.

A sample of the tap water was collected and subjected to a major inorganic ion analysis with the results shown in Table III-5. The analytical methods used to obtain the data shown in the table were all in accord with the recommendations of the US Environmental Protection Agency (EPA, 1979). The appropriate EPA section number for each ion analysis is given in Table III-7. The cation-anion balance for this sample was within one percent.

Table III-5

Analysis of Richmond Tap Water
Used in Large Column Studies

Anions			Cations		
	mg/L	meq/L		mg/L	meq/L
NO_3	0.44	0.01	Na	6.7	0.29
SO_4	21	0.44	K	1.0	0.03
CO_3	4.8	0.16	Ca	20	1.0
HCO_3	52	0.85	Mg	3.1	0.26
PO_4	6.4	0.13			
OH		0.01			
Sum		1.60	Sum		1.58

Electrical conductivity = 0.11 mmhos/cm
pH = 9.0
Temperature = 18 ^{o}C

Composition of TDS Leached from Spent Shale

The composition of the TDS leached with time in the large packed column studies was investigated by collecting two effluent samples for inorganic ion analysis from a column packed with the (-1 to +1/2) size. The samples were collected 10 hours and 10 days after commencing leaching. The physical properties of the leachate were measured directly after collection and before the acidification discussed below. The results are tabulated in Table III-6.

The usual chemical precipitates, which formed immediately after sample collection in these two samples, were redissolved by decreasing the pH to about 6.5 with phosphoric acid. The amount of acid added is shown in Table III-6. Phosphoric acid was chosen because phosphate has not been reported to any significant degree in spent shale leachates or in wastewaters derived from the oil shale processes (Fox 1980). The samples were analysed for the most likely major ions, aside from those compounds associated with silica: Na, K, Ca, Mg, SO_4, NO_3, and the alkalinity ions. The results are summarized in Table III-7. The methods of analysis used to determine the ionic species were those prescribed by the EPA reference section listed in the table.

The cation-anion balances for the data shown in the table disagree by about 10 percent for the 10-hour sample and by 25 percent for the ten day sample. The latter indicates that either the methods of analysis were inaccurate or that some major cation was not determined. The amounts of phosphates as PO_4 added did match, within reason, the PO_4 concentrations found in the samples.

Table III-6

Spent Shale Leachates
Physical Properties

Parameter	10 Hour Sample	10 Day Sample
pH	11.4	11.1
EC - mmhos/cm	10.9	0.85
TDS - mg/L	10,250	580
Temperature - ^{o}C	18	18
Phosphoric acid added for acidification (mg/L as PO_4)	239	169

The accuracy of the analysis can also be checked with the values of TDS determined prior to acidification. Assuming that all of the carbonates are lost in the TDS procedure, that the phosphates did not exist in the original sample, and that the hydroxides are converted to oxides, TDS calculated from the data in the table indicate approximate values of 9500 mg/L for the 10 hour sample and 500 mg/L for the 10 day sample. These values are about 7 and 14 percent lower than the measured TDS in the original samples as tabulated in Table III-7. This indicates that compounds other than those identified are present in the leachates.

The analytical methods used may also be inaccurate for water of this quality (Farrier et al., 1979). For example, the sulfate ion was determined by a turbidimetric method in which the sample was

Table III-7

Spent Shale Leachates
Major Inorganic Ion Analysis
After Acidification with Phosphoric Acid

Ion	EPA Method	10 hr Sample (pH=6.5)		10 day Sample (pH=6.5)	
		mg/L	meq/L	mg/L	meq/L
NO_3	353.2	0.38	0.01	0.35	0.01
SO_4	375.4	6390	133	312	6.5
CO_3	310.1	0	0	0	0
HCO_3	310.1	201	3.3	48	0.79
PO_4	364.5	250	<4.8*	150	2.9*
Sum			<141		10.2
Na	273.1	2500	109	53	2.3
K	258.1	470	12	29	0.74
Ca	215.1	41	2.1	93	4.6
Mg	243.1	50	4.1	6.6	0.54
Sum			127.2		8.18

* Adjusted for phosphoric acid dissociation at pH of 6.5 and a temperature of 25 °C (Stumm and Morgan, 1981)

acidified with the resultant precipitate being measured. Other compounds could have also precipitated along with the sulfate.

The Mg, Ca, and carbonate concentrations found in the acidified samples require clarification. No analyses of the fresh leachates were made for specific ions or inorganic carbon. These leachates were clearly supersaturated with respect to air as evidenced by the immediate precipitation upon collection. The composition of these precipitates was not investigated. The carbonates found in the acidified samples were undoubtedly due in part to the absorption of atmospheric carbon dioxide by the leachates. The presence of the Mg ion indicates the possibility that Mg and Ca complexes may have been present in the original samples.

Regardless of the possible analytical errors and missed compounds, the analyses summarized in Table III-7 do demonstrate that Na, K, SO_4 and OH must represent the major portion, by weight, of the ions leached from spent shale. The predominate ions in the 10 hour leachate are Na and SO_4. Sulfate is also a principal ion in the 10 day leachate, but the Na ion has been displaced by the Ca ion.

An estimate of the contribution of inorganic ions by spent shale to leachates is shown in Table III-8. This table was prepared by assuming that the pH was that observed immediately after sample collection, and that the background contributions present in the tap water supply can be subtracted directly from the results.

Leachate Trace Organics

Thirty days after the pump was shut off, a sample of the leachate remaining in the large column containing the (-1/2 to +1/8) size shale was taken and analysed to identify trace organics. The

Table III-8

Estimated Contribution of Inorganic Ions to Leachate by Spent Shale

Ion	10 Hour Sample (pH=11.4)		10 Day Sample (pH=11.1)	
	mg/L	meq/L	mg/L	meq/L
NO_3	n*	n	n	n
PO_4	n	n	n	n
OH	-	2.5	-	1.3
SO_4	6370	133	290	6.0
CO_3	-	4.7	n	n
Sum		140		7.3
Na	2500	109	46	2.0
K	470	12	28	0.7
Ca	21	1.1	73	3.7
Mg	47	3.9	3.5	0.3
Sum		126		6.7

* negligible

leachate, made basic with NaOH, was extracted with nano-grade hexane. The extract was reduced to a volume of 0.1 cc and analysed for trace organics in a Finnigan Model 4023 gas chromograph-mass spectometer having a 30m OV-101 quartz capillary column. The residue from the hexane extract was methylated with $(CH_3)_2SO_4$. An internal standard

of perdeutero phenol (C_6D_5OH) was used. The residue was extracted with nano-grade hexane, the extract reduced, and phenols determined as methyl-phenyl ether. The compounds found and the respective concentrations are given in Table III-9.

Table III-9

Trace Organic Analysis
30 Day Quiescent Leaching Sample from
Large Column Containing (-1/2 to +1/8) Shale

Compound	Concentration, ppb
Phenol	5
o-cresol	3
p-cresol	2
2,6 dimethyl phenol	2
Methyl-ethyl phenol	0.7
3-methyl pyridine	2
Akylpyridines	1.8

The original sample was found to contain 6.6 mg/L of TOC. The shale from which the leachate was derived was leached with tap water for 360 hours. After the pump was shut off, the leachate was then allowed to sit in the pores for 30 days. During this time the TOC in the leachate increased from 2.5 mg/L at shut-off to 6.6 mg/L. The conclusions from the analysis are that most of the organics present are not (1) extractable with hexane, i.e. are polar, and (2) are not volatile.

Correlation of EC and TDS

The TDS determination is more useful then EC and also much more time consuming to run. The EC of nearly every leachate sample was determined with the TDS being measured only occasionally. An attempt was made to correlate observed EC and TDS for typical leachate samples.

In one experiment, a sample of (-1/2 to +1/8) sieve size shale was placed in a one-liter flask, and the voids filled with water to the top of the shale. The free-draining portion of the leachate was removed at various time intervals and analysed for EC, TDS, and pH. The portion removed was replaced with fresh distilled water. The results are tabulated in Table III-10.

The tabulation shows a decrease in the TDS/EC ratios with decreasing TDS and pH. The ratios cannot be checked theoretically because the ionic compositions of the leachates were not measured. It is, however, possible to show that the relative magnitude of the ratios are reasonable by assuming that the only ions present are sodium, sulfate, and hydroxide.

The leachates may be considered to be mixtures of sodium hydroxide and sodium sulfate. The amount of hydroxide is determined by the measured pH, and the total quantity of the two compounds is set from the calculated TDS. Conductivities may be calculated by applying equivalent conductance factors determined for the particular ions at the given ionic strength (Perry et al., 1973). Conductances calculated by this method ranged from approximately the same as observed

Table III-10

Relation of EC with TDS in Leachate
Collected from Non-steady Batch Experiment

Sample No.	Contact Time hrs.	pH	EC mmhos/cm	TDS g/L	TDS/EC
1	16.3	11.7	12.7	11.3	0.88
2	2.0	11.5	6.1	4.4	0.72
3	2.4	11.6	5.2	4.1	0.79
4	2.9	11.5	4.3	3.0	0.70
5	20.0	11.4	4.4	3.3	0.75
6	72.0	11.3	4.4	3.0	0.68
7	3.0	11.3	2.9	2.0	0.69

to about ten percent lower. The inclusion of small quantities of calcium and potassium, ions with higher conductances than sodium, would improve the fit of the calculated conductivities to the observed data. The simple analysis shows that the decreasing ratios of the magnitude shown in Table III-10 are reasonable for decreasing pH and TDS.

A serviceable estimate for the TDS in g/L may be obtained by multiplying the observed EC in mmhos/cm by 0.72. This factor is the average of the tabulated TDS/EC ratios, excluding that for sample 1, and is applicable for EC values less than about 8.0 mmhos/cm.

BATCH INVESTIGATIONS

Several kinds of batch studies were undertaken. These studies were used to define equilibrium relationships, determine time rates of change of solute concentrations, and estimate the soluble total organic carbon content of the solid shale. Solute is used in this report as a general term for the component of interest. Solutes considered in the present studies are primarily non-purgable total organic carbon (TOC) and electrical conductivity (EC).

Equilibrium Relationships

A representative sample of shale was taken from the (-1 to +1/8) size range, crushed in a jaw crusher, and ground in a mortar to pass a #45 (0.354 mm opening) mesh screen. Varying amounts of the powdered shale were added to 50 mL of distilled water in 250-mL flasks to obtain solid-liquid ratios (S/L) of 1.5 to 0.01 g shale/mL water. The flasks were placed on a shaking table and shaken for 21 days at temperatures of 22 +/- 1 ^{o}C. At the end of the period the flasks were removed, the leachate decanted and centrifuged, and the EC, TOC and pH measured. The experiment was repeated for 73 days, and it was concluded that twenty-three days was sufficient time to attain equilibrium for pulverized shale. The data shown in Table III-11 represent the results obtained after 73 days, for mixes 1 through 6 and after 21 days for mixes 7 through 11. TOC data are shown plotted against the S/L ratios in Figure III-6.

The TOC data may be fit to a straight line as shown on Figure III-6. A definite non-linear relationship is seen to exist below TOC

concentrations of 6 mg/L. No attempt was made to define this relationship because of equipment and analytical limitations at TOC levels in this low range.

An isotherm relating TOC concentrations in the solid phase to those existing at equilibrium in the liquid phase was constructed following the method used by Amy (1978). The average TOC content in the unleached shale was assumed to be 1.7 weight percent as determined by the wet oxidation test. A mass balance was then made between the solid and liquid phases in each of the flasks of the batch study to find the amount of TOC, in mg/g, remaining in the solid phase at equilibrium. This value was plotted against the corresponding liquid TOC concentration for each of the solid-liquid mixtures. An isotherm calculated by this method is shown in Figure III-7.

Rates of Increase of Leachate Solutes

Several batch studies were conducted to investigate solute build-up in leachates.

Table III-11

Equilibrium Achieved in Agitated Batch Studies with Pulverized Spent Shale (< 0.35 mm mesh size) at 22 °C

Mix	Wt. Shale g	Vol Water mL	S/L* Ratio g/mL	TOC mg/L	EC mmhos/cm	pH
1	75	50	1.5	105	-	12.7
2	50	50	1.0	75	-	12.6
3	40	50	0.8	55	12.0	12.6
4	30	50	0.6	42	9.8	12.6
5	20	50	0.4	33	7.4	12.5
6	11.5	50	0.23	19	5.8	-
7	10	50	0.2	22	4.9	12.2
8	5	50	0.1	9	3.2	-
9	1	50	0.02	6	1.50	-
10	0.75	50	0.015	8	1.35	-
11	0.50	50	0.01	7	0.92	-

* Solids to Liquid Ratio

Rate of Increase of Leachate EC. The purpose of this study was to monitor the time rate of change of leachate EC in shaking batch studies conducted with three different solid-liquid ratios. This differs from the equilibrium shaking batch studies in which concentrations were measured only after long contact times. Ground shale passing a #45 screen was added to 50 mL of water contained in 250-mL

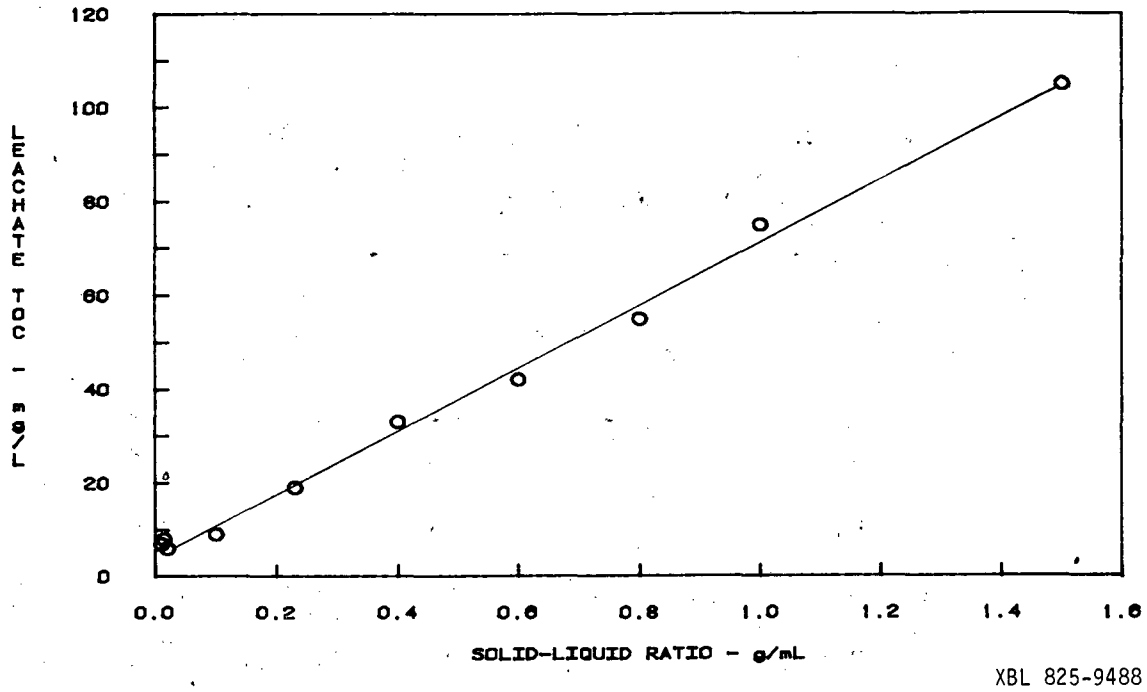

Figure III-6. Relation between leachate TOC and solid-liquid ratio at equilibrium in shaking batch studies at 22 °C.

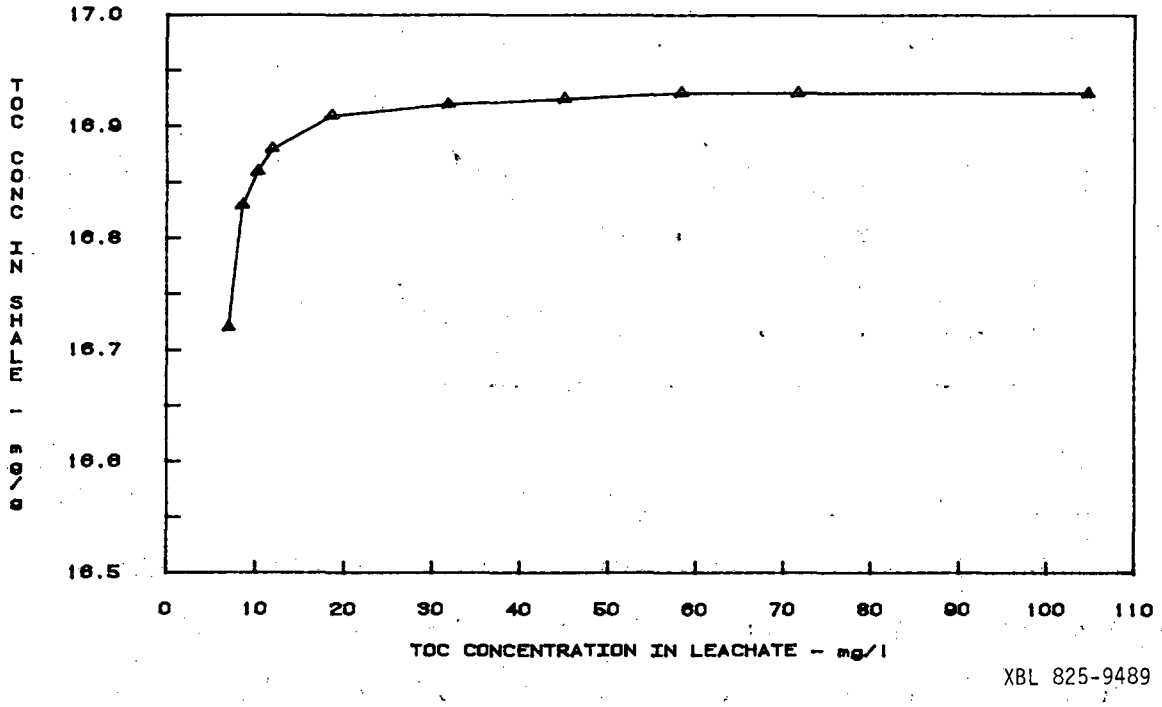

Figure III-7. Equilibrium isotherm for ground spent shale and distilled water at 22 °C.

flasks in S/L ratios of 0.075, 0.015, and 0.3 g shale/mL water. The flasks were placed on a shaking table for 56 days at room temperatures. Periodically samples of leachate were removed, centrifuged to separate the solids, and measured for EC and pH. Both solids and liquid were returned to the 250-mL flask and the shaking continued. The results are tabulated in Table III-12.

Table III-12

Increase of Solute EC with Time
Pulverized Spent Shale in Agitated Flasks

	Solid-Liquid Ratios (g/mL)					
	0.3		0.15		0.075	
Time hrs	pH	EC mmhos/cm	pH	EC mmhos/cm	pH	EC mmhos/cm
0.2	10.9	3.5	10.9	2.1	10.8	1.4
0.8	10.9	3.5	10.9	2.3	10.8	1.5
7.2	-	4.3	-	2.9	-	1.9
25	-	4.4	-	3.1	-	1.9
56	11.3	4.6	11.2	3.1	11.0	2.0
254	11.6	5.7	-	4.3	-	2.4
1350	11.8	7.9	11.5	4.8	11.1	3.1

Long-term Leaching of Shale Types. The purpose of this study was to determine if there were significant differences in the leachable TOC derived from grey, black, and tan shales. Samples of shale typifying each of the three colors were selected from drums containing

shale larger than 3 inches in diameter and crushed. Black, grey, and tan particles in the (-2.8 mm to +1.4 mm) size range were leached with one pore volume (includes both external and internal voids) of distilled water for 253 days in 1 liter flasks at room temperatures. The results are shown on Table III-13. Although there were gross differences in the 253 day EC values of the three types of shale, the corresponding TOC concentrations were essentially the same: consequently, further studies were conducted without regard to shale colors.

Table III-13

Comparison of Spent Shale Solutes
Black, Tan and Grey Types
2.8 mm to 1.4 mm Mesh Size Range

	17 Days Leaching			253 Days Leaching		
Shale type	pH	EC mmhos/cm	TOC mg/L	pH	EC mmhos/cm	TOC mg/L
Black	12.1	-	25	12.1	6.6	36
Tan	12.2	-	21	12.1	23.7	37
Grey	12.0	-	20	12.1	13.8	37

Long-Term Leaching of Column Dumps. After certain small column runs were completed, a liter of shale and one pore volume of the final leachate were removed and stored in flasks at room temperature. The purpose was to obtain an estimate of the equilibrium concentrations that would be established in a leachate remaining in contact

with previously well-leached shale. A tabulation of results is shown on Table III-14. The shales were all taken from the (-1/2 to +1/8) size range and were leached in small columns at pore velocities of less than 9 cm/hr.

Table III-14

Long Term Leaching
Leached Spent Shale Derived from Column Studies

		Starting Condition			Terminal Condition		
Run no.	Age mo.	pH	EC mmhos/cm	TOC mg/L	pH	EC mmhos/cm	TOC mg/L
A	19	11.4	1.8	3.5	12.0	9.5	16
B	17	11.5	1.6	4.0	12.0	9.2	20
C	16	11.8	1.8	<3.0	12.1	14.7	23

Leaching of a Shale Slab in a Stirred Solution. A single piece of grey shale was suspended in a beaker containing two liters of stirred deionized water. The purpose was to investigate the internal diffusion of solute within the solid phase. The shale piece had dimensions of approximately 10 x 12 x 1 cm and weighed 308 g. The increase with time in solute TOC proved too small to be monitored reliably, but the increase in EC was significant as shown in Table III-15.

Soluble TOC Content of Spent Shale. An attempt was made to determine the total amount of TOC which can be leached from the spent

Table III-15

Increase in Solute EC with Time for a Single Piece of Shale Suspended in Agitated Water

Time hrs	EC mmhos/cm
0.02	0.02
0.08	0.04
1.0	0.12
1.9	0.17
5.6	0.33
8.8	0.42
18.8	0.55
25	0.63
66	0.81
129	0.95
162	1.06
379	1.17
457	1.32
650	1.36

shale. Twenty grams of pulverized shale passing a #45 screen was added to one liter of distilled water in a flask and placed on a shaking table at room temperature. Periodically, the liquid was removed, centrifuged to separate solids, measured for TOC, EC, and pH and then discarded. Suspended solids were returned to the flask for further leaching with fresh water. The experiment was continued

until the TOC in the samples dropped to about 1 mg/L. The total TOC leached amounted to about 0.25 percent of the dry shale weight. The value represents the minimum TOC which may be leached from the spent shale, and it might be compared with the value of 1.7 percent obtained by wet oxidation of the shale. The amount of TOC removable by long term leaching with water is probably intermediate between the two.

SMALL COLUMN STUDIES

Extensive leaching studies were conducted with spent shale packed in 11.4 cm diameter columns. These were followed by shorter duration investigations involving 30 cm diameter columns.

A schematic of the small column system is shown on Figure III-8.

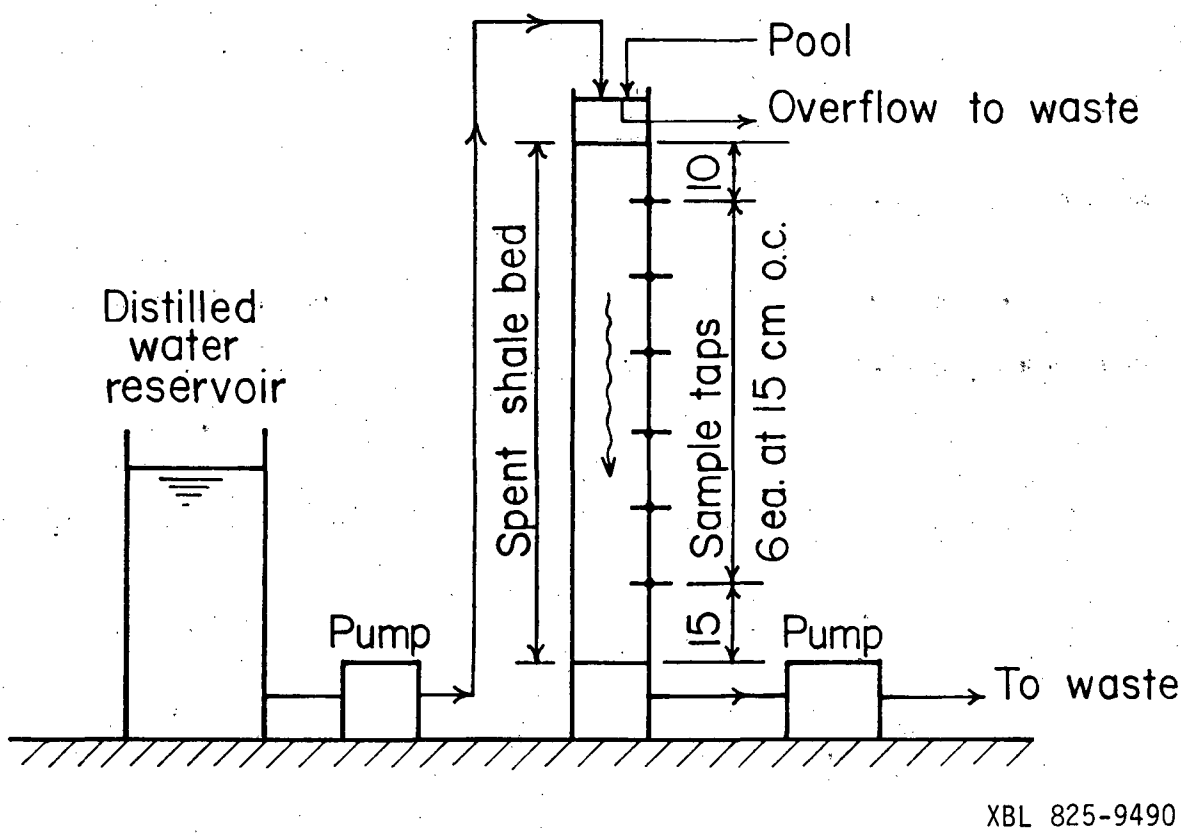

Figure III-8. Schematic of small column leaching apparatus.

Columns

Two identical lucite columns 11.4 cm in diameter by 1.2 m long were constructed to leach a one-meter-deep shale bed. The shale was supported by a 10-cm-high stainless steel wire mesh stool inserted into the bottom of the columns. Spaces were thus provided at both top and bottom of the column for water pools. Six sample taps were inserted at 15-cm intervals along the column as shown in the figure.

The sample taps were 1/8-inch tygon tubing passed through rubber stoppers inserted into holes drilled in the column wall. The tygon tubes extended to the center of the column cross-section and were protected from crushing by jackets of hard PVC tubing fitted over the softer tygon. The outside end of the tap was closed with a clamp which could be released for sampling.

The column was originally designed for upflow operation with water entering into the bottom pool and the leachate leaving from the top pool. For certain reasons to be discussed subsequently, the flow direction was reversed after several runs, with water entering at the top and leachate leaving from the bottom. In the case of the down-flow mode of operation, the packed shale was capped with a 2-cm thick layer of 2-mm sand supported by a stainless wire screen. The water supply pump delivered water at a slightly greater rate than necessary for the desired leaching flow. The excess was wasted from the upper pool. This arrangement eliminated the problem of solute build-up in the top pool caused by back diffusion from the shale bed.

Water Supply and Pumps

The spent shale was leached with distilled water in the small column studies. The water was stored in as many as five 20-liter Nalgene plastic or glass bottles, depending upon the number of columns in operation and the leaching rate. Initially, some difficulty was experienced with an increase with time in the background levels of TOC in the water supplied to the columns. This was corrected by draining, cleaning, and refilling the bottles daily. Water temperatures varied between 22 ^{o} and 24 ^{o}C .

The water was conveyed in either tygon or silicon tubing throughout the system. The tubing was passed through a model 7567 Cole Palmer Masterflex pump. Pump heads were selected for the applicable flow range. Constant column flow rates were maintained by a similar pump placed in the outlet line leading from the bottom pool. Frequent time-volume determinations indicated that flows were maintained within plus or minus two percent of the desired value.

System Operation

The following discussion is applicable to the downflow mode, but it also holds in general terms for column runs in the upflow mode.

Most of the studies were made with the (-1/2 to +1/8) size shale. The ratio of the column diameter to the mean particle diameter employed was about 16. The smaller this ratio, the more likely the possibility of fluid short-circuiting down the walls of the column. The bed material was carefully placed with the external voids being well distributed throughout the bed. The wall effects

appeared to be insignificant during the course of the experiments. No attempt was made to check the plug flow characteristics of the water phase. To do so would have been laborious due to the high internal porosity of the solids and the high pH which tends to destroy the fluorescence of most fluorescent dye water tracers.

Shale of the selected size was lightly screened with a #8 sieve (2.36 mm opening) to remove accumulated fines. The shale was carefully placed in 5 to 10 cm increments and compacted by impact on the column sides and bottoms. The sample taps were installed as the shale levels reached the level of the tap holes.

The columns were commonly filled with water before starting a run. Several methods of accomplishing this were investigated:

1. Filling the packed column rapidly from the bottom pool.

2. Filling the packed column rapidly, first from the bottom and then from the middle in sequence.

3. Filling the packed column slowly from the bottom pool.

4. Filling the packed column slowly from each sample tap in sequence.

The last scheme was the most successful, based on the uniformity of leachate concentrations contained within the column at the start of the run proper. In this method, water was pumped from the reservoir through each sample tap in sequence from the bottom upward, with each tap being used to fill the 15-cm-height tributary to the tap. After the water had risen a short distance into the bed, the water

supply was switched temporarily to a pre-measured 4-liter volume of water. The corresponding rise in the bed for this volume was used to evaluate the bed porosity. The filling was then continued until the water reached the sand layer at the top of the column, with the inlet pool being filled from the top. The inlet pump remained on after filling, and a small amount of water was wasted from the pool to eliminate solute build-up from back diffusion as much as possible.

The columns were allowed to set for at least an hour after filling to permit establishment of a uniform concentration gradient. Leachate samples were taken from each tap and from the upper pool just prior to the start of pumping. In general, a run was discontinued when the TOC in the effluent decreased to less than 2 mg/L, but difficulties were encountered with this criterion as discussed subsequently.

Quiescent Leaching

In two column runs, the leachate was allowed to set in the pores of the leached shale after terminating the run. The subsequent increases of TOC, EC, and pH in the leachate were monitored for several hundred hours. The results are summarized in Table III-16. Refer to Table III-17 for information on the particular column operation. TOC concentration data are plotted versus time on Figure IV-5 in the next chapter.

Sampling Procedures

The methods used for sample analyses required the removal of a total of at least 35 mL from the six sampling taps within a 5 minute

Table III-16

Quiescent Leaching in Columns
Subsequent to Column Runs

Run No.	Time hrs.	pH	EC mmhos/cm	TOC mg/L
D-6	0	-	0.6	1.0
D-6	144	-	-	5.1
D-6	451	-	7.2	9.7
D-6	936	-	9.6	15
D-6	1099	-	-	15
D-6	1632	12.0	10.1	20
D-7	0	-	0.6	0.9
D-7	91	-	2.3	3.6
D-7	115	-	2.5	6.2
D-7	431	-	6.1	9.6
D-7	595	-	9.9	13
D-7	1030	-	-	16
D-7	1151	-	10.1	13
D-7	1941	12.2	10.8	17

period of time. Because the range of leaching flows studied extended from 5 to 55 mL/min, it is apparent that incautious sample withdrawal would disturb the plug flow regime in the liquid phase. Leachate samples were taken in the direction of flow to minimize the potential disruption. Three mL of fluid were first wasted to clear the tap of the last withdrawal, and a similar amount was then withdrawn into a

glass vial. Samples were usually taken at intervals considerably greater than one hour to permit restoration of plug flow.

Results

A summary of operating parameters for ten small column runs is given in Table III-17. Leachate pH, EC, and TOC data for these runs are tabulated in Appendix A in Tables A-1 through A-27. TOC data in this table are adjusted to correct for influent water background levels. Measured TOC in effluents was, in general, 1 to 1.5 mg/L higher than values shown in the table. Adjusted values less than 1 mg/L are shown as < 1 mg/L because of analytical accuracy limitations.

Table III-17

Small Column Experiments
Summary of Operational Parameters

Run No.	Shale Size	Total Porosity	External Porosity	Flow Rate mL/min	Flow Mode	Pore Vel. cm/hr	Fill Type
U-1	A	0.63	0.48	7.1	up	8.7	F-M
U-2	A	0.63	0.48	7.1	up	8.7	S-B
D-1	B	0.58	0.43	6.3	down	8.6	F-B
D-2	C	0.60	0.45	15	down	20	S-T
D-3	C	0.63	0.48	5.0	down	6.1	S-T
D-4	A	0.61	0.46	12	down	16	S-T
D-5	A	0.61	0.46	39	down	50	S-T
D-6	A	0.58	0.43	53	down	73	S-T
D-7	A	0.59	0.44	55	down	71	S-T
D-8	D	0.60	0.45	20	down	26	S-T

Legend

A (-1/2 to +1/8) in. mesh size shale
B (-3/4 to +1/2) in. mesh size shale
C (-1 to +1/2) in. mesh size shale
D (-1/2 to +1/4) in. mesh size shale
F-B Fast fill from bottom pool
F-M Fast fill from bottom pool and then middle
S-B Slow fill from bottom pool
S-T Slow fill from each sample tap

The runs described in Table III-17 cover a wide range of operating conditions. Most runs were conducted with (-1/2 to +1/8) material, although larger material was used in three columns as shown in the table. The total porosity values are calculated from the change in bed water level due to the introduction of a known volume of water. External porosities shown are based on a calculated internal porosity of fifteen percent. The pore velocities are calculated from the average flow rate and the assumed external porosity. The fast and slow methods of filling the pores are relative. Fast fill was accomplished by filling the column with gravity flow of water from a reservoir in about two minutes, while slow fill was done with the tubing pumps operating at a rate of about 175 mL/min. Run U-2 was filled at a rate of 7 mL/min, the same used for leaching.

The column experiments were originally designed for upflow leaching primarily because initial conditions are more simply described for modelling purposes. For example, water can be introduced at the same rate and direction as used for leaching in the upflow mode, whereas an abrupt discontinuity is introduced between filling and leaching operations in the downflow mode. When the column is filled from the bottom, the direction of flow must be changed before leaching flow is started. If the column is filled from the top, three-phase flow conditions exist as the water trickles through the unsaturated shale bed. Another reason for selecting the upflow mode was that it simulated the probable path taken by the returning groundwater in field in-situ retorts.

The upflow mode was abandoned after several runs. Density gradients caused by local differences in leachate dissolved solids concentrations created currents in the macro-pores counter to the direction of net flow. These currents back-mixed the solute in the bed pores and tended to blur the concentration profile.

The effects can be seen clearly by referring to data from runs U-1 and U-2 presented in Tables A-1 through A-5 in Appendix A. Both runs are for the upflow case, differing mainly in the method used for the initial filling with water. The U-1 column was first filled rapidly from the bottom pool and then leaching flow at a slower rate was begun immediately. The column of run U-2 was filled from the bottom at the same rate used for subsequent leaching. Samples were taken at regular intervals as the front passed by the sample taps.

Data from U-1, in Tables A-1 and A-2, are affected by the initial filling operation. The rapid filling and the immediate start of leaching flow resulted in a poor initial distribution of solute concentrations. Concentrations observed in the center of the column were generally higher than at either end. One would expect that concentrations would increase in the direction of flow as mass was transferred from the solids to the liquid. It is hypothesized that concentration profiles did act in this manner during the initial filling stage. After the slower leaching flow was established, dissolved salt concentration gradients were such as to cause some of the denser leachate to drop back in the column.

U-2 data, presented in Tables A-3, A-4, and A-5 decrease in the direction of flow. In this case, density counter-currents were

sufficiently strong to overcome the relatively slow upward leachate flow. Calculations showing the validity of the hypothesized back-flow of solute will be presented in Chapter V.

Runs D-1 through D-8 were conducted under downflow conditions. In general, concentrations at any given time increased in the direction of flow and decreased with time at any given bed level. The natural density stratification from light at the top of the bed to dense at the bottom discouraged the formation of density currents.

Data from the small column runs will be analysed in a later chapter. It is worthwhile, however, to comment on the overall quality of the data from downflow leaching of shale in the small columns.

Conductivity data were well behaved. Smooth decreases with time at constant distances and uniform increases with distance at constant times were the rule. EC decreased from initial levels as high as 10 mmhos/cm to as low as 0.1 mmhos/cm after several hundred hours of leaching.

TOC data were not as well behaved. In early leaching stages, TOC did drop relatively smoothly from initial concentrations of 30 to 50 mg/L to about 5 mg/L. Thereafter, although the general trend of the data was downward, inexplicable increases were often noted. Some of these increases were short term peaks and others occurred over several hours.

The tails of the TOC break-through curves below about 2 mg/L did not exhibit the smooth decrease with time observed for EC. This is

attributed, at least in part, to the loss of analytical accuracy at low TOC values.

LARGE COLUMNS

The large column system included three columns, a constant head water supply tank connected to the city water supply, and outlet pumps. A flow schematic is shown on Figure III-9.

Columns

The large columns were located at the Richmond Field Station of the University of California, Berkeley. Three vertical columns, one foot in diameter by 10 feet long, were constructed from corrugated steel culverts. Steel plates were welded on the bottoms and all joints were sealed with epoxy cement. Thirty cm high steel cage stools were placed in the bottom of each column to support the shale bed and to provide a space for a lower pool.

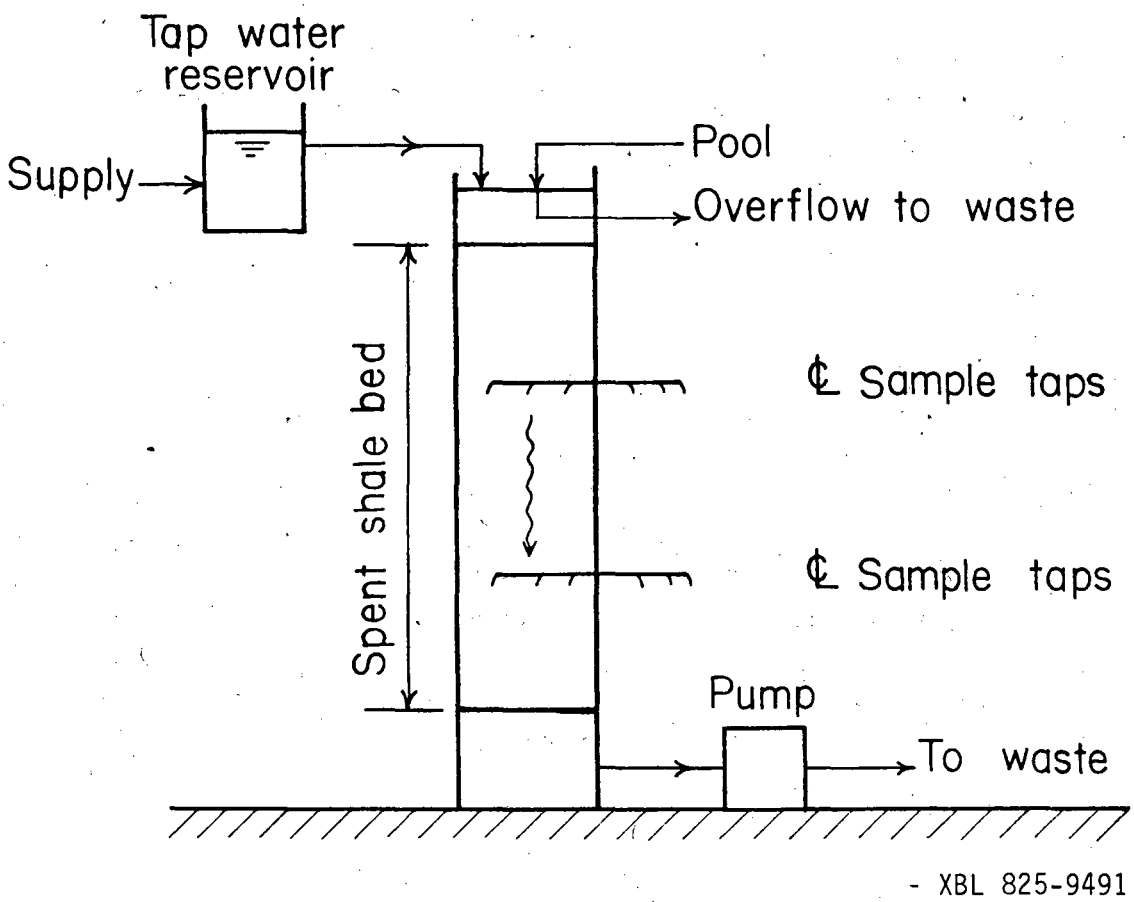

Figure III-9. Schematic of large column leaching apparatus.

Holes were drilled into the culvert walls for sample taps, inlets, and outlets. Sample taps were constructed of 1/2 inch plastic pipe passing through a rubber stoppers which in turn were inserted and clamped into holes drilled in the column walls. The pipes served as conduits for three tygon tubes, 1/8 inch in diameter, which carried leachate samples from the pores to the outside of the column. The tubes projected about 3 cm into the shale bed from holes drilled 7.5 cm on centers along the axis of the plastic pipe. These holes were located so that, when the sample tap was inserted through the culvert wall, the center tube terminated at the center of the cross-section. It was thus possible to sample at the center and quarter points on the column diameter. There were two sample tap locations, as shown on the schematic, 65 and 145 cm from the top of the bed.

The upper end of the shale bed was covered with a stainless steel wire mesh supporting a four cm thick bed of 2 mm dia sand with a water pool on top. As in the smaller columns, excess water was wasted from the top pool.

Water Supply and Pumping

Municipal tap water was conveyed to a constant head tank and then fed by gravity to the inlet pools located on the top of the columns. Leaching flow rates were established by pumping from the column effluent lines in the manner described previously for the small column studies.

Column Operation

The columns were loaded with the aid of a cherry picker hoist. Shale was poured into the columns directly from the drums and tamped lightly with a steel rod. The sampling taps were inserted at the appropriate time during the filling procedure. One column was filled with (-1/2 to +1/8) material and the other two with (-1 to +1/2) material.

The voids in the packed bed were filled slowly from the bottom up with water conveyed from the constant head tanks. Twenty liters of water were used to estimate bed porosity in the manner described previously for the small columns. Filling from the bottom continued until the water reached the sand layer. The flow from the constant head tanks was then diverted to the upper pool. Inflow continued after the pool was filled and a slight waste maintained to keep the pool clear. The column was allowed to set for 4.5 to 6 hours to allow the concentration patterns in the bed to stabilize.

Just before the run was started, leachate samples were taken from the sample taps and inlet pools. The outlet pump flow rates were set and downward leaching flow established in the shale bed. Samples were taken at frequent intervals.

The large columns had to be operated outdoors, unlike the small column studies which were performed in a temperature controlled laboratory. The diurnal temperatures variations were therefore considerably greater in the large columns, and the experiments had to be terminated when a heat wave struck the area. Diurnal variations of

12 °C or greater with a maximum temperature of 30 °C were observed. It was strongly suspected that these temperature variations created density gradient driven free-convection currents in the shale beds which distorted the effluent break-through curves. This matter is discussed in more detail in Chapter V.

Sampling Procedures

Flow and concentration profiles in the large columns were less affected by the withdrawal of samples than the smaller columns because the volumes taken represented a smaller fraction of the the total flow. Samples were collected from the upper tap first. Five mL of fluid were wasted to clear the tube of previous withdrawals and four mL of leachate were then collected from each tap.

Results.

Column operating parameters are summarized on Table III-18. Leachate pH, EC, and TOC data are shown in Appendix A in Tables A-28 through A-36. Data are presented at the far, center, and near quarter points of the cross-section, with reference to the observer, at two levels. TOC data have been adjusted for raw water background TOC and thus reflect actual pick-up of solute during passage through the bed. Temperatures taken at the time of sampling are also shown.

Although detailed data analysis is delayed until Chapter V, several comments on the data are pertinent at this time. pH and EC data generally decreased with time at a given bed depth and increased with depth at a particular time. Significant variations in data, not consistent with plug flow conditions, were observed at both sampling

levels. It cannot be determined with certainity if these variations were caused by local variation in material composition or by poor flow distribution.

Dirunal temperature variations undoubtedly affected the data. Otherwise unexplainable increases between consecutive samples were noted particularly during the latter part of the run when afternoon temperatures attained 30 ^{o}C. The size of the shale also had a significant impact on the solute levels. Column LC-1 was packed with (-1/2 to +1/8) shale and had the highest initial solute concentration. This was also higher than observed in effluents from small columns packed with the same size of shale.

The setting time between filling and the start of leaching flow also affected the initial concentrations. Columns LC-2 and LC-3 were filled with the same size shale. Higher starting EC and pH levels in LC-2 reflected a longer setting time of 6 hours after filling versus 4.5 hours for LC-3. TOC data, in general, for the large columns dropped from initial levels in a manner similar to that observed for EC and pH until concentrations of about 5 mg/L were reached. Thereafter, both short and long term peaks were noted before levels tailed off.

Table III-18

Large Column Experiments
Summary of Operational Parameters

Run No.	Shale Size	Total Porosity	External Porosity	Flow Rate mL/min	Flow Mode	Pore Vel. cm/hr	Set Time hr
LC-1	A	0.56	0.41	63	dn	12.6	4.5
LC-2	C	0.57	0.42	32	dn	6.2	6.0
LC-3	C	0.57	0.42	62	dn	12.1	4.5

See Table III-17 for Legend

CHAPTER IV

LEACHING AND TRANSPORT MODEL

The advection-dispersion equation, Equation II-1 in Chapter II, was presumed to be applicable to the leaching and transport of the solute of interest, TOC, in a bed of spent shale.

$$\frac{\partial C}{\partial t} = E \frac{\partial^2 C}{\partial Z^2} - U_p \frac{\partial C}{\partial Z} - R_r - \frac{1}{m} \frac{\partial q}{\partial t} \qquad \text{(II-1)}$$

The equation is based on a mass balance on an elemental volume of bed. The change of leachate TOC concentration with time is expressed as the sum of changes due to dispersive, advective, reactive, and internal mass transfer mechanisms.

PHYSICAL MODEL

A physical model of the leaching and transport of TOC was proposed. This model was based on: (1) physical characteristics of the fixed bed, (2) observations of leachate behavior during column and batch tests, and (3) assumptions on rate limiting transport mechanisms and initial solute distribution in the solid and liquid phases.

Physical Characteristics of the Fixed Bed

The spent shale bed comprises shale particles of various sizes in contact. Channels are formed in the spaces between the particles. In addition, small pores, located within the solid particles, terminate on the outside walls of the shale and interconnect with the larger channels. The pores within the shale were formed during the thermal conversion of the kerogen. The escaping liquids and vapors

left a network of voids within the particles. The presence of this network was confirmed in the present study by subjecting selected shale particles to an internal porosity test in a pressurized mercury bath. Porosities of up to 50 percent of the total particle volume were found.

The pores in the two networks range downward in size from dimensions on the order of the particle diameter to a few microns. This distribution is characterized by considering that only two types of pores are present: macro-pores which occur in the spaces between the particles and micro-pores which occur within the particle. The two types of pores are further characterized by the method of solute transport. Viscous flow occurs only within the saturated macro-pores, wherein solute transport is by advective, dispersive, and diffusive mechanisms. Mass transport within the micro-pores is by diffusion only.

Mass Transfer Mechanisms

The transport of a solute from sites within the solid phase to the liquid phase may be represented by a series of transfer mechanisms, each one in the series applicable to a particular domain. The principal domains in the spent shale bed are:

1. The solid phase.

2. The interface between phases.

3. The surface of the solid phase.

4. The fluid within the micro-pores.

5. The fluid within the macro-pores.

The transfer of solute between phases is likely controlled by transport within one of these domains. Amy et al. (1980) found that internal diffusion within the particle was most likely controlling for one type of shale investigated and that either internal diffusion or surface reaction were likely rate limiting for another type of shale. Furthermore, Amy found that different mechanisms could be rate limiting at different times in the leaching process.

Possible rate limiting mechanisms were outlined in Chapter II as:

1. Diffusion within the solid phase.

2. Chemical reaction at the phase interface.

3. Diffusion on the particle surfaces.

4. Molecular and Knudsen diffusion within the micro-pores.

5. Diffusion through the phase interface.

6. Mechanical or hydrodymanic dispersion in the macro-pores.

TOC Break-through Curve

A schematic of a break-through curve depicting effluent TOC concentrations normalized to the concentration existing at the time of

passage of one pore volume of fluid, versus pore volumes of fluid passed is shown in Figure IV-1. A pore volume is defined as the product of passage time and pore velocity divided by the bed depth. This curve is typical of those observed in the column leaching experiments conducted under downflow conditions in a bed which was initially saturated with water and then allowed to stand for about two hours. Leachate flow was started at pore volume zero.

The break-through curve is arbitrarily divided into three stages. Stage I occurs during the period of passage of the first pore volume. Leachate concentrations were often observed to rise slightly from initial levels during this stage. A longer period of setting after filling with water would have reduced or eliminated this rise. The presence of a pre-Stage I is implied during which water is introduced to the bed and the leachate concentrations in the pores approach equilibrium. The concentration at time zero (start of pumping) depends primarily on the time of contact between the water and the shale and the phase equilibrium isotherms. The rise during Stage I is independent of leachate velocity. A similar rise would be seen in a static batch leaching test of the same duration since each element of moving water has the same leaching history with regard to the stationary shale particles.

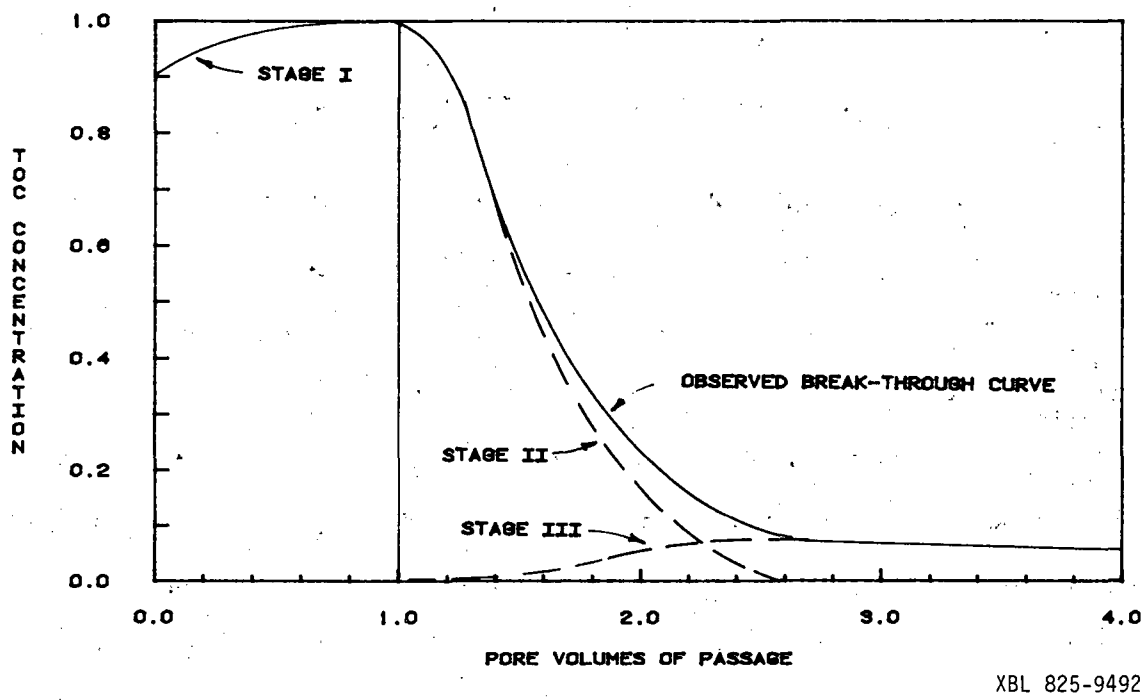

Figure IV-1. Schematic column break-through curve showing contributions of stage mechanisms.

Immediately upon the passage of one pore volume the normalized concentrations began a drop to 0.1 or less in the next two to three pore volumes. Thereafter, the concentration continued to decrease although at a greatly reduced rate.

Stages II and III each begin at unit pore volume and co-exist for the next few pore volumes as shown schematically on Figure IV-1. Stage II is dominant for two to three volumes and then disappears. Stage III is relatively small at first and then becomes dominant as Stage II disappears. The sum of the two stages is the observed break-through curve.

TOC Distribution in Solid Phase

The chemical characterization studies conducted on the spent shale, described in Chapter III, indicated that the total organic carbon content of the material was between 0.25 and 1.7 weight percent. These values are the TOC contents determined by the soluble TOC batch test and the hot acid methods, respectively. An 85 cm depth of spent shale in the small column therefore contained between 19 and 130 grams of TOC. This calculation is based on a cross-sectional diameter of 11.4 cm and a bulk density of 0.88 gm/cm^3. It is difficult to calculate with any degree of accuracy the total mass of organic carbon actually leached during a column study because the observed TOC concentrations in Stage III tend to lie near the limits of analytical accuracy. It is apparent, however, that only a portion of the available TOC is removed from the shale by the leachate in a run of normal duration. Take for example, a column in which the effluent concentration drops linearly with time in the first 20 hours

of operation from 40 to 4 mg/L and then continues at that level for 80 hours. A leaching flow of 20 ml/min would remove less than 1 g, or less than 5 percent of the soluble TOC in the solid. A large reservoir of solute thus must remain within the particle. Solute from this reservoir is released at a low rate, as evidenced by the low concentrations observed in Stage III effluent.

Physical Model of Leaching in Fixed Bed

An initial solute distribution was proposed wherein a portion of the soluble solid material lies on the surfaces of the dry shale and the remainder was distributed uniformly within the solid. Individual shale particles were modeled as cylinders having a radius 'b' and a height 'h' as shown on Figure IV-2.

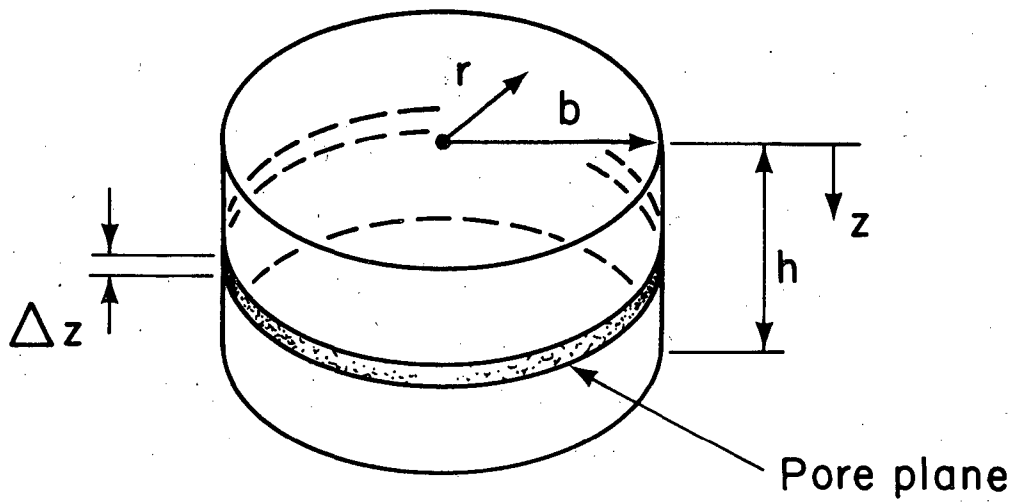

XBL 824 - 356

Figure IV-2. Model of Spent Shale Particle.

Solute transport occurs within pore planes perpendicular to the sides of the cylinders. No transfer between adjacent pore planes is assumed. Evidence for this assumption was presumptive. Raw shale consists of alternating layers of minerals rich and lean in organic content. The lean layer tends to retain integrity during retorting and remain relatively impervious to subsequent fluid movement. The principal porosity in the spent shale is thus concentrated in the formerly rich layers. Shale slabs subjected to long-term leaching in the present investigations delaminated along planes parallel to the slab face indicating that pore planes did exist within the shale. Water was able to enter along these planes and dissolve minerals in the pore walls, thus weakening the shale and causing the delamination.

Upon initial filling of the bed with water, all pores become saturated, and solute is transferred from the surface of the solid phase to the liquid. Solute is then transported within the micro-pores toward the macro-pores by molecular diffusion. The soluble material in the surface film becomes depleted quickly and additional solute moves toward the micro-pores from sites within the solid matrix.

MATHEMATICAL MODELLING

The original plan was to develop a mathematical model that would be applicable over the entire effluent solute break-through curve. After several false starts, it was found that the Stage II portion of the physical model alone could be represented by a model of simple diffusion from pores contained within the solid phase. Stage II is

the period of rapid drop in TOC content in effluent from an abandoned in-situ retort and is the period of most interest in an evaluation of intentional leaching as a viable control measure. It was decided to concentrate on developing a model for Stage II alone and to use this effort as a foundation for later investigations of the other stages. Following the development of the Stage II model, a simple Stage III model was proposed and tested. No model of Stage I was presented. Sophisticated models of Stages I and III can not be developed until more information on the chemistry of the solid and liquid phases is available including the effects of pH, ionic strength, and organic and inorganic solubility on the mass transfer mechanisms.

The problem of diffusion into spherical particles having a uniform internal porosity was solved analytically by Rosen (1952, 1954). This did not fit the obvious physical situation encountered in spent shale beds of approximately cylindrical particles containing well defined pore planes.

The following defines the physical model in a form suitable for mathematical modeling:

1. The pores of the shale particle are saturated with water at the beginning of Stage II and the solute originally in the surface film has been transferred to the liquid phase.

2. The solute contained within the liquid phase at the time of passage of the first pore volume of fluid is removed by the mechanisms of Stage II.

3. The solute that is transported between phases after the time of the first pore volume passage is removed by the mechanisms of Stage III.

MATHEMATICAL MODELLING OF STAGE II

The following are the basic assumptions used in the derivation of the Stage II model:

1. The basic element in the bed is a cylindrical particle, as shown in Figure IV-1, containing internal pore planes separated by laminar sheets of zero porosity. Channels within the pore plane are assumed to be straight, i.e. without tortuosity.

2. The primary mechanism of mass transport in the pore planes is pure Fickian diffusion. No Knudsen or surface diffusion was assumed.

3. Internal porosity was represented simply as the volume of the pore planes per unit volume of the solid.

4. Resistance to diffusion through a surface liquid film was ignored for reasons of scale. Eventually the model will be applied in field situations to large particles where the contribution of film resistance is small.

5 The contribution of dispersive and reactive mechanisms were neglected at this stage of the model development. Ultimately the effect of these mechanisms must be included in the model formation.

The mathematical representation of the above required the use of cylindrical instead of spherical functions. No solutions to this particular problem were found in the literature, so a unique solution involving Laplace Transforms was developed.

The advective-dispersive equation, Equation II-1, was rewritten in the following form to describe the physical model:

$$\frac{\partial C}{\partial t} + U_p \frac{\partial C}{\partial Z} + \frac{1}{m} \frac{\partial q}{\partial t} = 0 \qquad \text{(IV-1)}$$

in which:

C = Concentration of solute in fluid phase in macro-pores

t = Time

Z = Distance in direction of flow

q_a = Concentration of solute in fluid phase in micro-pores

U_p = Pore velocity

m = Ratio of macro-pore volume to micro-pore volume

Equation IV-1 was coupled with the Fickian diffusion equation:

$$\frac{\partial q}{\partial t} = D_m \nabla^2 q \qquad \text{(IV-2)}$$

in which:

D_m = Molecular diffusion coefficient

∇^2 = Laplacian operator for the applicable coordinate system.

The solution of Equations IV-1 and IV-2 is described in detail in Appendix B. A brief outline of the method of solution follows. Equation IV-1 is transformed to Equation IV-3 by the substitution of time and distance parameters; $\theta = t - (Z / U_p)$ and $X = Z / m\ U_p$.

$$\frac{\partial C}{\partial X} + \frac{\partial q}{\partial \theta} = 0 \qquad \text{(IV-3)}$$

The concentrations in the micro- and macro-pore fluids at time zero are q_o and C_o, respectively. The concentrations in the macro-pore fluid and at the surface of the shale at later times, C and q_s, respectively, vary with time. Time is defined in terms of θ, the time after the arrival of the first pore volume of fluid at a given location.

The solute of interest distributed within the pore planes is at concentration q_i which varies with time and the distance from the center of the particle, r. The average concentration, q_a within the particle is:

$$q_a = \frac{2}{b^2} \int_0^b r q_i dr \qquad \text{(IV-4)}$$

Diffusion from the micro-pores for the situation presumed to exist in the physical model can be represented by the superposition of solutions of Equation IV-2 for two cases considered by Crank

(1976). Superposition was valid because the diffusion is presumed to be a linear process.

Let $H_1(r, t)$ be the analytical solution for diffusion into initially empty pores from a surface having a unit concentration, q_s. Let $H_2(r, t)$ be the solution for diffusion out of pores having an initial concentration of q_o, toward an external surface having a concentration of zero. Assume that resistance to transfer through the phase interface is negligible and that the concentration at the surface is the same as the surrounding fluid in the macro-pores.

Application of the convolution theorem yields:

$$q_i(r,t) = \int_0^t q_s(\lambda) \frac{H_1(r,t-\lambda)}{\partial t} d\lambda + q_o H_2(r,t) \qquad \text{(IV-5)}$$

in which:

$q_i(r, t)$ = Concentration within pore plane at radius r and time t

$q_s(\lambda)$ = Concentration at particle surface at time λ

Crank's expressions for H_1 and H_2 were substituted into Equation IV-5, with q_a being computed with Equation IV-4. The derivative was then taken with respect to θ to yield Equation IV-6.

$$\frac{\partial q_a(X,\theta)}{\partial \theta} = \frac{4Dm}{b^2} \sum_1^\infty \frac{\partial \int_0^\theta C(r,\theta) \exp\left[-D_m \alpha_n^2 (\theta - \lambda)\right] d\lambda}{\partial \theta} - \frac{4 q_o D_m}{b^2} \sum_1^\infty \exp\left[-D_m \alpha_n^2 \theta\right] \qquad \text{(IV-6)}$$

in which:

D_m = Diffusion coefficient.

b = Particle radius

α_n = $[\ 0_n\ ]$ / b in which $[\ 0_n]$ are the zeros of a Bessel function of zero order.

The last equation was combined with Equation IV-3 and, with Laplace transforms, converted into an ordinary differential equation and solved to yield:

$$C(X,\theta) = q_o + (C_i - q_o)\ \mathcal{L}^{-1}\left\{\frac{1}{s}\exp\left[-\alpha X \sum_{1}^{\infty}\left(\frac{s}{s + D_m\alpha_n^2}\right)\right]\right\} \qquad \text{(IV-7)}$$

in which:

$C(X, \theta)$ = Concentration in macro-pores at distance X and time θ

q_o = Concentration in micro-pores at time zero

C_i = Concentration in influent to bed.

$\mathcal{L}^{-1}$ = Inverse of Laplace transform

s = Transform variable.

α = $4\ D_m\ /\ b^2$

For convenience remove constants from within the inverse function and rewrite as:

$$U(X,T) = \mathcal{L}^{-1}\left\{\frac{1}{s}\exp\left[-\alpha X\sum_{1}^{\infty}\left(\frac{s}{s+[O_n]^2}\right)\right]\right\} \qquad \text{(IV-8)}$$

in which:

$[O_n]$ = Zeros of the Bessel function of the zero order.

$T = D_m \quad \theta/b^2$

Assuming that $q_o = C_o$ and $C_i = 0$:

$$\frac{C(X,T)}{C_o} = 1 - U(X,T) \qquad \text{(IV-9)}$$

Equation IV-9 is the mass transport equation for Stage II. Solution of this equation gives a set of concentrations varying with time for a given bed depth. The dimensionless length and time parameters, αX and T, are expressed hereafter in mnemonic form as ALPHAX and TIME, respectively. The time-length parameter introduced below becomes TIME/ALPHAX.

Solution by Numerical Inversion

Equation IV-9 was solved by numerical inversion of the transformed function with the aid of programs from the LBL Computer Center Library. These programs were LAPINV, developed by Willis

(1975) and FLINV, a program which is part of the International Mathematics and Statistics Library (IMSL). LAPINV was used to obtain solutions of Equation of IV-9 and FLINV was used for verification of LAPINV solutions of test examples. A listing of the LAPINV computer program is included in Exhibit C-1 of Appendix C.

The inversion of Equation IV-9 was direct. The first 20 terms of the infinite series in the transformed mode were solved numerically. The zeros of the Bessel functions were taken from 10-place tables (Abramowitz, 1964). Equation IV-9 was then inverted by LAPINV for several values of ALPHAX over a range of TIME parameters. Solutions of Equation IV-9 are shown in Exhibit C-2 of Appendix C for ALPHAX values from 0.01 to 10 and for TIME values from 7.9 to 10^{-4}. These solutions are also shown graphically on Figure IV-3. Normalized concentrations for each length parameter ALPHAX are plotted against the time-length parameter, TIME/ALPHAX, defined as TIME divided by ALPHAX. Note that by so doing the D/b^2 term is removed from the ordinate.

Verification of Solution

The numerical inversion of a Laplace transform is a risky procedure. There is no positive way to prove that the resulting solution is the correct one. One method often used to test an inversion technique is to use it to solve functions which can be inverted analytically and determine the error. Both programs, LAPINV and

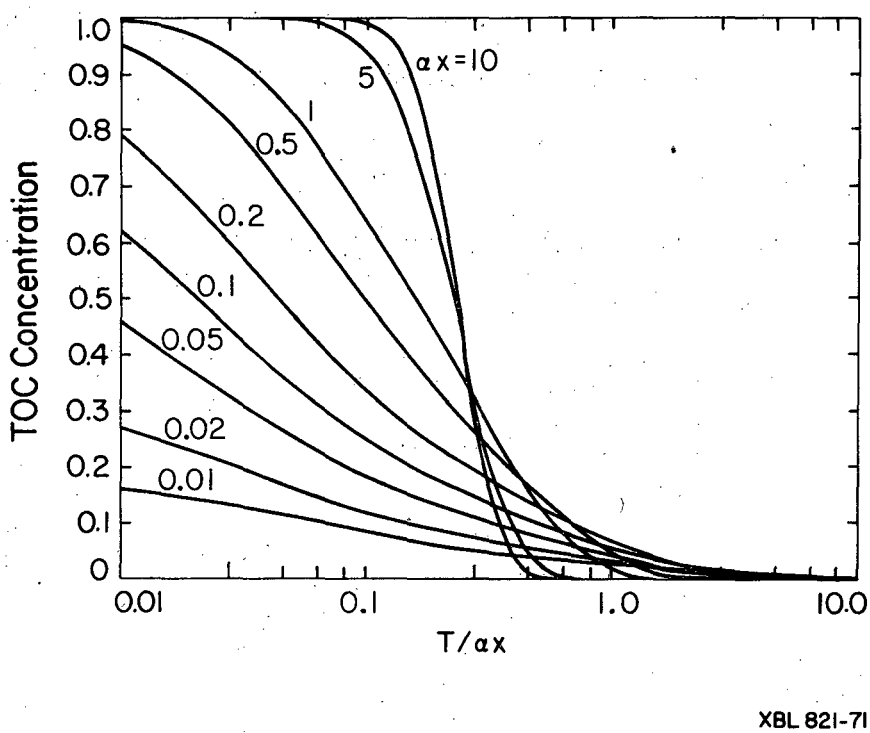

Figure IV-3. Leachate solute concentration as a function of ALPHAX and TIME/ALPHAX.

FLINV, were found to be accurate for inversion of simple functions. LAPINV was tested on several more complex problems common in reactor analysis. In general, the LAPINV inversions of smooth functions were comparable with published analytical solutions. On the other hand the LAPINV inversions of functions containing spike and step inputs did not compare favorable with published solutions. In these inversions, a false dispersion was introduced by the numerical techniques employed. Spike functions were transformed into peaks having finite heights and broad bases and the step functions were smoothed at the shoulders into S-curves.

LAPINV was tested with the first term of the expansion of Equation IV-8.

$$U'(X,T) = \mathcal{L}^{-1}\left\{\frac{1}{s}\exp\left[-\alpha X\left(\frac{s}{s + [0_n]^2}\right)\right]\right\} \qquad \text{(IV-10)}$$

in which:

$$[0_1] = 2.4048255577$$

It can be shown that there is a mathematical equivalence between Equation IV-10 and the J function defined by:

$$J(a,b) = 1 - \exp[-b]\int_0^a \exp[-\xi]\, I_o(2\sqrt{b\xi})\, d\xi \qquad \text{(IV-11)}$$

in which:

(a,b) = Variables for which the J function is evaluated.

I_o ( ) = Modified Bessel function

Tabulations of the J function are found in Sherwood et al. (1975). The equivalence between the U' and J functions occurs when the functions are evaluated for the parameters within the brackets of Equation IV-12. Note the similarity of parameters for the two functions. The first parameter of the J function is ALPHAX, the same parameter at which U' is evaluated. The second parameter of the J function differs from the second parameter of the U' function only by the factor $[O_1]^2$.

$$U'(X,T) = J(\alpha X, [O_1]^2 T) \qquad \text{(IV-12)}$$

The two functions, plotted against the product of TIME/ALPHAX and $[O_1]^2$, are shown on Figure IV-4 for comparison. The J function was evaluated by setting ALPHAX equal to unity and then taking values of J from tables in Sherwood et al. (1975) for several ratios of TIME/ALPHAX * $[O_1]^2$. U' was evaluated by also setting the length parameter, ALPHAX, equal to one and then inverting by LAPINV. The J function is shown as a continuous line on Figure IV-4 and the U' function is shown as discrete points. The correspondence is excellent. The LAPINV inversion of Equation IV-10 was also verified by FLINV.

These verification tests of FLINV and LAPINV present strong

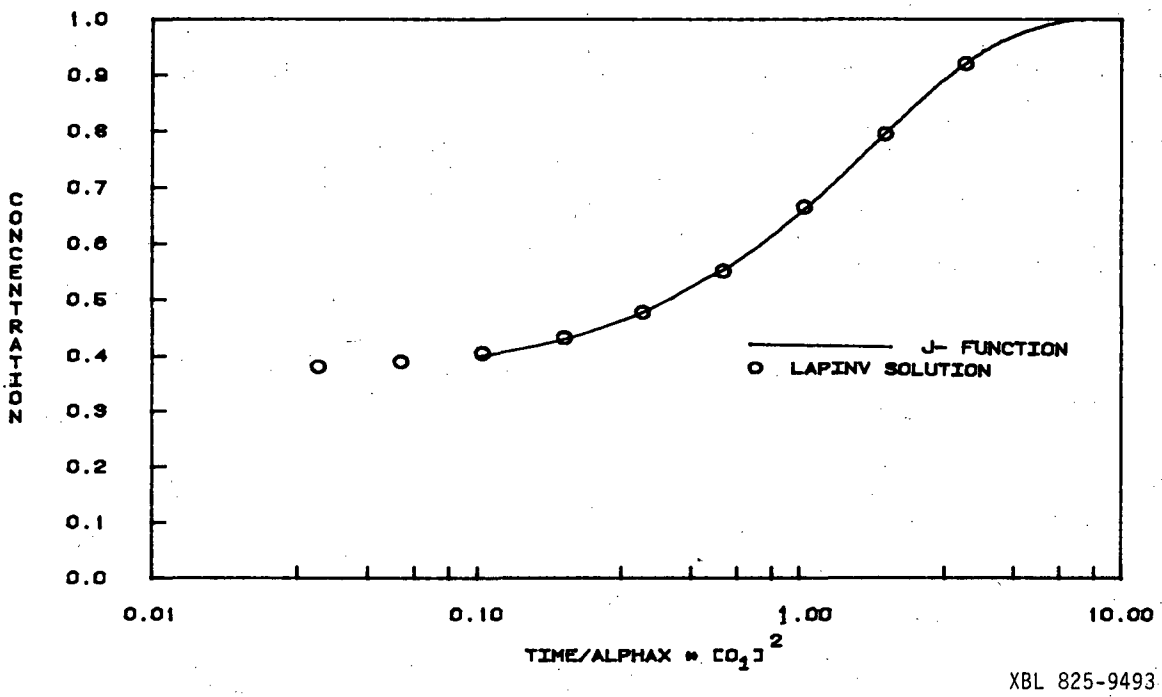

XBL 825-9493

Figure IV-4. Comparison of J-function with the LAPINV inversion of Equation IV-10.

evidence that the solutions of IV-9 by LAPINV are satisfactory for the purposes of the study.

MATHEMATICAL MODEL OF STAGE III

Stage III leaching mechanisms were modeled independently of Stage II. The Stage III model is not applicable during the first few pore volumes passages when Stage II removal mechanisms dominate. After Stage II disappears, Stage III was assumed to attain steady state. This condition was the basis for the Stage III model. It is presumed that the reservoir of solute remaining within the shale is sufficiently large to maintain steady-state conditions for an indefinite period. In reality, the tail of the break-through curve will show a gradual decrease with time as the resistance to solute travel within the solid phase increases and the reservoir becomes depleted.

Physical Model of Stage III

The loss of TOC from the solid phase within a unit volume of bed was equated to the corresponding gain in the liquid phase. The rate of transfer across the phase interface is expressed in terms of a mass transfer coefficient.

Mathematical Model of Stage III

The physical model is expressed mathematically in differential form as:

$$\varepsilon \frac{dC}{dt} = \rho_B \frac{dq}{dt} \cdot 1000 \qquad \text{(IV-13)}$$

in which:

ε = External porosity

C = Solute concentration in liquid phase (mg/L)

ρ_B = Bulk density (g/cm^3)

q = Solute concentration in solid phase (mg/g)

t = Time (hr)

Equation IV-13 can be coupled with Equation IV-14 relating the change in solid solute to a mass transfer coefficient and a concentration gradient driving force.

$$\rho_B \frac{dq}{dt} = Ka(C_e - C) \qquad \text{(IV-14)}$$

in which:

K = Mass transfer coefficient ($mg/hr\text{-}cm^3\text{-}mg/L$)

a = Interfacial area (cm^2)

C_e = Equilibrium concentration in liquid phase in contact with solid phase

C = Liquid phase concentration

Substitution of Equation IV-13 into IV-14 yields:

$$\frac{dc}{dt} = \frac{1000}{\varepsilon} Ka(C_e - C) \qquad \text{(IV-15)}$$

Equation IV-15, solved by separation of variables and integration, yields Equation IV-16. Concentrations were normalized with C_e. The initial concentration at the start of leaching is C_o. Equation IV-16 is valid only for the units listed above.

$$K = \ln \left[\frac{1 - C_o/C_e}{1 - C/C_e} \right] \frac{\varepsilon}{a\ t\ 1000} \qquad \text{(IV-16)}$$

Mass Transfer Coefficient

The quiescent leaching experiment, described in Chapter III, was the source of data for the determination of the mass transfer coefficient, K. Observed concentrations, normalized with C_e, are plotted versus time on Figure IV-5. Experimental variables were substituted into Equation IV-16, and the equation trial fitted to the plotted data for various assumed values of K. Variables used were: bulk density of 0.88 g/cm^3, external porosity of 0.45, equilibrium concentration of 22.5 mg/L, initial concentration of 1.0 mg/L, and surface area of 2.3 cm^2/cm^3.

The equilibrium concentration was based on long-term batch tests of leached spent shale obtained from column dumps, as described in Chapter III. The value of 22.5 mg/L was the mean of the terminal TOC values of tests B and C shown in Table III-14. The surface area was based on a typical cylindrical particle having a diameter of 0.7 cm, a height of 0.2 cm and a solid density of 2.2 g/cm^3. The surface area determined by this method is less than values measured by Carley (1980) for crushed raw oil shale particles. Carley found a mean A/V

(surface area/particle volume) factor of 11.4 for crushed shale in the 5/16 to 3/8 inc size range. The lower value used in the present study compensated for the assumption that diffusion in the cylinderical element is normal to the axis of the cylinder.

Equation IV-17, containing the above values, is plotted on Figure IV-5 for K values of 1.5, 2.0, and 3.0 x 10^{-7} mg/hr-cm^2-mg/L. The data are generally encompassed by the upper and lower curves; therefore, the median K value was taken to be representative of the shale.

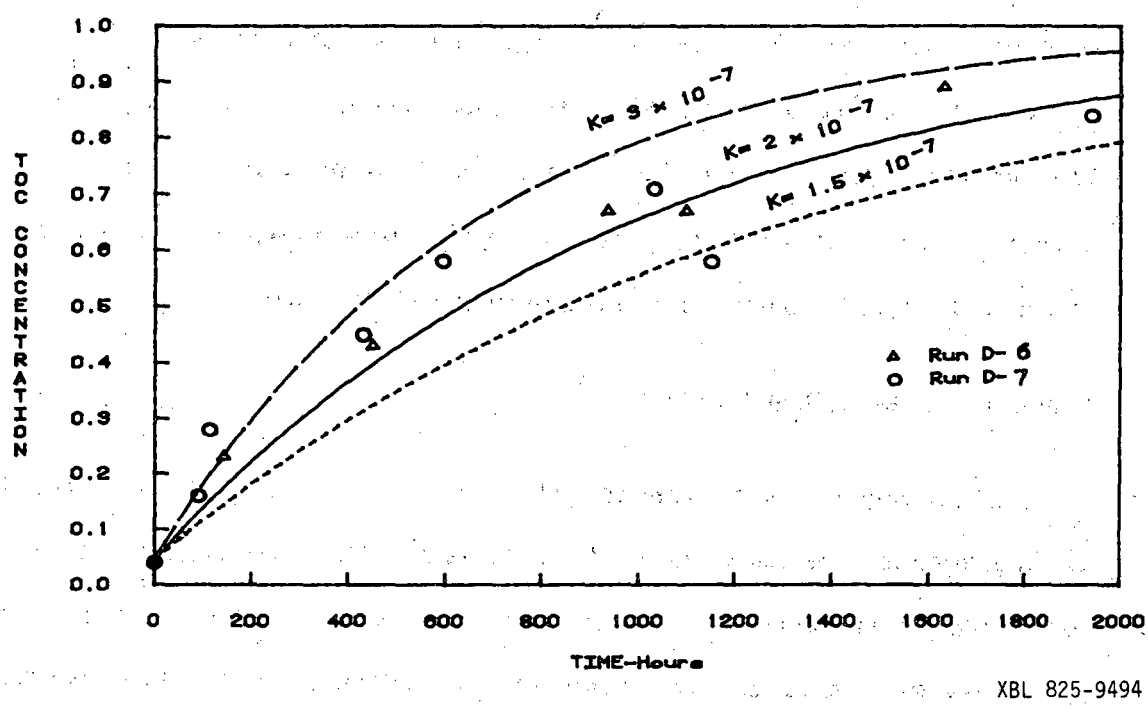

Figure IV-5. TOC concentration versus time for quiescent leaching studies in small columns.

CHAPTER V

MODEL VERIFICATION AND ANALYSES OF RESULTS

The mass transfer models of Chapter IV were derived without regard to specific compounds and should be generally applicable for transport of any solute in the system described by the physical model. A primary objective of this study was to model transport of organic compounds from in-situ spent shale. Models were therefore tested and verified with TOC data taken from leaching experiments. The general approach used for model verification was to first derive kinetic coefficients from selected small column experiments and then test these coefficients with data obtained from other column runs.

STAGE II MODEL VERIFICATION

The Stage II model presented in Chapter IV is a simplification of the mechanisms involved in the transfer of solute within the shale bed. The derivation and application of the model presumes: (1) a two phase system containing a homogeneous solid phase comprising uniform particles and a liquid phase moving under plug flow conditions and (2) that one mass transfer mechanism would be rate limiting. These conditions were met with varying degrees of success in the experiments.

Despite the care taken to pack the columns in a homogeneous manner, the column studies indicated that some portions of the bed tended to release TOC and salts more readily than other portions. Individual shale particles, while generally cylindrical in shape, tended toward the angular and also varied significantly from the average dimensions used to typify the media. Ideal plug flow

conditions were approached but not necessarily attained in the small column experiments. Free convection currents in the liquid phase, driven by density gradients caused by local differences in temperature and salt concentration, were undoubtedly present. Some transfer mechanisms, such as transport through the liquid film at the interface and the simultaneous occurrence of Stage III mechanisms during Stage II, were not included in the model. All of the above factors tend to produce a flatter break-through curve than predicted by the Stage II model.

Calculation of Diffusion Coefficients

The Stage II model was fitted to the higher observed TOC concentrations only. The primary reason for this was that measured TOC was more inaccurate at low concentrations. The higher concentrations were also affected less by the factors neglected in the derivation of the Stage II model. The general rule was to use only those observations having a normalized TOC concentration C/C_o of 0.40 or more. C_o represented the weighted mean average of the TOC concentrations observed just before the time of passage of the first pore volume. Reference to the tables in Appendix A shows that considerable variations in TOC measurements existed over the length of the columns during this period. These variations were most likely due to the non-homogeneity in the bed. Extreme high values were not included in the computation of C_o.

The time of passage of the first pore volume was estimated with the aid of the expression, $U_p\ t\ /\ Z$; in which U_p was the estimated

mean pore velocity; t the time of observation; and Z the depth to the sample point.

Unfortunately the TOC concentration often dropped too rapidly to permit the collection of many observations of C/C_o in excess of 0.40. Decreasing the sampling time interval during the period of rapid TOC decrease would have produced more data in this region but the column flow regime and the concentration profiles would have been distorted excessively. Those runs which contained one or more C/C_o in excess of 0.40 are listed in Table V-1 and are plotted on Figures V-1 through V-11.

The Stage II model results proved quite sensitive to the value of the internal porosity; consequently, analyses were made for internal porosities varying from 0.10 to 0.20, a range based on the limited particle porosity studies described in Chapter III. A summary of parameters used in analyses with an internal porosity of 0.15 is shown on Table V-1. Similar summaries for internal porosities of 0.20 and 0.10 are shown on Tables V-2 and V-3, respectively.

The curves shown on Figures V-1 through V-7, V-9, and V-11 represent the break-through curves predicted by the Stage II model for an internal porosity of 0.15. Solutions could not be obtained at this porosity for two cases, runs D-7 and D-8 at bed depths of 70 cm: consequently, the break-through curves shown on Figures V-8 and V-10 are for an internal porosity of 0.20. The reason for the inability to obtain a solution for these two runs will be discussed subsequently.

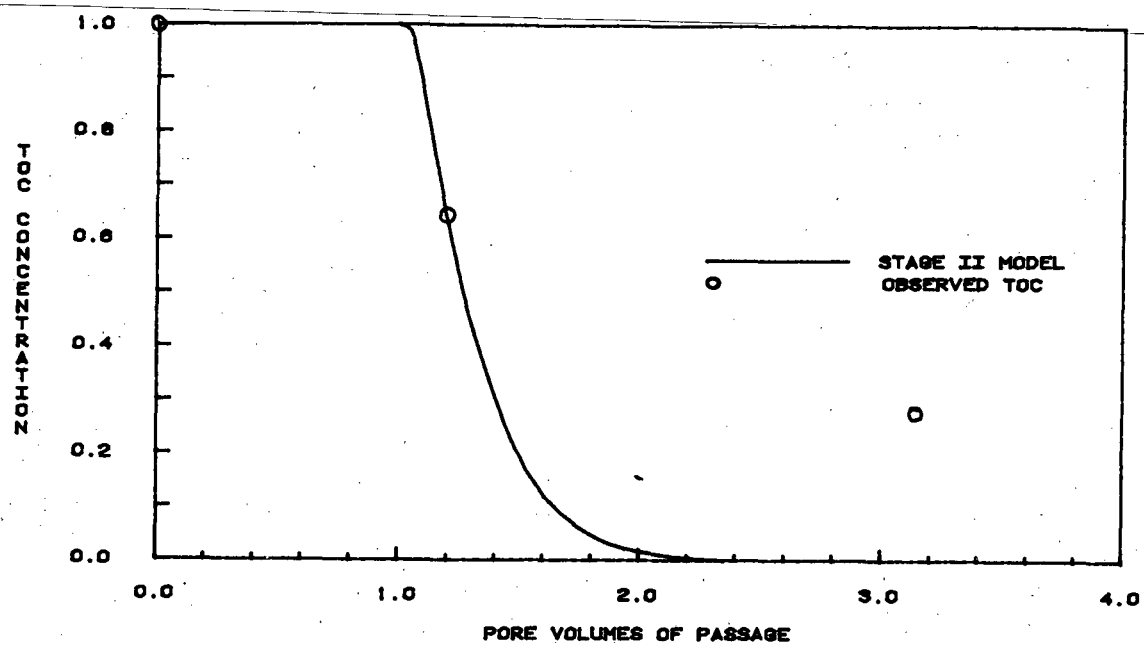

XBL 825-9495

Figure V-1. Break-through curve and normalized observed TOC concentrations plotted versus pore volumes of passage. Run D-1, 25 cm bed depth, and 0.15 internal porosity.

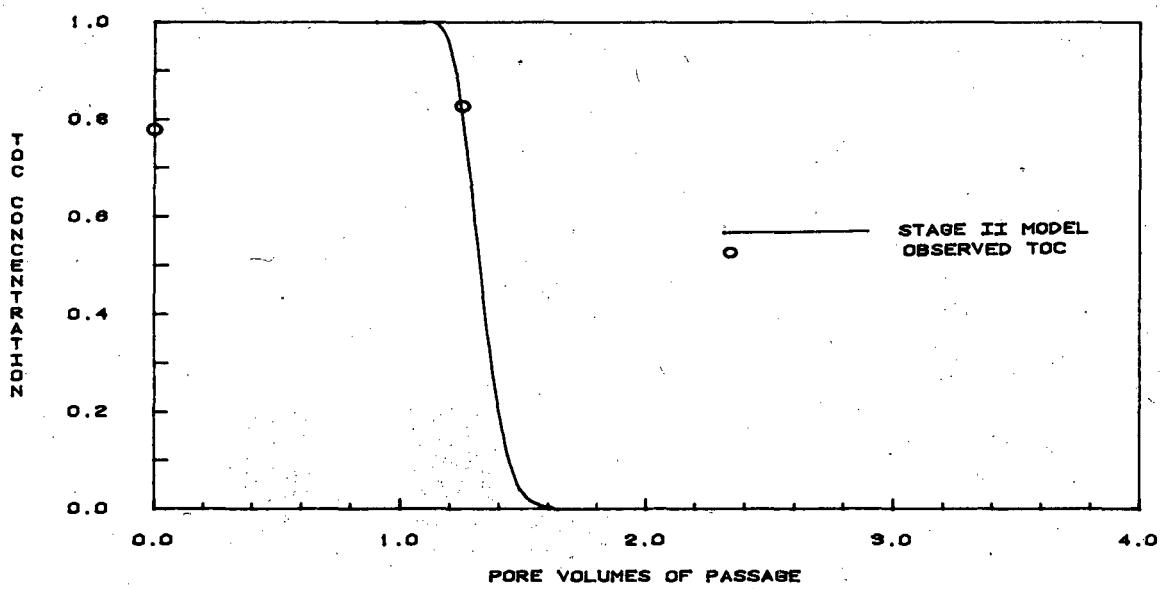

XBL 825-9496

Figure V-2. Break-through curve and normalized observed TOC concentrations plotted versus pore volumes of passage. Run D-2, 55 cm bed depth, and 0.15 internal porosity.

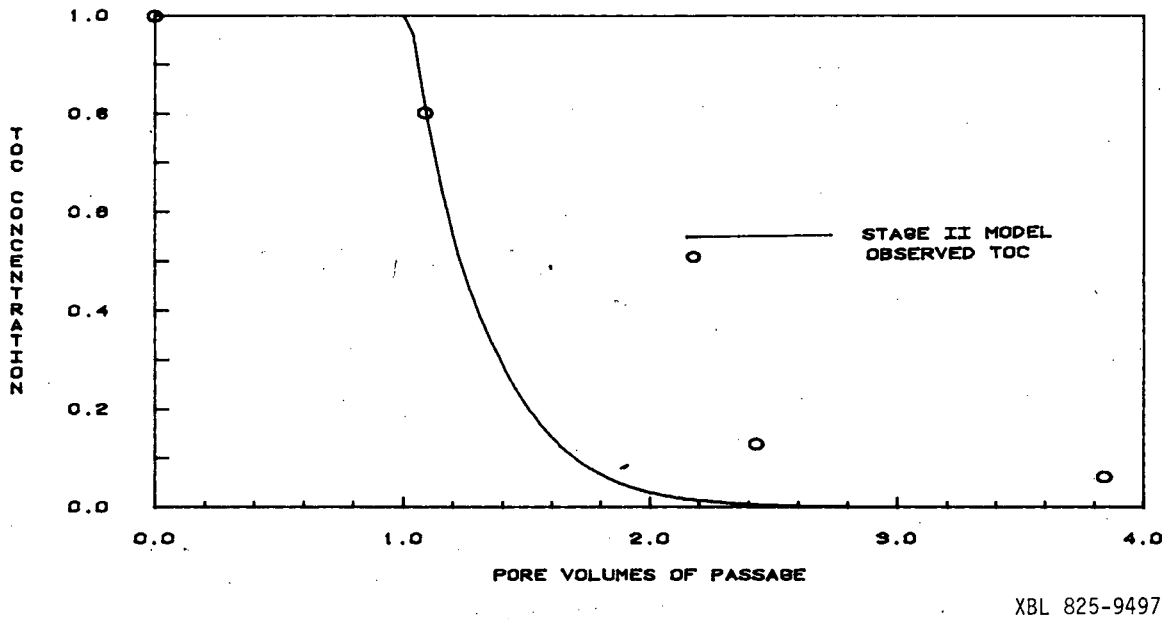

Figure V-3. Break-through curve and normalized observed TOC concentrations plotted versus pore volumes of passage. Run D-4, 25 cm bed depth, and 0.15 internal porosity.

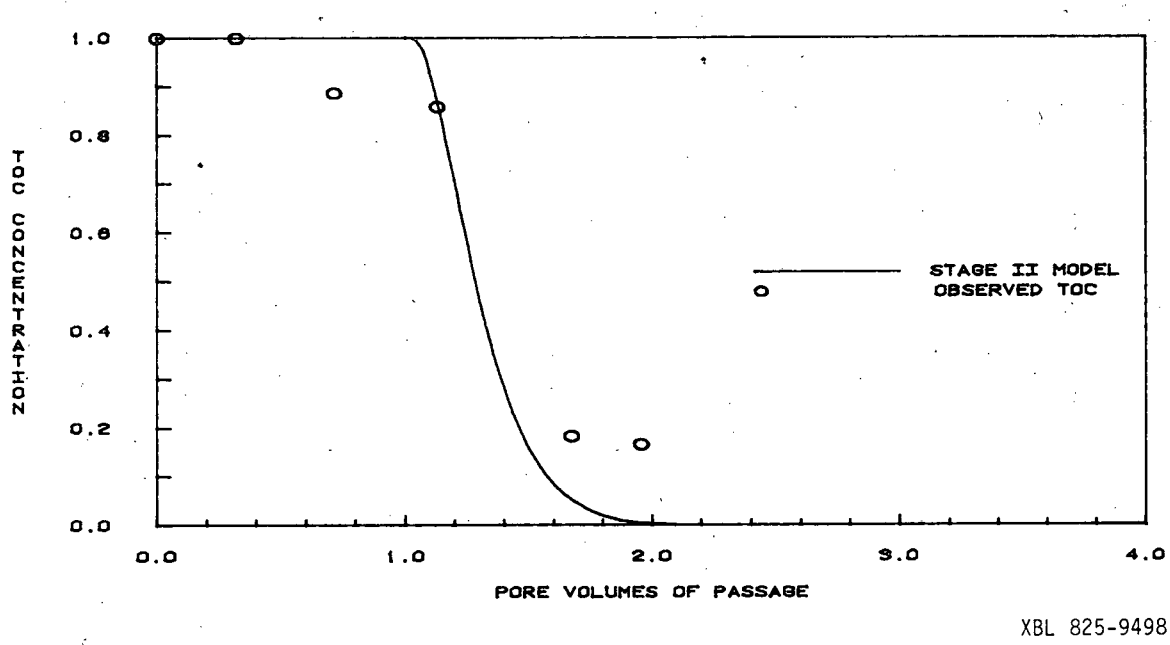

Figure V-4. Break-through curve and normalized observed TOC concentrations plotted versus pore volumes of passage. Run D-4, 85 cm bed depth, and 0.15 internal porosity.

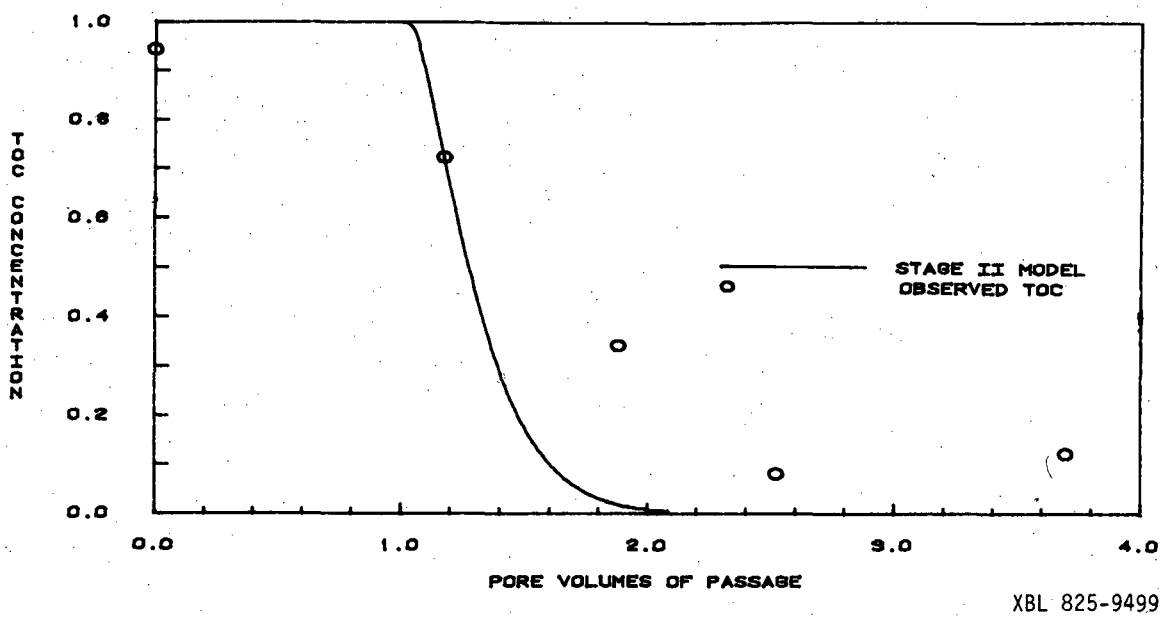

Figure V-5. Break-through curve and normalized observed TOC concentrations plotted versus pore volumes of passage. Run D-5, 85 cm bed depth, and 0.15 internal porosity.

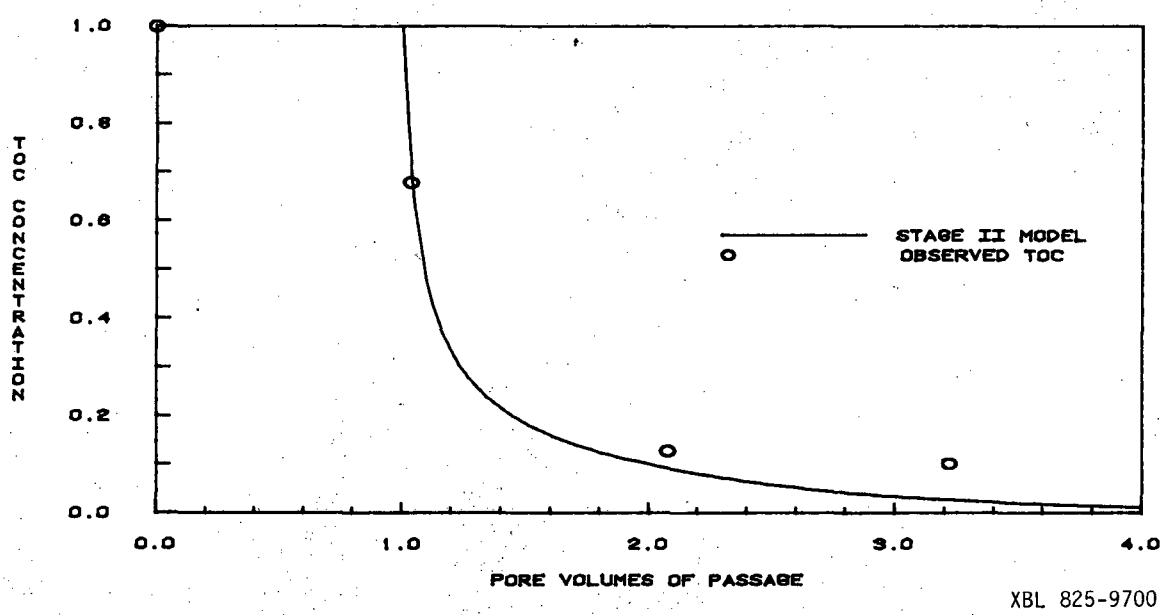

Figure V-6. Break-through curve and normalized observed TOC concentrations plotted versus pore volumes of passage. Run D-6, 70 cm bed depth, and 0.15 internal porosity.

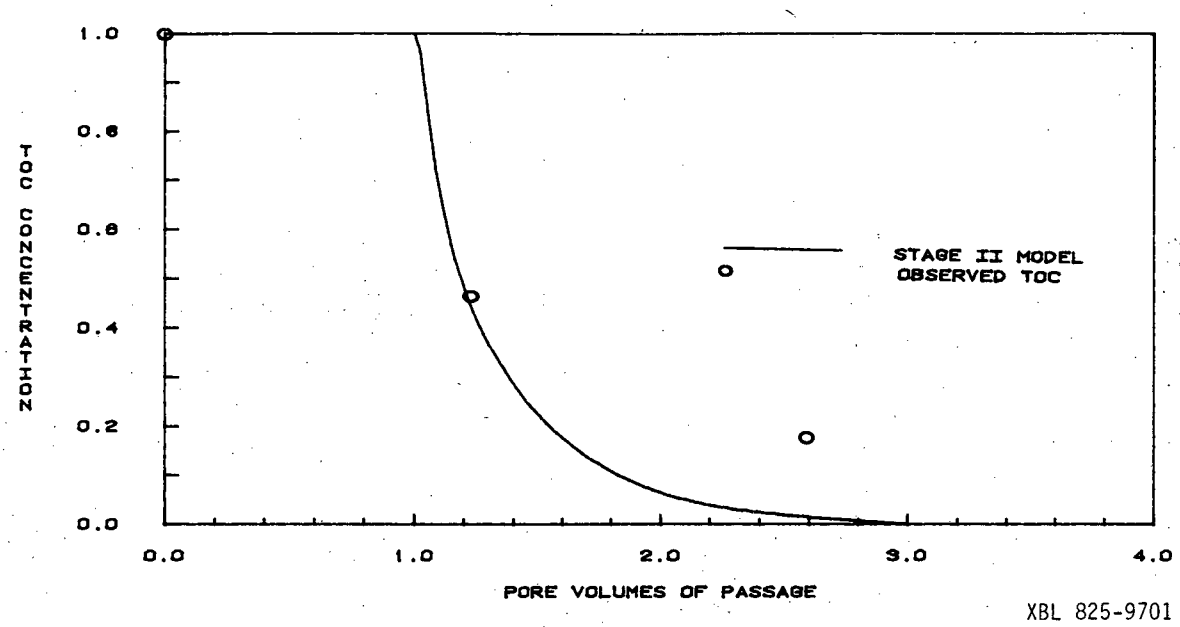

Figure V-7. Break-through curve and normalized observed TOC concentrations plotted versus pore volumes of passage. Run D-7, 55 cm bed depth, and 0.15 internal porosity.

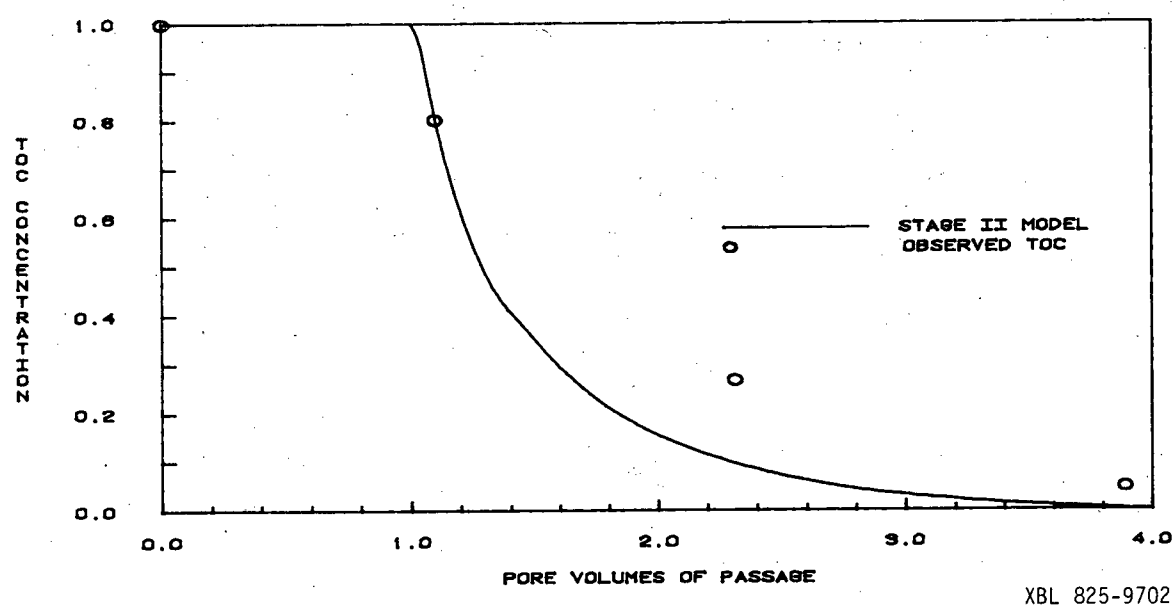

Figure V-8. Break-through curve and normalized observed TOC concentrations plotted versus pore volumes of passage. Run D-7, 70 cm bed depth, and 0.20 internal porosity.

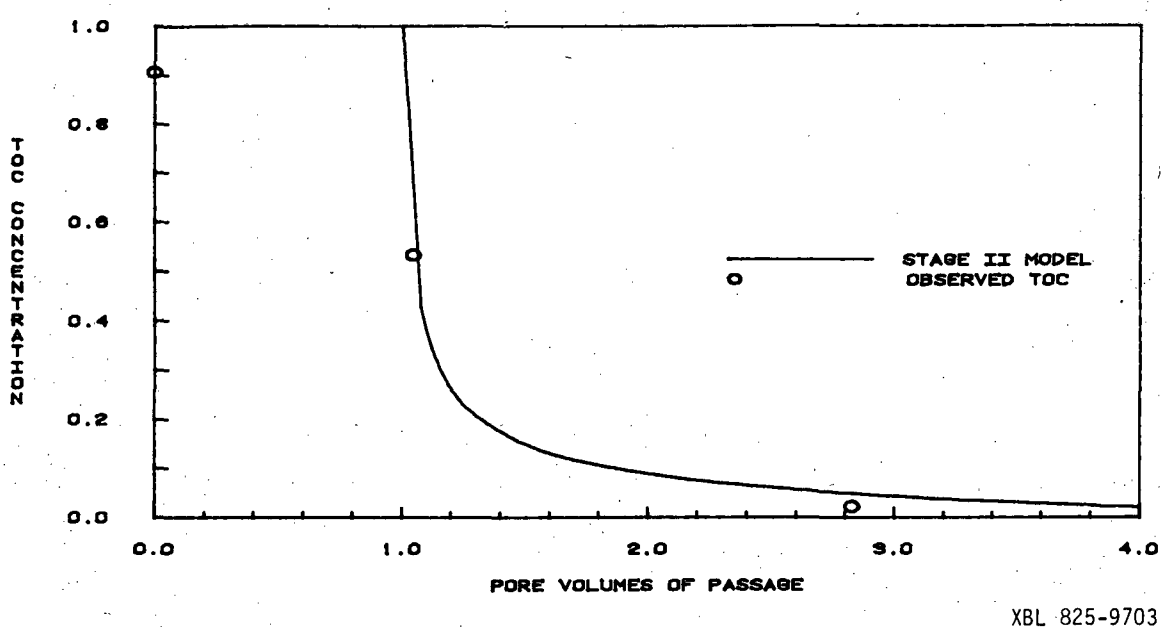

Figure V-9. Break-through curve and normalized observed TOC concentrations plotted versus pore volumes of passage. Run D-8, 25 cm bed depth, and 0.15 internal porosity.

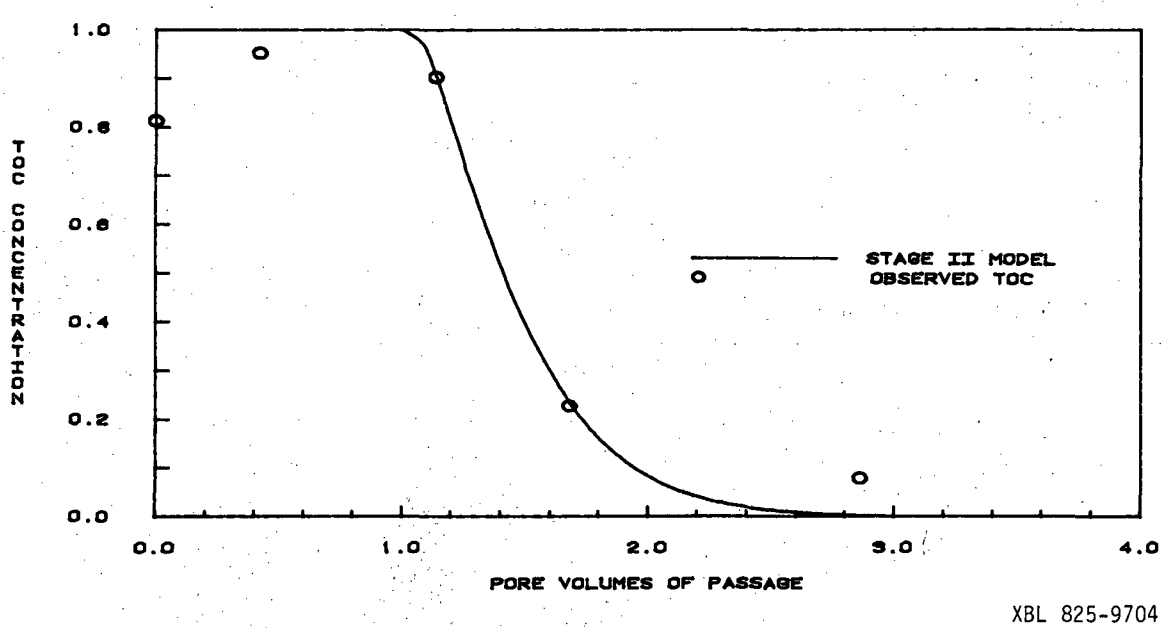

Figure V-10. Break-through curve and normalized observed TOC concentrations plotted versus pore volumes of passage. Run D-8, 70 cm bed depth, and 0.20 internal porosity.

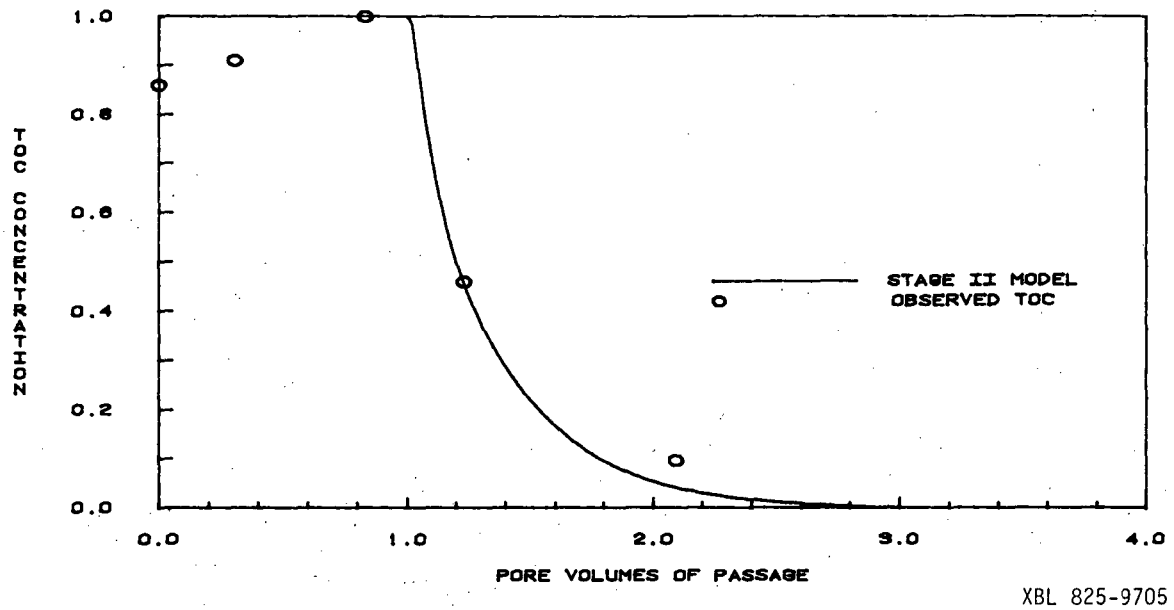

Figure V-11. Break-through curve and normalized observed TOC concentrations plotted versus pore volumes of passage. Run D-8, 85 cm bed depth, and 0.15 internal porosity.

Table V-1

Small Column Diffusion Coefficients
Internal Porosity of 0.15

Run no.	Z Bed Depth cm	b Part. Radius cm	C_o Norm. Conc. mg/L	U_p Pore Vel. 10^{-3} cm/sec	ALPHAX	D_m/b^2 10^{-4} sec^{-1}	D_m Diff. Coef. 10^{-5} cm^2/sec
D-1	25	0.4	30.0	2.4	2.0	1.4	2.2
D-2	55	0.8	19.5	5.5	14.8	11.1	70.0
D-4	25	0.4	35.5	4.4	1.3	1.8	2.9
D-4	85	0.4	35.5	4.4	3.0	1.2	1.9
D-5	85	0.4	36.5	13.9	2.4	3.0	4.8
D-6	70	0.4	37.5	20.2	0.29	0.60	1.0
D-7	55	0.4	35.5	20.9	0.80	2.2	3.5
D-7	70	0.4	35.5	20.5	nd*	nd	nd
D-8	25	0.5	21.5	7.3	0.18	0.40	1.0
D-8	70	0.5	21.5	7.3	nd	nd	nd
D-8	85	0.5	21.5	7.3	0.94	0.60	1.5

*nd - not determined

The Stage II model of Chapter IV was fit to the observed data by a trial and error process. Dimensionless time, distance, and time/distance parameters were used throughout as defined by Equations V-1 through V-3, respectively. The pore volume passage equation defined above was related to the ratio of the dimensionless

Table V-2

Small Column Diffusion Coefficients
Internal Porosity of 0.20

Run no.	Z Bed Depth cm	U_p Pore Vel. 10^{-3} cm/sec	ALPHAX	D_m/b^2 10^{-4} sec^{-1}	D_m Diff. Coef. 10^{-5} cm^2/sec
D-1	25	2.7	3.0	1.5	2.4
D-2	55	6.1	22.4	12.4	79.0
D-4	25	5.0	2.6	2.7	4.3
D-4	85	5.0	5.6	1.7	2.7
D-5	85	15.5	4.8	4.5	7.2
D-6	70	22.8	0.90	1.4	2.2
D-7	55	23.7	1.25	2.6	4.2
D-7	70	23.7	0.80	1.3	2.1
D-8	25	8.2	0.50	0.82	2.0
D-8	70	8.2	2.16	1.25	3.1
D-8	85	8.2	1.25	0.60	1.5

time/distance parameter as illustrated in Equation V-4. The variables are as defined in Chapter IV.

The internal porosity of the shale was first estimated and then U_p and the porosity ratio factor m computed. These factors, together with real time t and depth Z for a given observed TOC concentration, permitted the estimate of the TIME/ALPHAX parameter with the aid of Equation V-4. A trial value for ALPHAX was selected from Figure IV-3

Table V-3

Small Column Diffusion Coefficients
Summary for Internal Porosity of 0.10

Run no.	Z Bed Depth cm	U_p Pore Vel. 10^{-3} cm/sec	ALPHAX	D_m/b^2 10^{-4} sec^{-1}	D_m Diff. Coef. 10^{-5} cm^2/sec
D-2	55	4.9	5.8	6.5	41.6
D-5	85	12.5	1.0	1.9	3.0
D-8	85	6.5	0.60	0.57	1.4

$$\text{ALPHAX} = \frac{4D_m}{b^2} \frac{Z}{mU_p} \tag{V-1}$$

$$\text{TIME} = \frac{\theta D_m}{b^2} \tag{V-2}$$

$$\text{TIME/ALPHAX} = \frac{\theta_m U_p}{4Z} \tag{V-3}$$

$$\text{Pore Volumes} = [\text{TIME/ALPHAX}] \frac{4}{m} + 1 \tag{V-4}$$

for the appropriate normalized concentration C/C_o. This trial ALPHAX defined a set of concentrations for a range of TIME parameters which, after conversion with Equation IV-4, were plotted on graphs of observed data similar to those shown on Figures V-1 through V-11. The value of ALPHAX was adjusted until the trial break-through curve passed through the desired points. In general, the adjustment was sensititive to variations of about two percent in values of ALPHAX. After obtaining the best-fit curve, the ratio D_m/b^2 was computed from Equation V-1 and the factor D_m estimated by using the appropriate average particle radius b. The results of these analyses for porosi-

ties of 0.15, 0.20, and 0.10 are shown on Tables V-1 through V-3, respectively.

The foregoing analyses involved a considerable number of trial break-through curves. The process was facilitated by first tabulating solutions of Equation IV-9, the Stage II model equation, for a wide range of ALPHAX and TIME parameters. A typical table of such output is shown in Appendix C. Concentrations for a given ALPHAX could thus be determined directly by interpolation.

An examination of Figure IV-3 illustrates another reason for not considering low C/C_o ratios when attempting to fit the Stage II model to the observed results. The model output becomes insensitive to ALPHAX for large values of ALPHAX and relatively small C/C_o ratios. Also, the relationship between C/C_o and ALPHAX reverses at TIME/ALPHAX ratios of about 0.25. Above this value C/C_o increases with decreasing ALPHAX, the reverse of the situation at lower ranges of TIME/ALPHAX. This tends to make the interpretation of the experimental data confusing and difficult at low C/C_o ratios.

Despite these difficulties, markedly similar estimates of the diffusivity coefficients, D_m, were obtained for all runs conducted with an average media radius of 0.4 to 0.5 cm as shown on Tables V-1 through V-3.

Sensitivity of Analyses to Experimental Variables

The sensitivity of the analyses to experimental variables can be determined by investigating the dimensionless length and time parameters defined by Equations V-1 and V-2.

ALPHAX, the parameter which defines the shape of the Stage II break-through curve, is primarily a function of two variables: the reciprocal characteristic time factor, D_m/b^2, and the internal porosity. The other variables are relatively well defined by experimental controls.

The effects of changes in ALPHAX upon TIME/ALPHAX can be seen on Figure V-12 on which are plotted break-through curves for ALPHAX values of 0.5, 1.0, 5.0, and 10.0. For illustration, a ten-percent increase in ALPHA from 1.0 to 1.1 at a concentration of 0.6 would increase TIME/ALPHAX by about six percent. The change in pore volume passages, calculated for a porosity ratio m of 3, would be less than one percent.

The sensitivity of ALPHAX and thus the calculated diffusion coefficient D_m to errors in the observed normalized concentration C/C_o can also be seen on Figure V-12. It was estimated that the coefficient of variation of TOC concentrations above 10 mg/L was 5 percent. The ratio C/C_o will have a coefficient of variation equal to or greater than this value. Consequently, the 95 percent confidence limit on a C/C_o of 0.50 would be at least +/- 0.05. Within this limit, for example, ALPHAX could vary from 0.5 to about 0.9 at a TIME/ALPHAX factor of 0.12. Different ranges may be calculated depending on the selected values of C/C_o and TIME/ALPHAX.

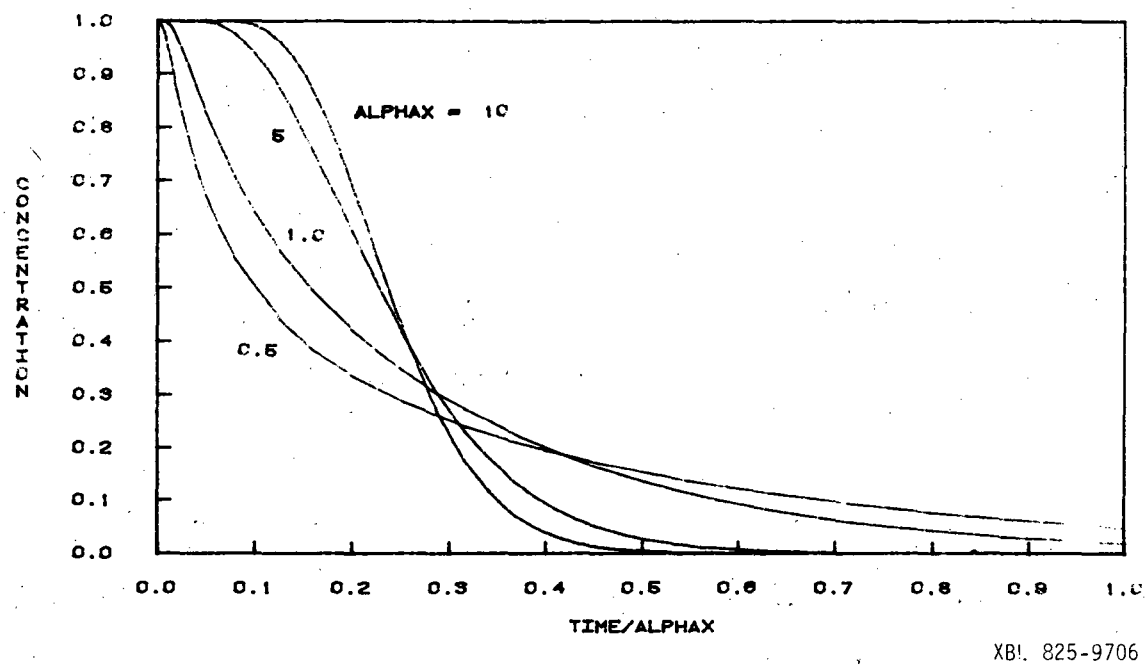

Figure V-12. Arithmetic plot of dimensionless break-through curves for ALPHAX parameters of 0.5, 1.0, 5.0, and 10.0.

Dispersion

The dispersion term in Equation II-1 was not included in the derivation of the Stage II model because of the assumption of plug flow. Furthermore, no attempt was made to determine an experimental value of the dispersion coefficient in the spent shale beds. Micro-pores within the particles would have detained a portion of any tracer used and the dispersion coefficient determined from the distorted break-through curve would have been incorrect. Coating the shale particle surfaces to seal the micro-pores would have been difficult and there would have been no assurance that the dispersion in a bed of coated particles would be the same as that which would exist in a bed of uncoated particles.

An attempt was made to evaluate the relative magnitude of the dispersive mechanisms by using a solution to Equation V-5.

$$\frac{\partial C}{\partial t} = E \frac{\partial^2 C}{\partial Z^2} - U_p \frac{\partial C}{\partial Z} \qquad \text{(V-5)}$$

This dispersion equation is derived from Equation II-1 by neglecting the reactive and internal mass transfer terms.

Ogata and Banks (1961) solved equation V-5 for a semi-infinite fixed bed containing fluid at concentration C_o at time zero. At all greater times the concentration in the fluid at distance zero was held at the influent concentration C_i, and the concentration at infinite distance in the bed approached C_o. These boundary conditions are simplifications of the actual situation in the column but are sufficient to illustrate the potential impact of dispersion.

The Ogata and Banks solution is given by Equation V-6.

$$C/C_o = 1 - \frac{1}{2}\left\{\text{erfc}\left[\frac{\sqrt{\frac{U_p Z}{E}}}{2\sqrt{\theta}}(1-\theta)\right] + \exp\left(\frac{U_p Z}{E}\right)\text{erfc}\left[\frac{\sqrt{\frac{U_p Z}{E}}}{2\sqrt{\theta}}(1+\theta)\right]\right\} \quad \text{(V-6)}$$

in which:

C/C_o = Normalized effluent concentration

erfc = Complimentary error function

U_p = Pore velocity

Z = Length of column

E = Dispersion coefficient

θ = Pore volume passage term - U_p t / Z

t = Time of observation

Solutions of Equation V-6 for Run D-8 at 85 cm are shown on Figure V-13 for axial dispersion coefficients of 10^{-2} and 0.5×10^{-2} cm^2/sec. Values of U_p and Z were taken from Table V-1 for an internal porosity of 0.15.

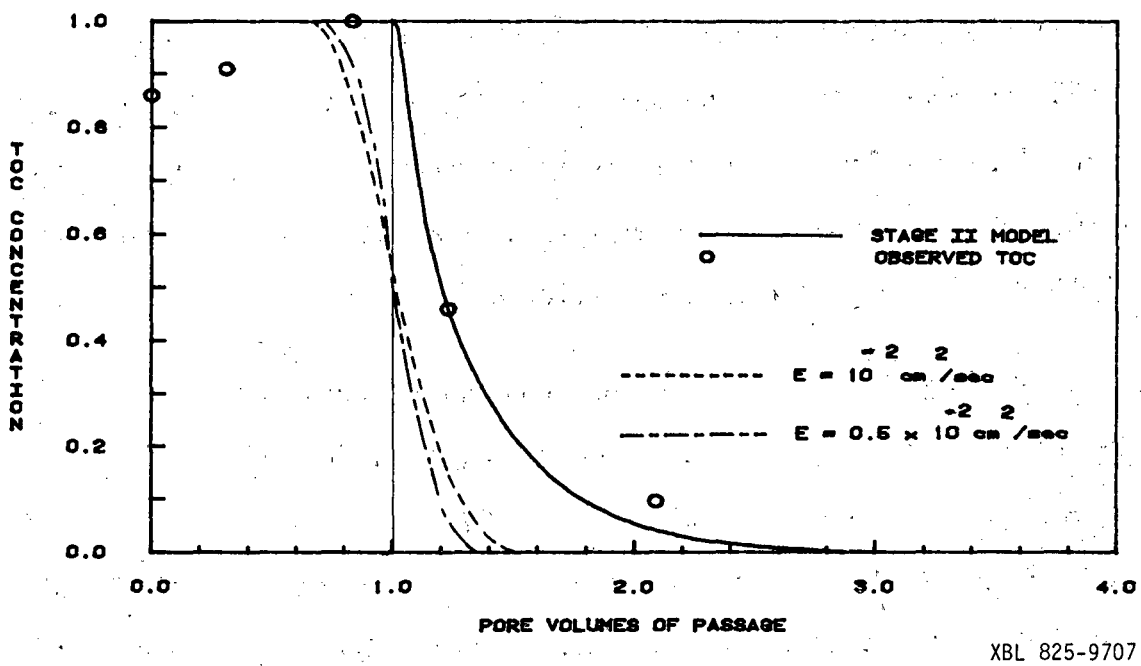

Figure V-13. A comparison of dispersive mechanisms with observed TOC data and the Stage II model for Run D-8 at 85 cm. Internal porosity = 0.15.

The first of the coefficients was derived from a correlation of a large amount of published data on axial dispersion in beds (Sherwood et al., 1975). This coefficient may be in error by a factor of two or more. The correlation by Sherwood el al. was based on particle Peclet and Reynolds numbers for flow in beds of uniform spherical particles. Dispersion in a bed of mixed sizes and shapes has been little studied, and there is no reliable means to relate the mean particle diameter characterizing a bed of heterogeneous shale fragments to dispersion in the pore fluid (Sherwood et al., 1975). The second coefficient is an arbitrary reduction of 50 percent of the first to illustrate the sensitivity of the dispersive break-through curve to the axial dispersion coefficient.

The Stage II model and the normalized observed TOC for the run, as shown on Figure V-11, are plotted on V-13 for comparative purposes. The dispersive mechanism, for an axial coefficient of 10^{-2} cm^2 /sec, is observed to contribute to the observed break-through curve for about half of the duration of Stage II. The mechanism for the smaller coefficient is seen to contribute less to the observed break-through curve, particularly at the point of observation used to define the Stage II curve. The TOC observation at 0.8 pore volume offers evidence that dispersion may not have been as severe as indicated by the larger coefficient.

Dispersion curves were calculated from Equation V-6 for each run in Table V-1 and were compared with the Stage II model and observed data for the particular run. In each case, the dispersive mechanisms calculated with a dispersion coefficient of 10^{-2} cm^2 /sec were shown

to contribute in some degree to the observed break-through curve at the point of observation defining the Stage II curve.

The uncertainity in the dispersion coefficient precludes the calculation of the actual contribution of the dispersive mechanisms to the observed break-through curve. In addition, the solutions of Equations V-6 and the Stage II model are not additive, even though they are based on the same original equation. The following general observations can, however, be made.

1. Dispersive mechanisms may have contributed to the observed break-through curves upon which the calculated diffusion coefficients were based. If this is correct, these coefficients may also include some contribution from dispersion.

2. A fifty percent reduction in the axial dispersion coefficient was shown to reduce the dispersive contribution to the observed break-through curves significantly and furthermore that this revised coefficient may be reasonable based on observed data.

3. Based on the foregoing, it will be necessary to either include axial dispersion in further studies of Stage II leaching mechanisms or show conclusively that it may be safely neglected for the conditions of the experiment.

An approach for future investigations is suggested by Figure V-13. The inclusion of the axial dispersion term in the derivation of the Stage II model, along with internal mass transfer, would define a model in which the dispersive and diffusive mechanisms are additive.

Experimental verification could then be directed toward defining either the axial dispersion coefficient or the internal diffusion coefficient. The determination of either factor would then permit the calculation of the other coefficient. The contribution of each mechanism to the total observed break-through curve could then be investigated for a range of conditions. A comparison of the experimental and calculated factors with those in the literature would also aid in the identification of the rate-limiting mechanisms involved.

Analysis of Calculated Diffusion Coefficients

The diffusion coefficients listed in Table V-1 for Runs D-1 and D-4 through D-8 vary from 1.0 to 4.8 x 10^{-5} cm^2/sec. The value for run D-2 was more than an order of magnitude higher, reasons for this will be discussed subsequently.

A principal assumption in the derivation of the Stage II model was that one mechanism would be rate limiting and that this mechanism might be identified by the size of the coefficient determined from analysis of the experimental data. One means of mass transfer within the pore planes of the physical model is molecular diffusion. Experimental values of molecular diffusion of organic compounds at very low concentrations in water are in the order of 10^{-5} cm^2/sec (Sherwood et al., 1975). Typical values are 0.58, 1.0 and 1.5 x 10^{-5} cm^2/sec. for pyridine, benzoic acid and oxalic acid, respectively. The mean of the calculated diffusion coefficients in Table V-1, excluding D-2, is 2.4 x 10^{-5} cm^2/sec. This is slightly larger than the typical diffusivities given for organic compounds in water. The relatively good agreement appears to confirm that molecular

diffusion in the pore planes is a primary mechanism of mass transport and that the Stage II model is a valid representation of the mechanisms involved.

The reason for the high value of diffusivity calculated for Run D-2 cannot be determined with certainity. The shale used in this run, (-1 to +1/2 inch), was larger than that used in the other small columns listed in Table V-1 and consequently bigger pore channels may have been formed. There was thus more chance for leachate channelization in run D-2 with subsequent early break-through and late tailing of solute. The high diffusivity factor therefore probably reflects a significant contribution from a distorted break-through curve.

One of the more significant factors affecting the magnitude of the calculated diffusion coefficients may be the amount of unknown internal porosity and the relationship of this internal porosity to the total porosity. Varying the porosity factors was seen to have a significant impact on the size of the calculated coefficient. Decreasing the internal porosity from 0.20 to 0.10 decreased the calculated diffusion coefficients for run D-5 from 7.2 to 3.0 x 10^{-5} cm^2 /sec, as shown in Tables V-2 and V-3. On the other hand, a similar decrease in internal porosity decreased the coefficient for run D-8 at 85 cm only from 1.5 to 1.4 x 10^{-5} cm^2/sec.

The selection of a particular value for internal porosity defines other porosity factors such as external porosity and the m ratio, as well as associated parameters including pore velocity. A decrease in internal porosity results in a reduced pore velocity.

The reduction of pore velocity below a certain point leads to an infeasible solution because the pore volume passage factor becomes less than unity. All runs analysed for an internal porosity of 0.20 gave feasible solutions, as shown in Table V-2. Two runs for the 0.15 case were infeasible, as shown in Table V-1. Only the three runs shown in Table V-3 resulted in feasible solutions for an internal porosity of 0.10.

The impact of a change in internal porosity on the break-through curve and the plotted data may be seen by comparing Figure V-11 with Figures V-14 and V-15. These three figures present the data from Run D-8 at 85 cm for internal porosities of 0.15, 0.20, and 0.10, respectively. Stage II model curves are seen to become steeper and the plotted observed data to move toward the left as the internal porosity decreases.

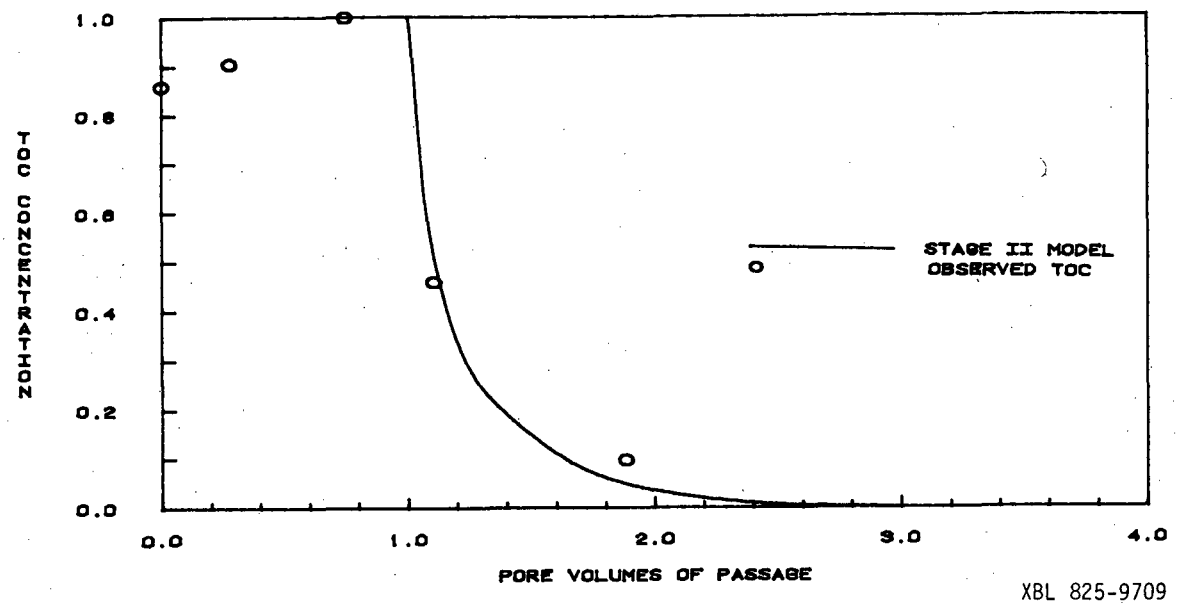

Figure V-14. Break-through curves and normalized observed TOC concentrations plotted versus pore volumes of passage. Run D-8, 85 cm bed depth and 0.20 internal porosity.

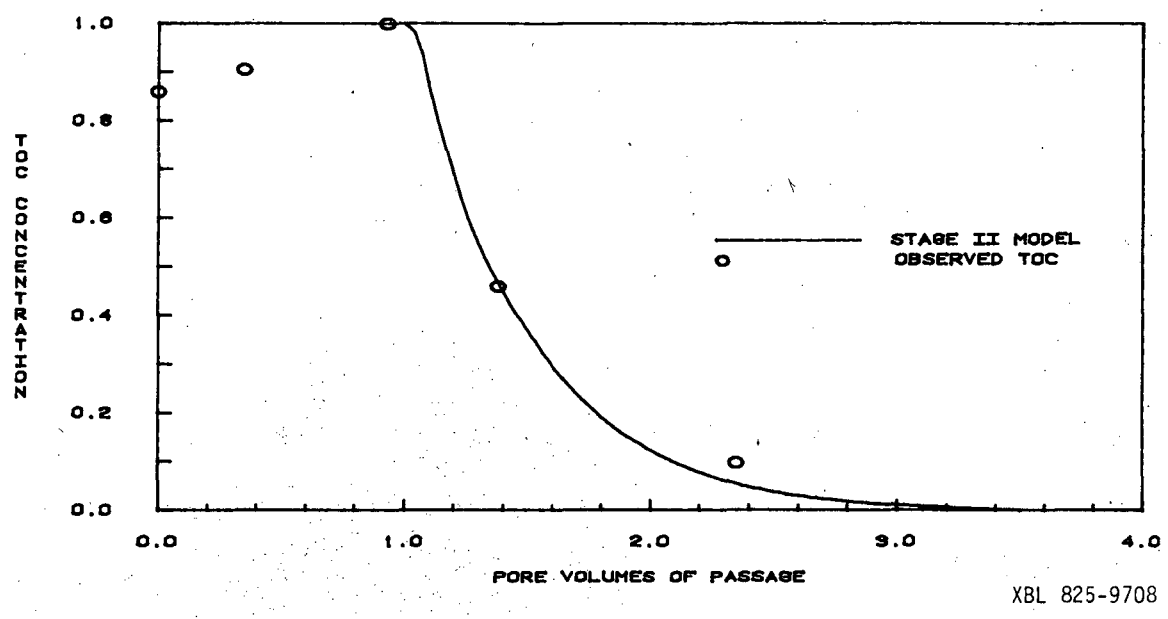

Figure V-15. Break-through curves and normalized observed TOC concentrations plotted versus pore volumes of passage. Run D-8, 85 cm bed depth and 0.20 internal porosity.

An increase in the assumed total porosity, while holding internal porosity constant, was also shown to decrease the computed diffusion coefficients. The total porosity for Run D-5 was arbitrarily increased from the measured 0.61 to 0.65. Such an increase could be realistic if the micro-pores were not completely filled at the time of measurement. The calculated diffusion coefficient at a bed depth of 85 cm for an internal porosity of 0.20 was reduced from 7.2 to 2.7 10^{-5} cm^2 /sec as shown in Tables V-2 and V-3.

It may be concluded that a better definition of the porosity relationships would result in diffusion coefficients that are more representative of molecular diffusion and therefore the selection of this mechanisms a rate limiting process is entirely reasonable.

STAGE III MODEL VERIFICATION

Low but significant TOC concentrations were observed long after the cessation of the Stage II mechanisms. Run D-2 is an example, as shown in Table A-12 in Appendix A. TOC effluent levels in the order of 1 mg/L were still being observed after 748 hours of leaching.

Stage III mechanisms were characterized by a mass transfer coefficient determined from the quiescent leaching studies of Chapter III. It was assumed that the mechanisms involved in Stage III are similar to those which occurred during quiescent leaching. In each case, readily available solute had been removed from the surface of the solid phase prior to the start of the process and the leachate concentrations were at low levels. The principal difference was that the fluid moved at low velocities during Stage III and was at rest

during quiescent leaching. The rate limiting mechanisms of Stage III were assumed to be not affected by the liquid velocity.

A mean mass transfer coefficient K of 2.0×10^{-7} mg/hr-cm^2-mg/L, defined by Equation IV-16 and derived from the quiescent leaching studies described in Chapter III, was used in the Stage III model.

The Stage III model was verified by first expressing the differential equation of IV-14 in finite terms and then solving for the loss in TOC from the solid phase for an assumed concentration gradient between phases. The gain in leachate TOC concentration due to a loss from a known amount of shale was then computed for a given flow rate and then compared with observed data.

Equation IV-14 expressed in finite form is:

$$\frac{\Delta q}{\Delta t} = \frac{Ka}{\rho_B} (C^* - C) \qquad \text{(V-7)}$$

in which:

Δq = Change in TOC in solid phase (mg/L)

Δt = Change in time (hrs)

K = Mass transfer coefficient (2×10^{-7} mg/hr-cm^2-mg/L)

a = Interfacial area (2.3 cm^2/cm^3)

ρ_B = Bulk density (0.88 gm/cm^3)

C^* = Phase equilibrium concentration in leachate (22.5 mg/L)

C = Leachate concentration (mg/L)

The loss in solid TOC per unit weight of shale for the parameters in the above tabulation and an assumed concentration gradient of 22.4 mg/L (i.e. C = 0.1 mg/L) was 1.2×10^{-5} mg TOC transferred per g of shale per hour. The corresponding loss in solid TOC for a 100-cm-deep bed in a small column for this rate was calculated to be 0.11 mg/hr. This amount of TOC would increase effluent TOC concentrations by about 0.1 mg/L in a leachate flow of 20 ml/min. A smaller leachate flow of 5 ml/min would attain a slightly higher concentration of 0.3 mg/L.

The observed effluent TOC concentration during Stage III in the small columns can be verified only in a general manner by referring to the tabulated TOC data in the tables in Appendix A. After 10 hours of operation, observed TOC concentrations in many of the small columns dropped to below 1 mg/L. The precision of analyses is not sufficient to verify that concentrations actually dropped to the low levels predicted by the solution of the model.

The confirmation, however, that calculated concentrations are in the correct order of magnitude is encouraging and offers evidence that the assumptions used in the derivation of the Stage III model are reasonable. It is hypothesized that the Stage III mechanisms involve the release of TOC by slow dissolution of the mineral matrix from the pore walls and the subsequent diffusion of TOC within the

micro-pores, through the phase interface and into the macro-pores. Some transport of TOC within the mineral may also be involved. The low value of the mass transfer coefficient K is indicative of the types of mechanisms hypothesized in Stage III leaching. It is two to three orders of magnitude lower than coefficients observed for cases in which mass transfer from surfaces through interface films was rate limiting (Sherwood et al., 1975).

In future investigations it should be possible to incorporate Stage III in the leaching and transport model along with the Stage II and dispersive mechanisms. One approach might be to include Stage III in the form of Equation IV-14. The rate of mass transfer during Stage III would then be governed by the concentration gradient between phases. Inclusion of a TOC source term would allow the Stage III concentrations to drop as the source in depleted.

ANALYSIS OF LEACHING IN LARGE COLUMNS

Normalized observed TOC concentrations from the three large column experiments, plotted against pore volumes of passage, are shown on Figures V-16 through V-21. Stage II model break-through curves are also shown for comparison purposes. Calculations are based on an internal porosity of 0.15 and a constant diffusivity coefficient of 2.4×10^{-5} cm^2 / sec. A summary of parameters used in the calculations is shown in Table V-4 and additional data is given in Table III-18.

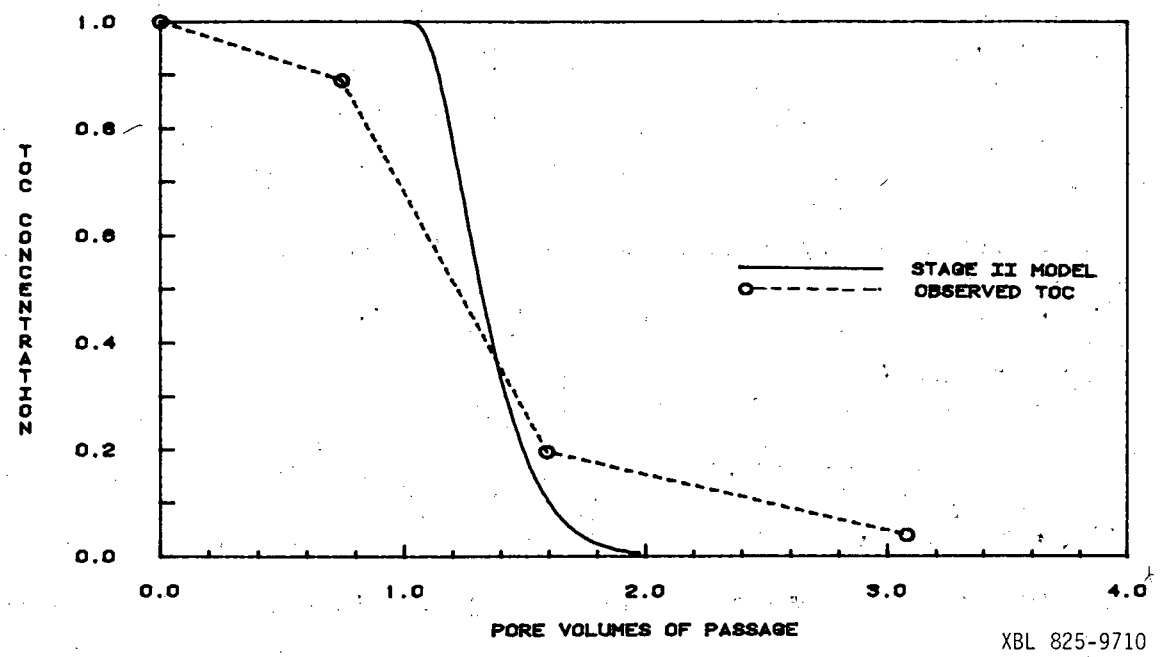

Figure V-16. Break-through curve and normalized observed TOC concentrations plotted versus pore volumes of passage. Run LC-1, 58 cm bed depth, and 0.15 internal porosity.

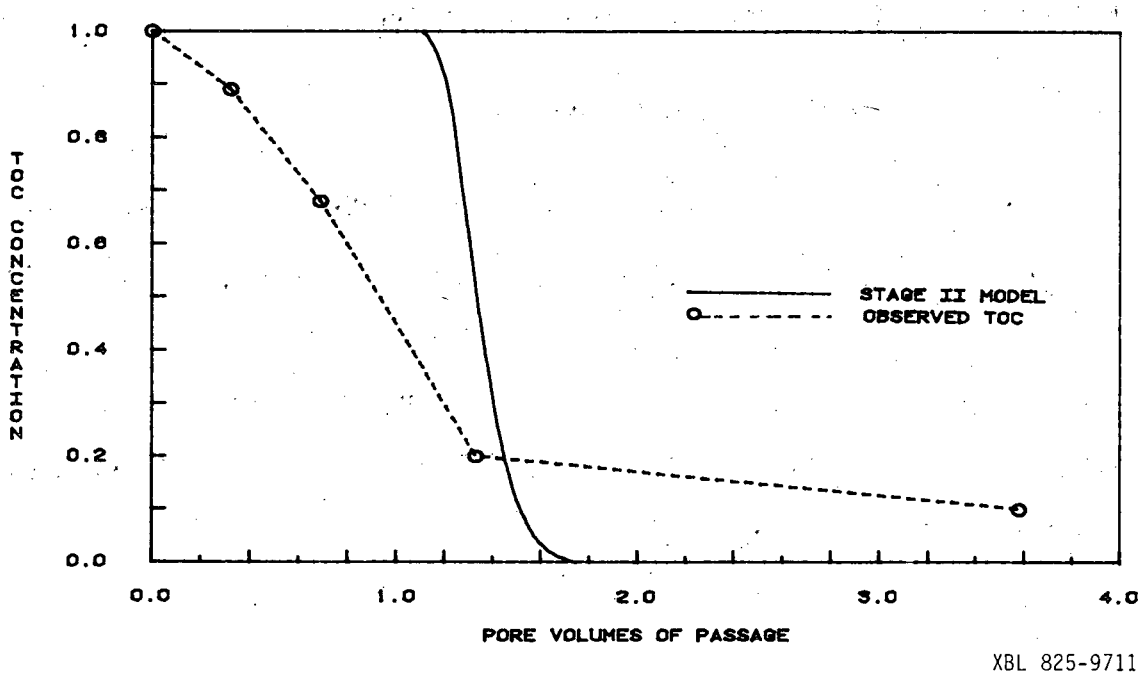

Figure V-17. Break-through curve and normalized observed TOC concentrations plotted versus pore volumes of passage. Run LC-1, 134 cm bed depth, and 0.15 internal porosity.

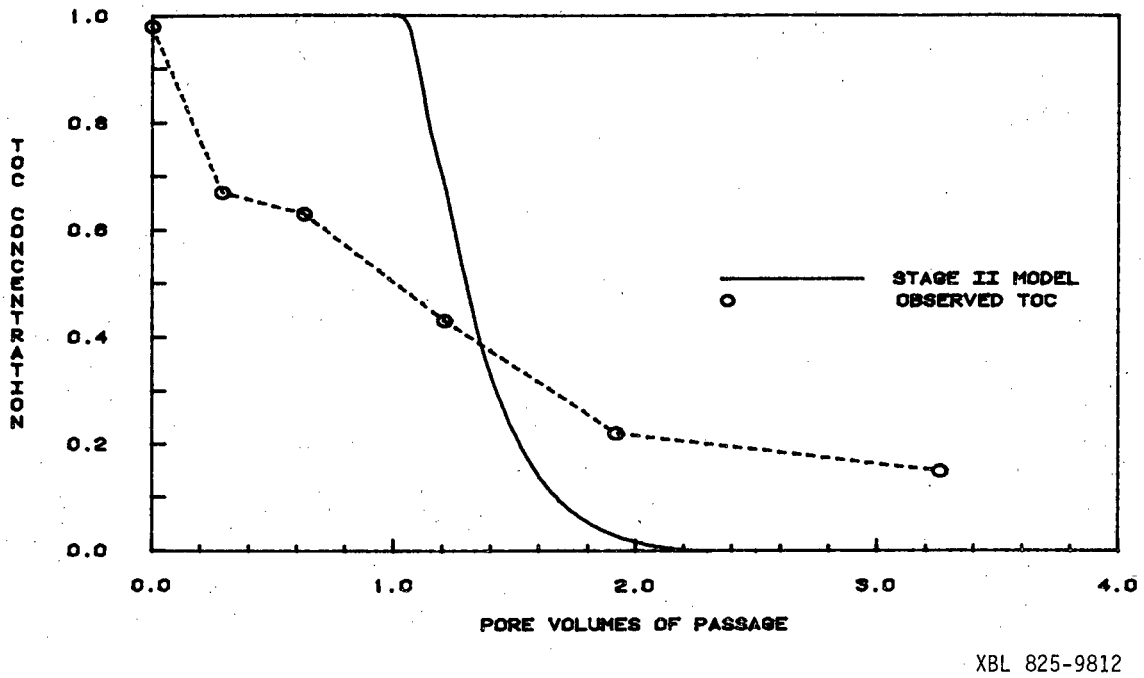

Figure V-18. Break-through curve and normalized observed TOC concentrations plotted versus pore volumes of passage. Run LC-2, 68 cm bed depth, and 0.15 internal porosity.

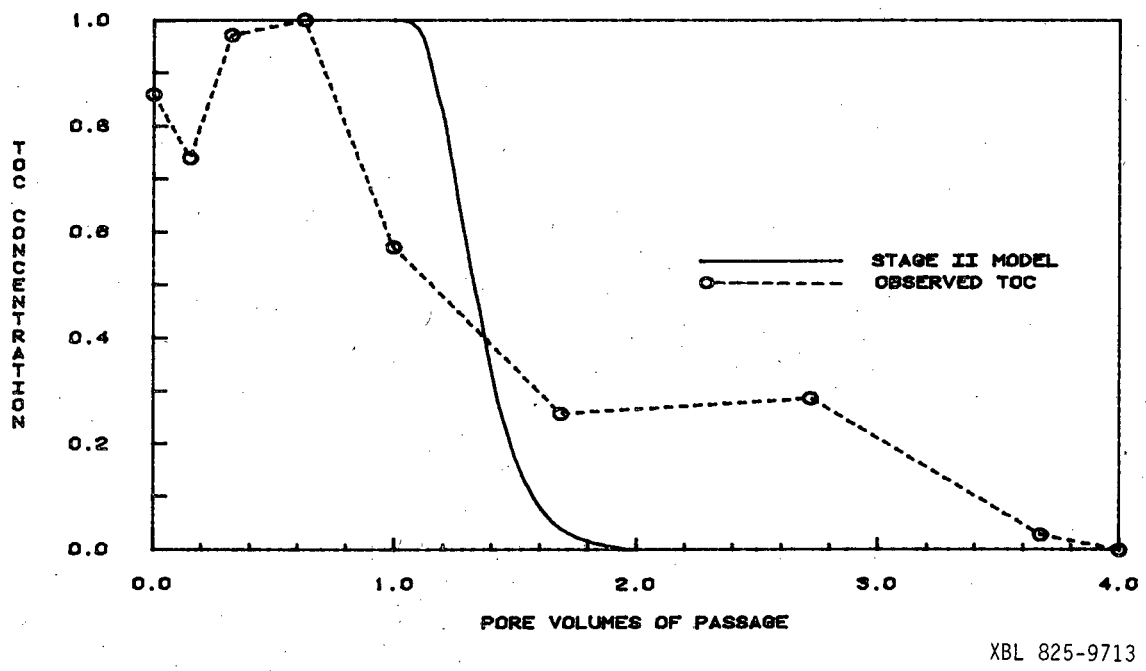

Figure V-19. Break-through curve and normalized observed TOC concentrations plotted versus pore volumes of passage. Run LC-2, 145 cm bed depth, and 0.15 internal porosity.

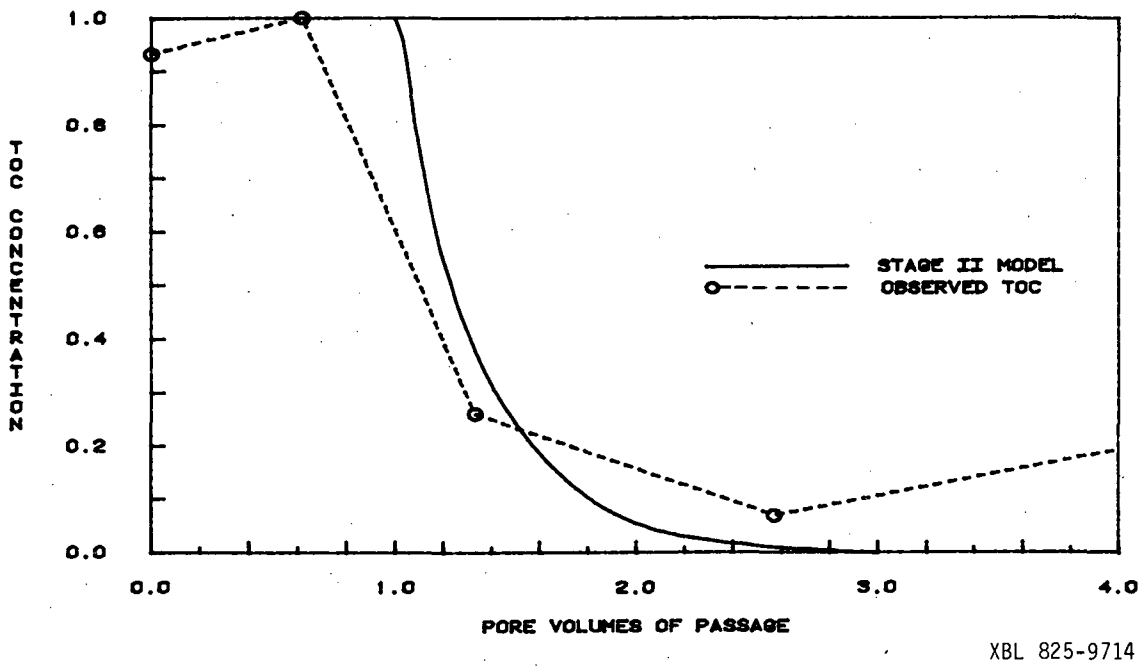

Figure V-20. Break-through curve and normalized observed TOC concentrations plotted versus pore volumes of passage. Run LC-3, 68 cm bed depth, and 0.15 internal porosity.

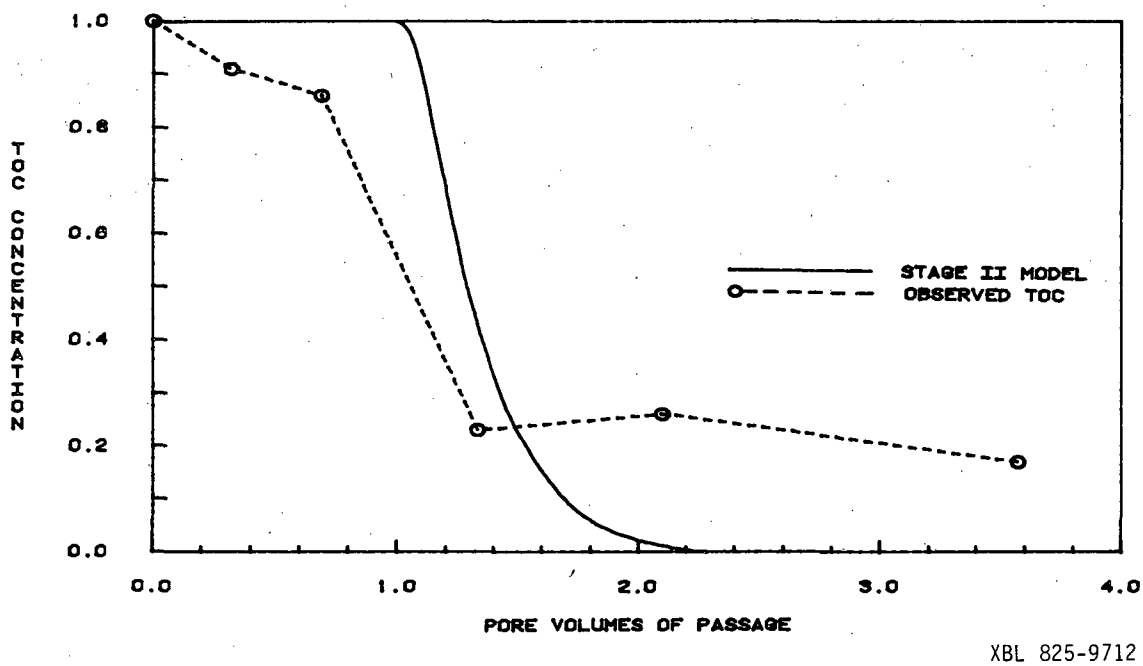

Figure V-21. Break-through curve and normalized observed TOC concentrations plotted versus pore volumes of passage. Run LC-3, 145 cm bed depth, and 0.15 internal porosity.

Table V-4

Large Columns
Summary of Parameters used for Calculation
of Break-through Curves

Run no.	Z Bed Depth cm	b Part. Radius cm	C_o Norm. Conc. mg/L	U_p Pore Vel. 10^{-3} cm/sec	ALPHAX	D/b^2 10^{-4} sec^{-1}	D_m Diff. Coef. 10^{-4} cm^2/sec
LC-1	58	0.4	60	3.4	3.7	1.5	2.4
LC-1	134	0.4	60	3.4	8.6	1.5	2.4
LC-2	68	0.8	35	1.7	2.1	3.8	2.4
LC-2	145	0.8	35	1.7	4.4	3.8	2.4
LC-3	68	0.8	46	3.4	1.1	3.8	2.4
LC-3	145	0.8	46	3.4	2.3	3.8	2.4

The plotted data exhibit the early break-through and late tailing characteristics of dispersive mechanisms; consequently, no verification of the Stage II and III models could be made with the large column data. The distortion precluded the calculation of Stage II diffusivities by the methods used for the small columns because there were no concentration data available from which to calculate the Stage II model parameters. In addition, the distorted tails of the break-through curves were too high to provide verification of the Stage III model. Column LC-2 was the only one to attain the low levels below 1.0 mg/L necessary to verify the Stage III model and these were not reached until after the passage of more than 4 pore volumes.

An attempt was undertaken to determine the reasons for the distortion of data by comparison with the more successful small column experiments. The latter were packed with shale taken from the same size classifications and were operated in a similar manner to the large columns. A major difference, however, was that the large columns were operated outdoors instead of in the laboratory. The small column data did not exhibit the significant drop before the passage of the first pore volume, as seen in the larger column data. TOC observations in the Stage III region were also generally lower in the small column results.

Data taken across the cross-section evidenced non-plug-flow conditions in the large columns. Significant variations, greater than can be explained by non-homogeneity of the shale, are seen in Tables A-28 through A-36 in Appendix A for EC, pH, and TOC data. No consistent pattern of solute transport could be identified as illustrated by reference to the EC data given in Tables A-29, A-32, and A-35. Maximum or minimum EC values can not be correlated with tap location. Coefficients of variation of 10 percent or more are prevalent in these tables for data measured at the three taps at any one time and location.

Dispersion curves, calculated with the aid of Equation V-6, were superimposed on plots of observed data to determine if a consistent pattern of dispersion could be identified. In general, the trend of observed data was represented reasonably well by the slope of the calculated dispersion curves but the data tended to lie above that predicted by the dispersion equation, indicating the presence of

other solute contributing mechanisms. No further analyses were made to determine the amount of the contribution because neither the Stage II model nor Equation V-6 were applicable in the circumstances. The Stage II model is not valid prior to the passage of the first pore volume and Equation V-6 is only approximately correct at intermediate lengths in finite columns.

The possibility of dispersion caused by free-convection currents was also examined. These currents could be driven by density gradients caused by local variations in dissolved salt content or temperature in the fluid. The general problem of density gradients has been discussed by Mandelbaum and Bohm (1973) who found it necessary to compensate for free-convection effects due to density differences during mass transfer at low flow rates.

Krupp et al.(1969) investigated the displacement of liquids in vertical columns containing beds of glass beads by fluids of higher and lower densities. A 0.1N $CaCl_2$ solution (density = 1.005), initially in the bed pores, was first displaced by water. The situation was then reversed with water becoming the displaced fluid. Break-through curves were measured for both upward and downward displacements at several velocities. The data of Krupp et al. showed definite signs of early break-through and late tailing when heavier fluid was uppermost in the column.

The effects of density gradients were observed in small column upflow experiments conducted during the present study when free-convection currents were sufficient to overcome plug flow and almost completely mix the solute throughout the bed.

The magnitude of these free-convection currents may be estimated by a method suggested by Skelland (1974). This method was based on a model of the boundary layer created when flow passes by a vertical flat plate. A density gradient is formed in the boundary layer by the dissolution of solute from the solid phase represented by the plate. This gradient varies from a high of p_o at the phase interface to p_∞, the density in the bulk fluid at the far edge of the boundary layer. The vertical component of this gradient becomes the driving force for the free convection currents.

Maximum velocities in the density currents, calculated by the method, for several fluid density gradients are tabulated in Table V-5.

Table V-5

Maximum Velocity in Macro-pores
Due to Density Gradients

Fluid Density g/cm^3		Maximum Velocity cm/sec
Interface p_o	Bulk Fluid p_∞	U_{max}
1.005	1.002	0.041
1.004	1.003	0.024
1.0036	1.0034	0.011

A fluid density of 1.005 corresponds to a dissolved salt concentration of about 7500 mg/L, a value frequently attained in early stages of many of the batch and column tests.

There exists no evidence to support the belief that density gradients due to salts alone were sufficient to create free convection currents in excess of forced convection because this effect appeared to be relatively minor in the small columns operated in the downflow mode. It is, however strongly suspected that temperature gradients may have been the cause of the distorted break-through curves in the large columns. The water supply used for leaching was taken from an underground service and had a temperature in the order of 17 ^{o}C during the run. The columns were located in a sheltered area in an angle formed by two buildings and were exposed fully to the sun during daylight hours. Unfortunately, temperatures were recorded only at the time of sampling, but daytime temperatures ranging from 26 ^{o} to 29 ^{o}C were recorded in a metal-sheathed building located directly adjacent to the columns. It was therefore likely that temperatures considerable in excess of 17°C were obtained in the columns since the exteriors were not insulated.

It is reasonable to assume that denser threads of fresh water at 17 ^{o}C extended down through the warmer bed from the pool at the top. Soluble salts would move from the solid to the liquid phases thus increasing the density of all the fluid more or less uniformly with little regard to temperature differences. The cooler, more dense, threads of fluids would tend to move faster than lighter fluids carrying the same amount of solute. Solute contained in the lighter, less dense fluid would be delayed thus contributing to the extended tail.

The densities of water at 17 ^{o} and 22 ^{o}C are 0.9988 and 0.9978 respectively, a density difference of 0.001 g/cm^3. A difference of this magnitude for the concentration model assumed by Skelland produces a velocity of 0.024 cm/sec, a value several times higher than the forced convection velocities as shown in Table-18. It can be presumed, therefore that a significant potential exists for dispersion due to temperature gradients.

The following conclusions were reached even though the large column experiments were not successful in providing data for verification testing of the Stage II and III models.

1. Further pilot-scale column leaching experiments should be conducted under temperature controlled conditions to minimize the effects of temperature caused density gradients. The entering water should be at the same temperature as the water in the columns.

2. The presence of free convection currents caused by density gradients must be considered in field scale application of a leaching and transport model to an abandoned in-situ retort. Two particular circumstances can be identified in which free-convection currents driven by density gradients may be significant:

   a. Density gradients will be created by differential leaching as returning groundwater passes through the abandoned retort.

b. Density gradients of considerable magnitude may be caused by the differentials in temperature between the heated rock and the entering groundwater.

CHAPTER VI
SUMMARY, CONCLUSIONS AND RECOMMENDATIONS

STUDY OBJECTIVES

The objectives of the study were to:

1. Identify Rate-Limiting Mechanisms

   Evaluate mass transfer mechanisms involved in the leaching of in-situ spent shale by water and determine which are rate-limiting.

2. Determine Response of Mass Transfer Coefficients to System Changes

   Evaluate changes in mass transfer coefficients with respect to changes in bed media, approach velocity and bed porosity.

3. Model Transport Mechanisms

   Develop a mathematical model of the variation of concentration of organics with time and depth in a spent shale bed.

SUMMARY OF STUDY

A series of batch and column experiments were conducted to leach spent shale obtained from the 10-ton simulated in-situ retort of the Laramie Energy Technology Center. The inorganic and organic content of the shale and leachate were characterized by electrical conductivity (EC) and total organic carbon (TOC). The primary solute of interest for model development, testing and verification was TOC.

A schematic of a typical column effluent break-through curve was the basis of the physical and mathematical models. Three stages of mass transfer were assumed. Stage I takes place and is completed during the period before the first pore volume of fluid passes through the bed. Stages II and III start immediately upon passage of the first pore volume. Stage II is dominant at first and then disappears, leaving Stage III to continue alone for an indefinite period.

The basic element in the spent shale bed was assumed to be a cylinder containing pore planes lying normal to the axis. Bed porosity was characterized by a bi-modal system containing large and small pores. Solute transport in the micro-pores, within the pore planes, is by diffusive mechanisms alone. Transport in the macro-pores among the bed media is by convective, dispersive, and diffusive mechanisms.

Solute transport begins immediately upon the introduction of water to the dry bed. Soluble material moves from the surface of the solid to the liquid in the micro-pores until phase equilibria is reached.

The solute present at the time of the first pore volume passage of leachate is removed from the micro-pores by stage II mechanisms As soon as the concentration in the micro-pores drops, additional material is transported from the solid phase to the micro- pore liquid. The removal of this solute is accomplished by Stage III mechanisms. The depletion of soluble material at the particle surface forces solute to move to the phase interface from sites within the mineral matrix. After the Stage II solute has been removed, the transport of Stage III solute approaches steady state. Stage II and

Stage III solute are thus present in the micro-pores at the same time.

Mathematical models were formulated for Stage II and Stage III mechanisms.

Stage II effluent break-through curves, developed from the solution of the model, were then fit to selected data from a series of small column leaching experiments. Diffusion coefficients calculated from the parameters defining the applicable curves were compared with published data to verify that the underlying assumptions were valid and that the rate-limiting mechanism was correctly chosen. The Stage III model was verified with data from the small column.

FULFILLMENT OF OBJECTIVES

1. Identify Rate Limiting Mass Transfer Mechanisms

Mass transfer mechanisms acting within the solid and liquid phases of the spent shale bed and the domains in which they are applicable were enumerated. A rate-limiting mass transfer mechanism was then hypothesized for each of the three stages of the assumed physical model.

Stage I. The Stage I rate-limiting mechanism was assumed to be mass transfer from a surface layer of readily soluble material across the phase interface to micro-pore fluid. Phase equilibrium was assumed to be reached by the end of Stage I. The existence of this mechanism was not verified. However, the assumption appears to be

reasonable in view of the rapid transfer of solute evidenced by the fast build-up of leachate concentrations during this stage.

Stage II. The rate-limiting mechanisms was assumed to be mass transfer by molecular diffusion within the micro-pores driven by the concentration gradient between the micro- and macro-pore systems. Diffusion coefficients varying from 1.0 to 4.8 x 10^{-5} cm^2/sec were calculated from experimental data. The values were close to 10^{-5} cm^2/sec, a mean value for diffusion of weak concentrations of organic compounds in water. This was taken as confirmation that the selection of molecular diffusion in the micro-pores as rate-limiting was reasonable. It was shown that small amounts of dispersion in the macro-pores could account for the slightly higher values of the calculated coefficient. Dispersive mechanisms distort the break-through curves and thus contribute to the calculated Stage II coefficients.

Stage III. The rate-limiting mechanism in Stage II was presumed to be transport within the boundaries of the solid phase. A mass transfer coefficient of 2 x 10^{-7} mg TOC transfer per hr per cm^2 per mg/L of gradient was obtained from static leaching tests. The low value of the observed mass transfer coefficient was taken as evidence of the type of rate-limiting mechanism present. The mechanism was not identified per se, but it is quite likely that dissolution of the minerals in the pore walls plays a significant role. Dissolution would release TOC from a large reservoir of TOC within the solid. The presence of this reservoir was confirmed by chemical analysis of the shale.

2. Determine Response of Mass Transfer Coefficients to System Changes.

Changes in mass transfer coefficients were evaluated with respect to changes in bed media size, approach velocity, and bed porosity. Significant factors were found to be porosity relationships within the bed and the physical characteristics of the system which affected the amount of fluid dispersion.

Porosity relationships must be well defined to obtain a realistic estimate of the rate-limiting dispersion coefficient. Internal and external porosity of the shale in the column beds were not measured directly in the present experiments. The sensitivity of the calculated diffusion coefficients to the porosity relationships was tested by varying the porosity parameters over reasonable ranges. Reduction of internal porosity from 0.20 to 0.15 and, in some cases, to 0.10 reduced calculated diffusion coefficients significantly. The increase of total porosity from 0.61 to 0.65 while holding internal porosity constant was also shown in one case to decrease the calculated diffusion coefficient.

Dispersion was shown to contribute to a small extent to the calculated dispersion coefficient. Bed dispersion is a function of pore velocity, particle size, and temperature and density gradients. The relatively low velocities used in the experiments minimized the effects of the first two items. Density gradients caused by local temperature and concentration differences in the leachate were shown to have a considerable impact on the results, particularly in the early small column upflow experiments and in the large columns.

3. Model Transport Mechanisms

Mathematical models of Stage II and Stage III mechanisms were developed, solved, and verified. No model was developed for Stage I. The derivation of the Stage II model involved several simplifying assumptions, including the presumption of plug flow, the conservation of solute, and the neglect of Stage III mechanisms during Stage II. The resulting equation, based on the classic advection-dispersion equation, was solved by a numerical inversion of a Laplace transform.

The Stage II model was shown to be a realistic representation of the portion of the break-through curve immediately after the passage of the first pore volume.

The Stage III mathematical model was derived from a mass balance of solute in the system. A mass transfer coefficient, derived from long term static leaching studies, completed the Stage III model. The Stage III model was verified to a limited extent. The assumptions used in the derivation of the model were found to be reasonable. The inclusion of the Stage III model, as formulated, in the overall physical and mathematical model for use in further leaching investigations was justified.

RECOMMENDATIONS

Discrete observations and conclusions, identified during the course of the study, are discussed in the context of two general recommendations:

1. Future studies of spent shale leaching must give due consideration to mass transport kinetic mechanisms. The development of physical and mathematical kinetic models early in the investigation is recommended.

2. A multi-disciplinary approach should be used to formulate these models and to conduct the investigations.

Model Framework

Physical and mathematical models of mass transport in spent shale should be developed at the start of any future leaching study. Detailed characterization studies of shale and leachate without consideration of intra- and inter-particle mass transport tend to become little more than tabulations of species concentrations valid only for a given material leached under a particular set of conditions. Extrapolation of results to other materials or conditions is impossible.

The validity of the approach was shown in the present study. Complex advection and inter-particle mass transport phenomena were reduced to manageable dimensions by appropriate assumptions. The assumptions were based on experimental observations and were included in the physical and mathematical models. The model was shown to represent experimental data fairly well in the applicable region of the break-through curve. In addition, the use of the model aided in the identification of additional mechanisms which, upon incorporation, would likely improve the model performance.

The advection-dispersion equation, represented by Equation II-1, is recommended for use as the basis of the mathematical model. This equation includes terms for dispersion, advection, reaction, and internal mass transport. Source terms can be readily added to meet the requirements of the physical model.

Momentum and energy transport can also be included in the mathematical model based on Equation II-1. This aspect was not explicitly discussed in this study but becomes obvious upon recognizing the similitude that exists among transport phenomena (Bird et al., 1960).

It should be emphasized that this recommendation does not imply that models be derived to include all heat, momentum and mass transport mechanisms. Such an effort would be counter-productive as some mechanisms are insignificant, undefined or not pertinent to the problem at hand. Simple models may be expanded as the need requires.

Multi-disciplinary Approach

The study of leaching of spent shale in abandoned in-situ retorts is an ideal application of the multi-disciplinary effort because of the complexity and diversity of the subject. Available and attained knowledge in several disciplines can be readily integrated by the physical and mathematical models described above.

In the present study, several disciplines were referenced, including chemical engineering, geo-physics, geo-chemistry, and soil science. For example, the work by Rasmunsen and Neretricks on the transport of radio-nuclides in fractured systems has direct

application to leaching of spent shale because of the similarity of the transport mechanisms and the physical systems.

Specific areas in leaching of spent shale in abandoned in-situ retorts where multi-disciplinary input may be helpful are:

1. Physical characterization of a mixed bed of shale particles to define, preferably on a statistical basis, internal and external porosity relationships and particle surface area, shape and size. This will become important as the scale of the system increases. The larger the particles in the retort the more difficult it will be to characterize the bed.

2. Chemical characterization of spent shale to define species type and distribution. This will be crucial in studies of Stage III leaching when mass is transferred by low rate mechanisms. The use of EC and TOC as characteristic indicators was justified in the present study. Their use, however, in further studies as the solute of interest is not recommended as they can not represent changes with time in individual species. Dissolution investigations and transport of organics should be conducted with specific species as tracers.

3. The identification and definition of mechanisms of mass, energy and momentum transport. These mechanisms will become significant, particularly during large scale investigations. Specific examples include the effects of

density gradients and dispersion in beds of mixed particles sizes and shapes. Approximations valid for homogeneous and uniform particles in laboratory columns may not be applicable to abandoned retorts.

4. The formulation and analysis of the mathematical models of transport. The advective-dispersive equation has been applied to many different systems. Numerous numerical techniques are available for the solution. These range for the numerical inversion of Laplace Transforms used in the present studies to powerful finite element analysis techniques.

APPENDIX A
COLUMN LEACHING DATA

Leaching conditions for columns in this appendix are summarized in Tables III-17 and III-18 for small and large columns, respectively. Missing data are identified by a dash (-). TOC concentrations less than 1.0 mg/L are shown as <1. Far, Cent. and Near in Tables A-28 through A-36 refer to the sample tap locations at the quarter points of the column cross-section.

TOC leaching data are discussed in the text of this report in terms of pore volumes, defined as the product of clock time since the start of flow and interstitial velocity divided by the length of column to the point of interest. A summary of interstitial (pore) velocities for the small and large columns follows for an assumed internal porosity of 0.15. These velocities may be used along with the applicable time and distance to calculate the pore volumes of passage at any of the sample points.

Column No.	Pore Vel. cm/hr
U-1	8.7
U-2	8.7
D-1	8.6
D-2	20
D-3	6.1
D-4	16
D-5	50
D-6	73
D-7	71
D-8	26
LC-1	12.6
LC-2	6.2
LC-3	12.1

Table A-1

Small Column U-1

Electrical Conductivity of Leachate

Series	Time	Electrical Conductivity-mmhos/cm						
		Leaching Distance-cm						
	hrs	15	30	45	60	75	90	105
10	1.0	6.8	9.5	11.2	12.0	-	10.5	8.0
20	3.0	5.2	7.2	9.8	10.4	9.5	9.2	8.3
30	9.0	6.1	-	-	-	-	-	-
40	19	-	-	-	-	-	-	-
50	26	3.1	3.3	3.6	-	3.9	-	3.6
60	43	1.9	2.4	2.8	-	2.7	-	2.5
70	51	1.4	1.9	2.3	-	2.4	-	2.2
80	67	1.3	1.6	2.1	-	2.0	-	1.9

Table A-2

Small Column U-1

Total Organic Carbon in Leachate

Series	Time	Total Organic Carbon - mg/L						
		Leaching Distance-cm						
	hrs	15	30	45	60	75	90	105
10	1.0	26	29	34	36	34	32	28
20	3.0	18	25	33	34	31	30	29
30	9.0	21	23	20	-	20	-	16
40	19	12	11	17	-	14	-	16
50	26	10	6.3	4.5	-	7.9	-	8.5
60	43	3.3	1.3	5.1	-	3.5	-	3.4
70	51	7.3	4.9	4.6	-	-	-	3.8
80	67	1.0	2.5	3.4	-	3.9	-	5.5

Table A-3

Small Column U-2

pH of Leachate

Series	Time hrs	pH Leaching Distance-cm 15	30	45	60	75	90	105
10	2.2	-	*	*	*	*	*	*
20	3.0	-	*	*	*	*	*	*
30	3.8	-	*	*	*	*	*	*
40	4.8	-	-	*	*	*	*	*
50	6.8	12.20	12.10	11.60	*	*	*	*
60	11	11.80	11.90	11.90	11.90	11.90	*	*
70	14	-	-	-	-	-	-	-
80	23	11.91	11.90	11.85	11.85	11.82	11.80	11.80
90	28	11.85	11.85	11.85	11.80	11.75	11.70	11.65
100	32	11.90	11.85	-	11.80	11.80	11.80	11.80
110	47	11.90	11.85	11.85	11.82	11.75	11.82	11.80
120	55	11.90	11.90	11.85	11.90	11.80	11.80	-
130	72	-	11.95	11.90	11.90	11.85	11.82	-

* Dry material, no sample

Table A-4

Small Column U-2

Electrical Conductivity of Leachate

Series	Time	Electrical Conductivity-mmhos/cm						
		Leaching Distance-cm						
	hrs	15	30	45	60	75	90	105
10	2.2	7.7	*	*	*	*	*	*
20	3.0	10.0	*	*	*	*	*	*
30	3.8	11.2	*	*	*	*	*	*
40	4.8	-	9.3	*	*	*	*	*
50	6.8	11.3	10.9	8.4	*	*	*	*
60	11	10.3	11.2	10.6	11.4	11.1	*	*
70	14	10.3	9.9	9.9	10.5	-	8.0	*
80	23	9.6	8.8	7.0	8.8	7.0	7.6	6.6
90	28	7.2	7.6	6.9	7.7	6.5	6.4	6.6
100	32	7.2	7.0	-	6.5	5.8	5.2	-
110	47	4.2	4.4	4.3	4.1	3.6	3.3	3.1
120	55	3.5	3.6	3.5	3.9	3.0	2.9	-
130	71	-	2.8	2.5	2.1	2.1	2.0	2.1

* - Dry material, no sample

Table A-5

Small Column U-2

Total Organic Carbon in Leachate

Series	Time hrs	Total Organic Carbon - mg/L						
		Leaching Distance-cm						
		15	30	45	60	75	90	105
10	2.2	31	*	*	*	*	*	*
20	3.0	23	*	*	*	*	*	*
30	3.8	31	*	*	*	*	*	*
40	4.8	-	33	*	*	*	*	*
50	6.8	40	34	32	*	*	*	*
60	11	28	35	28	34	32	*	*
70	14	35	32	31	37	29	30	*
80	23	24	23	21	20	17	16	17
90	28	-	-	-	-	-	-	-
100	32	30	25	20	24	21	21	19
110	47	12	11	14	19	17	15	-
120	55	12	12	12	8.0	8.0	8.0	7.0
130	71	8.0	15	12	13	13	13	8.0
140	80	4.3	5.5	4.6	4.8	4.7	4.8	3.1

* - Dry material, no sample

Table A-6

Small Column D-1

pH of Leachate

Series	Time Hrs	pH Leaching Distance-cm 10	25	40	55	70	85
00	0	12.50	12.50	12.42	12.36	12.38	12.39
10	3.5	11.98	12.37	12.72	12.74	12.72	12.67
20	9.1	11.93	12.16	12.33	12.58	12.70	12.72
30	19	11.85	11.94	12.11	12.23	12.26	12.38
40	46	11.33	11.70	11.94	11.98	12.00	12.07
50	115	11.44	11.61	11.87	12.11	12.26	12.10
60	139	11.44	11.95	12.26	12.16	12.51	12.38
70	212	11.36	11.75	11.86	11.90	11.97	12.05
80	289	11.47	11.80	12.04	12.12	11.98	12.03

Table A-7

Small Column D-1

Electrical Conductivity of Leachate

Series	Time	Electrical Conductivity - mmhos/cm					
		Leaching Distance-cm					
	Hrs	10	25	40	55	70	85
00	0	5.1	5.2	5.1	4.9	4.9	4.7
10	3.5	0.95	2.3	5.3	5.3	5.3	5.3
20	9.1	0.75	1.2	2.0	3.4	4.8	5.2
30	19	0.51	0.80	1.1	1.4	1.7	2.2
40	46	0.32	0.53	0.74	0.97	1.0	1.2
50	115	0.24	0.41	0.59	0.74	0.80	0.91
60	139	0.25	0.41	0.58	0.69	0.84	0.99
70	212	0.15	0.28	0.46	0.58	0.68	0.78
80	289	0.18	0.33	0.44	0.57	0.64	0.70

Table A-8

Small Column D-1

Total Organic Carbon in Leachate

Series	Time	Total Organic Carbon - mg/L					
		Leaching Distance-cm					
	hrs	10	25	40	55	70	85
00	0	21.6	26.6	23.0	23.7	20.8	20.1
10	3.5	17.2	18.7	29.0	30.6	27.7	32.4
20	9.1	5.5	10.5	15.5	24.5	34.5	36.5
30	19	4.5	7.5	10.5	10.5	12.5	13.5
40	46	8.5	9.5	4.5	9.5	12.5	12.5
50	115	5.0	8.1	4.6	3.1	8.8	11.3
60	139	3.8	5.3	5.6	5.3	8.3	7.7
70	212	2.2	<1	2.2	<1	5.2	<1
80	289	1.3	1.3	5.0	2.0	3.9	3.2

Table A-9

Small Column D-2

pH of Leachate

Series	Time	pH					
		Leaching Distance-cm					
	hrs	10	25	40	55	70	85
00	0	11.56	11.52	11.56	11.65	11.67	11.67
10	3.5	-	-	-	-	-	-
20	19	10.75	10.96	11.07	11.17	11.21	11.25
30	28	10.51	10.75	10.90	11.01	11.07	11.16
40	52	10.43	10.80	10.99	11.02	11.18	11.22
50	67	10.53	10.82	11.00	11.08	11.17	11.22
60	167	10.59	10.74	10.96	11.06	11.11	11.15
70	243	-	-	-	-	-	-
80	578	9.94	10.29	10.50	10.82	10.86	10.86
90	747	9.89	10.19	10.45	10.68	10.77	11.08

Table A-10

Small Column D-2

Electrical Conductivity of Leachate

Series	Time	Electrical Conductivity - mmhos/cm					
		Leaching Distance-cm					
	hrs	10	25	40	55	70	85
00	0	3.9	3.9	4.2	4.1	4.2	4.3
10	3.5	0.75	1.2	1.9	3.5	4.4	4.5
20	19	0.37	0.58	0.76	0.94	1.1	1.2
30	28	0.33	0.54	0.72	0.84	1.0	1.1
40	52	0.27	0.47	0.64	0.70	0.86	0.96
50	67	0.25	0.43	0.58	0.70	0.82	0.91
60	167	0.16	0.25	0.37	0.47	0.53	0.61
70	243	0.13	0.23	0.32	0.41	0.48	0.53
80	578	0.08	0.15	0.20	0.32	0.34	0.40
90	746	0.08	0.14	0.19	0.29	0.34	0.40

Table A-11

Small Column D-2

Total Organic Carbon in Leachate

Series	Time hrs	Total Organic Carbon - mg/L					
		Leaching Distance-cm					
		10	25	40	55	70	85
00	0	25.	18.	17.	15.	19.	22.
10	3.5	3.2	6.1	11.	16.	20.	20.
20	19	2.8	<1	1.1	1.4	<1	4.4
30	28	1.0	<1	1.4	<1	2.0	2.6
40	52	4.8	<1	<1	2.2	2.9	4.1
50	67	2.0	1.8	<1	3.9	2.0	<1
60	167	<1	<1	<1	<1	-	<1
70	242	-	-	-	-	-	-
80	578	5.0	2.0	<1	<1	1.0	1.0
90	748	1.0	1.2	<1	2.5	<1	<1

Table A-12

Small Column D-3

pH of Leachate

Series	Time	pH					
		Leaching Distance-cm					
	hrs	10	25	40	55	70	85
00	0.9	10.91	11.22	11.56	11.56	11.58	11.61
10	5.2	10.99	11.26	11.61	11.64	11.63	11.62
20	21	10.93	11.15	11.27	11.34	11.40	-
30	29	10.70	10.81	11.16	11.31	11.33	11.38
40	45	10.91	11.18	11.26	11.36	11.47	11.49
50	144	10.31	10.81	10.95	11.30	11.29	11.41
60	220	-	-	-	-	-	-
70	555	10.34	10.80	10.95	11.15	11.32	11.37
80	725	10.59	-	-	-	-	11.37

Table A-13

Small Column D-3

Electrical Conductivity of Leachate

Series	Time	Electrical Conductivity - mmhos/cm					
		Leaching Distance-cm					
	hrs	10	25	40	55	70	85
00	0.9	2.4	3.6	4.8	4.8	4.7	4.8
10	5.2	1.2	2.2	3.7	5.0	5.0	5.0
20	21	0.58	1.0	1.4	1.7	2.2	2.6
30	29	0.56	0.96	1.2	1.6	1.7	2.0
40	45	0.44	0.76	1.1	1.3	1.4	1.7
50	144	0.27	0.51	0.72	0.94	1.0	1.2
60	220	0.19	0.35	0.52	0.57	0.68	0.78
70	555	0.10	0.23	0.40	0.50	0.58	0.68
80	725	0.13	0.28	0.41	0.54	0.60	0.70

Table A-14

Small Column D-3

Total Organic Carbon in Leachate

Series	Time	Total Organic Carbon - mg/L					
		Leaching Distance-cm					
	hrs	10	25	40	55	70	85
00	0.9	16.	20.	19.	28.	20.	19.
10	5.2	8.0	11.	19.	25.	30.	25.
20	21	<1	1.5	2.7	4.4	8.0	5.1
30	29	-	-	-	-	-	-
40	45	<1	3.5	<1	3.8	1.8	<1
50	144	4.4	<1	<1	2.9	4.6	<1
60	220	1.7	2.8	-	-	<1	1.1
70	555	1.0	<1	1.6	1.7	<1	<1
80	725	4.3	<1	<1	<1	<1	<1

Table A-15

Small Column D-4

pH of Leachate

Series	Time	pH					
		Leaching Distance-cm					
	hrs	10	25	40	55	70	85
00	0	11.53	11.55	11.49	11.48	11.56	-
10	1.7	11.11	11.33	11.41	11.36	11.45	11.52
20	3.8	10.90	11.08	11.28	11.43	11.43	11.43
30	6.0	11.01	11.16	11.25	11.30	11.40	11.48
40	8.9	11.29	11.37	11.41	11.45	11.44	11.48
50	10	11.18	11.22	11.30	11.45	11.42	11.47
60	25	11.00	11.12	11.25	11.36	11.40	11.48
70	32	10.97	10.98	11.17	11.53	11.55	11.52
80	56	10.96	11.07	11.14	11.20	11.29	11.31

Table A-16

Small Column D-4

Electrical Conductivity of Leachate

Series	Time	Electrical Conductivity - mmhos/cm					
		Leaching Distance-cm					
	hrs	10	25	40	55	70	85
00	0	8.0	8.0	8.2	7.4	7.8	8.0
10	1.7	1.8	6.5	6.8	8.0	8.0	8.0
20	3.8	0.90	1.4	3.4	6.5	8.0	7.8
30	6.0	0.82	1.2	1.7	2.4	4.1	7.1
40	8.9	0.77	1.2	1.4	1.7	1.9	2.7
50	10	0.68	1.1	1.3	1.6	1.7	2.0
60	25	0.52	0.80	1.1	1.2	1.4	1.4
70	32	0.49	0.69	0.96	1.1	1.2	1.3
80	56	0.46	0.62	0.82	1.0	1.0	1.2

Table A-17

Small Column D-4

Total Organic Carbon in Leachate

Series	Time	Total Organic Carbon - mg/L					
		Leaching Distance-cm					
	Hrs	10	25	40	55	70	85
00	0	36.5	50.5	32.5	31.5	39.5	-
10	1.7	4.5	28.5	36.5	35.5	35.5	35.5
20	3.8	1.4	4.6	16.5	13.5	32.5	31.5
30	6.0	1.5	2.2	6.0	12.5	15.5	30.5
40	8.9	<1	3.1	2.4	2.9	4.2	6.5
50	10	<1	<1	<1	1.5	3.8	5.9
60	25	8.5	10.5	6.3	10.6	8.5	4.3
70	32	-	-	-	-	-	-

Table A-18

Small Column D-5

pH of Leachate

Series	Time	pH					
		Leaching Distance-cm					
	hrs	10	25	40	55	70	85
00	0	11.49	11.45	11.54	11.49	11.54	11.58
10	2.0	10.83	11.09	11.23	11.34	11.39	11.40
20	3.2	10.93	10.99	11.06	11.23	11.25	11.33
30	4.3	10.85	11.00	11.06	11.16	11.13	11.20
40	6.3	10.84	10.91	11.13	11.13	11.16	11.13
50	11	10.82	11.31	11.39	11.43	11.43	11.48
60	25	10.95	11.15	11.20	11.16	11.27	-
70	32	11.22	11.30	11.33	11.36	11.36	-

Table A-19

Small Column D-5

Electrical Conductivity of Leachate

Series	Time	Electrical Conductivity - mmhos/cm					
		Leaching Distance-cm					
	hrs	10	25	40	55	70	85
00	0	8.0	7.2	8.0	6.8	7.0	7.1
10	2.0	0.88	1.3	2.2	4.7	6.5	6.9
20	3.2	0.65	0.92	1.1	1.5	1.8	2.9
30	4.3	0.57	0.80	0.99	1.2	1.3	1.6
40	6.3	0.57	0.73	0.86	0.98	1.1	1.2
50	11	0.44	0.66	0.80	0.88	1.0	1.1
60	25	0.37	0.48	0.58	0.68	0.73	0.85
70	33	0.36	0.38	0.54	0.64	0.66	0.80

Table A-20

Small Column D-5

Total Organic Carbon in Leachate

Series	Time	Total Organic Carbon - mg/L					
		Leaching Distance-cm					
	hrs	10	25	40	55	70	85
00	0	40.5	39.5	38.5	28.5	33.5	34.5
10	2.0	2.8	2.3	7.7	18.5	29.5	26.5
20	3.2	1.9	<1	5.3	2.6	9.5	12.5
30	4.3	<1	<1	<1	2.8	1.1	3.0
40	6.3	3.3	1.9	1.6	2.3	19	4.5
50	11	<1	<1	3.5	-	3.2	1.9
60	25	5.1	5.1	-	-	-	-

Table A-21

Small Column D-6

Electrical Conductivity of Leachate

Series	Time	Electrical Conductivity - mmhos/cm					
		Leaching Distance-cm					
	hrs	10	25	40	55	70	85
00	0	8.8	9.1	9.0	9.2	9.8	10.2
10	1.0	0.82	1.5	2.8	5.4	7.4	8.5
20	2.0	0.58	0.83	1.1	1.4	1.8	2.6
30	3.1	0.50	0.72	0.90	1.1	1.2	1.4
40	4.5	0.48	0.64	0.82	0.91	1.1	1.2
50	5.4	0.47	0.62	0.78	0.92	1.0	1.1
60	21	0.29	0.43	0.53	0.58	0.64	0.70
70	29	0.30	0.40	0.50	0.64	0.70	0.72

Table A-22

Small Column D-6

Total Organic Carbon in Leachate

Series	Time	Total Organic Carbon - mg/L					
		Leaching Distance-cm					
	hrs	10	25	40	55	70	85
00	0	34.5	37.5	33.5	38.5	39.5	38.5
10	1.0	2.7	2.7	-	-	25.5	32.5
20	2.0	1.2	<1	1.9	4.2	4.8	5.9
30	3.1	7.1	1.1	1.4	8.9	3.8	4.3
40	4.5	<1	<1	<1	2.1	1.3	2.7
50	5.4	1.2	<1	<1	4.2	1.7	1.0
60	21	<1	<1	<1	<1	<1	<1
70	29.3	<1	<1	<1	<1	<1	<1

Table A-23

Small Column D-7

Electrical Conductivity of Leachate

Series	Time	Electrical Conductivity - mmhos/cm					
		Leaching Distance-cm					
	hrs	10	25	40	55	70	85
00	0	4.8	6.2	7.6	8.2	8.2	8.6
10	0.9	0.89	1.2	2.4	3.8	6.2	8.2
20	1.9	0.86	1.1	1.6	1.9	2.7	4.1
30	3.2	0.78	1.0	1.4	1.5	1.7	2.0
40	4.7	0.69	0.85	1.2	1.3	1.4	1.6
50	7.9	0.62	0.78	1.0	1.1	1.2	1.3
60	9.9	0.52	0.67	0.93	0.98	1.1	1.2
70	29	0.29	0.38	0.52	0.56	0.62	0.66

Table A-24

Small Column D-7

Total Organic Carbon in Leachate

Series	Time	Total Organic Carbon - mg/L					
		Leaching Distance-cm					
	hrs	10	25	40	55	70	85
00	0	30.5	33.5	31.5	36.5	39.5	36.5
10	0.9	2.8	3.0	10.5	16.5	28.5	37.5
20	1.9	3.3	3.5	7.5	6.3	9.5	18.5
30	3.2	1.3	1.8	1.6	3.5	1.7	5.1
40	4.7	<1	1.9	3.0	6.6	2.5	4.2
50	7.9	3.5	<1	4.2	<1	1.4	1.9
60	9.9	<1	<1	<1	<1	1.9	2.3
70	29	<1	<1	<1	<1	<1	<1

Table A-25

Small Column D-8

pH of Leachate

Series	Time	pH					
		Leaching Distance-cm					
	hrs	10	25	40	55	70	85
00	-4.0	10.08	10.13	10.28	10.28	10.28	10.32
10	-2.7	10.57	10.59	10.59	10.58	10.58	10.68
20	0	10.73	10.63	10.62	10.62	10.53	10.51
30	1.0	10.59	10.65	10.71	10.63	10.69	10.67
40	2.7	10.54	10.59	10.60	10.70	10.68	10.70
50	4.0	10.29	10.50	10.53	10.60	10.65	10.75
60	6.8	10.26	10.35	10.50	10.60	10.62	10.67
70	17	10.26	10.47	10.83	10.68	10.81	10.89
80	26	10.34	10.49	10.48	10.83	10.66	10.65
90	41	10.27	10.37	10.53	10.77	10.75	10.73

Table A-26

Small Column D-8

Electrical Conductivity of Leachate

Series	Time	Electrical Conductivity - mmhos/cm					
		Leaching Distance-cm					
	hrs	10	25	40	55	70	85
00	-4.0	3.5	2.9	3.0	3.0	2.9	2.7
10	-2.7	3.5	3.2	3.2	3.2	3.3	3.2
20	0	3.6	3.5	3.4	3.3	3.3	3.3
30	1.0	0.84	2.6	3.7	3.7	3.4	3.4
40	2.7	0.54	0.87	1.3	2.2	3.2	3.5
50	4.0	0.46	0.69	0.95	1.3	1.7	2.3
60	6.8	0.40	0.59	0.76	1.1	1.1	1.3
70	17	0.32	0.48	0.62	0.70	0.76	0.82
80	26	0.30	0.43	0.55	0.65	0.73	0.79
90	41	0.25	0.36	0.42	0.55	0.60	0.63
100	49	0.24	0.36	0.45	0.55	0.61	0.67

Table A-27

Small Column D-8

Total Organic Carbon in Leachate

Series	Time	Total Organic Carbon - mg/L					
		Leaching Distance-cm					
	hrs	10	25	40	55	70	85
00	-4.0	19.5	19.5	17.5	17.5	15.5	14.5
10	-2.7	-	-	-	-	-	-
20	0	23.5	19.5	19.5	23.5	17.5	18.5
30	1.0	2.5	11.5	22.5	21.5	20.5	19.5
40	2.7	<0.5	0.5	2.5	3.5	19.5	22.5
50	4.0	<0.5	<0.5	-	3.1	4.9	9.9
60	6.8	-	<0.5	0.5	0.5	1.7	2.1
70	17	0.7	<0.5	<0.5	<0.5	<0.5	<0.5
80	26	-	-	-	-	-	-
90	41	<0.5	<0.5	<0.5	<0.5	<0.5	0.6

Table A-28

Large Column LC-1

Leachate pH

		Leaching length - 58 cm				Leaching length - 135 cm			
Time Hrs	Temp °C	Far*	Cent.	Near	Mean	Far	Cent.	Near	Mean
0	22	12.26	12.21	12.26	12.24	12.24	12.13	12.16	12.18
3.5	21	12.16	12.21	12.18	12.18	12.23	12.16	12.12	12.17
7.5	20	11.59	11.67	11.65	11.64	12.17	12.10	12.04	12.10
14.5	17	11.48	11.55	11.44	11.49	11.85	11.90	11.87	11.87
23	24	-	11.34	11.03	11.19	11.43	11.43	11.43	11.43
39	17	11.19	11.40	11.18	11.26	11.48	11.47	11.48	11.48
63	18	11.28	11.45	11.03	11.25	11.46	11.64	-	11.55
85	17	11.40	-	-	11.40	-	-	11.61	11.61
110	18	11.23	-	-	11.23	11.36	-	-	11.36

* - Tap location
Far - Far quarter point of cross-section
Cent. - Center of cross-section
Near - Near quarter point of cross-section

Table A-29

Large Column LC-1

Leachate Electrical Conductivity

mmhos/cm

		Leaching length - 58cm				Leaching length - 135cm			
Time Hrs	Temp °C	Far	Cent.	Near	Mean	Far	Cent.	Near	Mean
0	22	14.6	16.8	16.2	15.9	16.4	14.4	13.2	14.7
3.5	21	12.0	12.5	13.0	12.5	15.0	13.4	12.6	13.7
7.5	20	3.5	4.2	4.1	3.9	12.2	12.0	11.5	11.9
14.5	17	2.2	2.6	1.9	2.2	5.5	6.2	5.1	5.6
23	24	-	2.1	1.7	1.9	3.0	2.8	2.6	2.8
39	17	1.4	1.7	1.2	1.4	2.2	2.0	2.2	2.1
63	18	1.1	1.5	0.98	1.2	1.9	1.6	2.0	1.8
85	17	1.0	1.4	0.98	1.1	2.0	1.5	1.8	1.8
110	18	0.94	1.3	0.85	1.0	1.9	2.2	1.7	1.9
135	18	0.91	0.82	0.86	0.86	1.8	1.5	1.6	1.6

Table A-30

Large Column LC-1

TOC Data

mg/L

		Leaching length - 58 cm				Leaching length - 135cm			
Time Hrs	Temp °C	Far	Cent.	Near	Mean	Far	Cent.	Near	Mean
0	22	50	72	71	64	63	59	52	58
3.5	21	48	47	54	50	55	51	44	51
7.5	20	12	12	9.0	11	38	41	36	38
14.5	17	1.3	4.0	2.0	2.4	14	10	10	11
23	24	-	-	-	-	-	-	-	-
39	17	5.0	5.0	5.0	5.0	6.0	4.0	7.0	5.7
63	18	10	6.0	5.0	7.0	5.0	7.0	7.0	6.3

Table A-31

Large Column LC-2

Leachate pH

Time Hrs	Temp °C	Leaching length - 69 cm Far	Cent.	Near	Mean	Leaching length - 145 cm Far	Cent.	Near	Mean
0	22	11.98	11.94	11.99	11.97	11.97	12.01	12.05	12.01
3.5	21	11.90	11.94	11.96	11.93	11.97	11.98	11.99	11.98
7.5	20	11.88	11.88	11.89	11.88	11.92	11.83	11.96	11.90
14.5	17	11.56	11.56	11.62	11.59	12.00	11.98	12.06	12.01
23	24	11.29	11.07	11.37	11.24	11.75	11.74	11.73	11.74
39	17	11.15	11.20	11.18	11.18	11.49	11.50	-	11.49
63	18	-	11.23	-	11.23	-	11.39	-	11.39
85	17	-	11.39	-	11.39	-	-	11.46	11.46
110	18	-	-	11.30	11.30	-	-	11.55	11.55
135	18	-	11.10	-	11.10	-	11.72	-	11.72
168	-	-	11.07	-	11.07	-	11.73	-	11.73

Table A-32

Large Column LC-2

Leachate Electrical Conductivity

mmhos/cm

		Leaching length - 69 cm				Leaching length - 145 cm			
Time Hrs	Temp °C	Far	Cent.	Near	Mean	Far	Cent.	Near	Mean
0	22	9.4	9.2	9.3	9.3	9.4	9.2	9.0	9.2
3.5	21	9.2	9.0	9.1	9.1	9.1	8.7	9.1	9.0
7.5	20	8.9	8.9	8.9	8.9	9.1	9.4	9.7	9.4
14.5	17	3.4	3.1	3.1	3.2	9.4	9.2	9.4	9.3
23	24	2.0	1.8	2.2	2.0	5.8	5.4	5.3	5.5
39	17	1.6	1.4	1.6	1.5	2.8	2.3	2.7	2.6
63	18	0.87	1.1	1.1	1.0	2.3	2.4	2.3	2.3
85	17	1.5	1.4	1.4	1.4	2.1	2.2	2.0	2.1
110	18	1.6	1.5	1.6	1.6	2.2	1.5	2.3	2.0
135	18	1.4	1.4	1.5	1.4	2.0	2.2	2.0	2.1
168	-	0.41	0.62	1.4	0.82	1.9	1.9	1.4	1.7

Table A-33

Large Column LC-2

Leachate TOC

mg/L

		Leaching length - 69 cm				Leaching length - 145 cm			
Time Hrs	Temp °C	Far	Cent.	Near	Mean	Far	Cent.	Near	Mean
0	22	44	31	30	35	30	34	25	30
3.5	21	44	23	29	32	30	26	21	26
7.5	20	30	31	29	30	35	-	33	34
14	17	12	4.1	-	8.0	31	40	33	35
23	24	14	8.0	6.0	9.1	22	18	21	20
39	17	7.0	7.0	4.0	6.0	13	6.0	-	9.5
63	18	9.0	5.0	6.0	6.7	10	12	8.0	10
85	17	-	1.1	-	1.1	-	-	1.0	1.0
110	18	-	-	-	-	-	<1	-	<1
135	18	6.0	3.0	3.0	4.0	-	3.0	3.0	3.0
168	-	-	<1	-	<1	-	<1	-	<1

Table A-34

Large Column LC-3

Leachate pH

		Leaching length - 69 cm				Leaching length - 145 cm			
Time Hrs	Temp °C	Far	Cent.	Near	Mean	Far	Cent.	Near	Mean
0	22	11.52	11.74	11.74	11.67	10.78	10.64	10.71	10.71
3.5	21	11.25	11.52	10.84	11.20	11.04	10.78	10.84	10.89
7.5	20	11.20	11.36	11.40	11.32	11.01	10.68	10.82	10.84
14.5	17	11.08	11.17	11.15	11.13	10.72	10.70	10.95	10.79
23	24	11.31	11.31	10.97	11.20	10.95	10.90	10.89	10.91
39	17	10.90	10.68	10.68	10.75	10.85	10.94	10.89	10.89
63	18	11.05	11.04	-	11.05	-	10.51	-	10.51
85	17	-	-	11.03	11.03	-	-	10.97	10.97
110	18	-	-	11.17	11.17	-	-	11.05	11.05
135	18	-	10.66	-	10.66	-	10.62	-	10.62
168	-	-	10.80	-	10.80	-	11.11	-	11.11

Table A-35

Large Column LC-3

Leachate Electrical Conductivity

mmhos/cm

		Leaching length - 69 cm				Leaching length - 145 cm			
Time Hrs	Temp °C	Far	Cent.	Near	Mean	Far	Cent.	Near	Mean
0	22	8.5	8.4	8.1	8.3	6.2	6.4	6.5	6.4
3.5	21	7.5	7.8	6.6	7.3	7.2	6.7	7.0	7.0
7.5	20	4.0	3.5	3.1	3.5	7.0	7.0	7.0	7.0
14.5	17	1.9	1.6	1.5	1.7	4.4	4.5	5.0	4.6
23	24	1.8	2.1	0.88	1.6	1.8	0.98	1.6	1.5
39	17	0.92	0.91	1.1	0.98	0.88	0.80	0.64	0.77
63	18	0.80	0.68	0.62	0.70	0.94	0.74	0.87	0.85
85	17	0.66	0.80	0.80	0.75	0.96	0.82	0.94	0.91
110	18	0.70	0.61	0.62	0.64	0.81	0.64	0.78	0.74
135	18	0.66	0.70	0.74	0.70	0.80	0.64	0.63	0.69
168	-	0.72	0.35	0.43	0.50	0.60	0.61	0.72	0.64

Table A-36

Large Column LC-3

TOC Data

mg/L

		Leaching length - 69 cm				Leaching length - 145 cm			
Time Hrs	Temp °C	Far	Cent.	Near	Mean	Far	Cent.	Near	Mean
0	22	74	38	41	51	43	-	46	45
3.5	21	50	49	38	46	43	30	32	35
7.5	20	18	9.0	9.0	12	26	29	32	29
14.5	17	7.0	3.0	4.0	4.7	20	19	23	21
23	24	10	6.0	10	8.7	8.0	6.0	15	9.7
39	17	7.0	13	19	13	3.0	11	8.0	7.3
63	18	6.0	5.0	3.0	4.7	5.0	5.0	11	7.0
85	17	-	-	<1	<1	-	-	4.0	4.0
110	18	-	-	13	13	-	-	12	12
135	18	5.0	3.0	5.0	4.3	12	6.0	12	10
168	-	-	5.0	-	5.0	-	1.5	-	1.5

APPENDIX B

STAGE II MODEL

DERIVATION

The basic element in the spent shale bed is cylindrical as shown in Figure B-1. Mass transport within the cylinder occurs in micro-pores contained within pore planes lying normal to the axis. The spaces between the particles are defined as macro-pores.

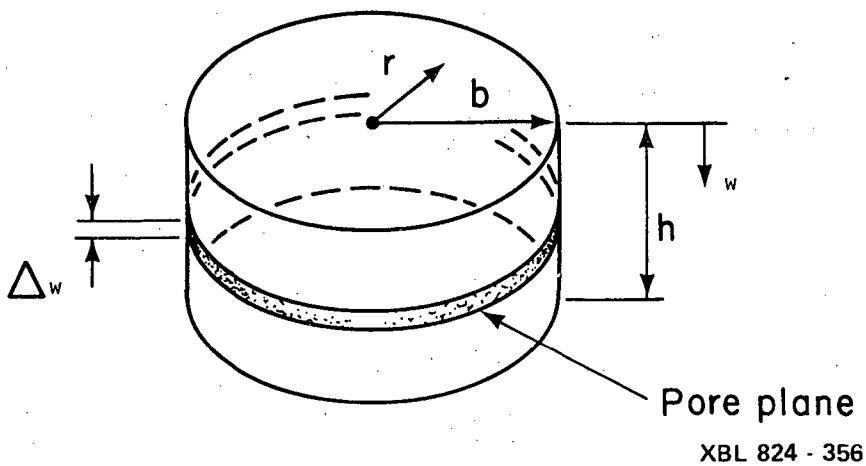

Figure B-1. Basic spent shale element in fixed bed.

Mass transport in the spent shale bed is assumed to be governed by Equation [A]. The rate of change of solute concentration is a function of advective and internal mass transfer mechanisms.

q_a = average

$$U_p \frac{\partial C}{\partial z} + \frac{\partial C}{\partial t} + \frac{1}{m} \frac{\partial q_a}{\partial t} = 0 \qquad [A]$$

in which:

U_p = Pore velocity

q_a = Average solute concentration in micro-pores

C = Solute concentration in macro-pores

m = Ratio of macro- to micro-pore volume

t = Time

z = Distance in direction of flow

The mean concentration q_a of solute in the cylinder is:

$$q_a = \frac{hn\Delta w \int_0^b 2\pi rq \, dr}{hn\Delta w\pi b^2} = \frac{2}{b^2} \int_0^b rq \, dr \qquad [B]$$

in which:

n = Number of pore planes per unit height of cylinder

w = Distance along particle axis

b = Radius of cylinder

r = Radial distance

h = Height of cylinder

q = Solute concentration at distance r and time t

Variables in Equation [A] are transformed with the following:

$$\theta = t - \frac{z}{U_p} \qquad X = \frac{z}{mU_p}$$

to obtain:

$$\frac{\partial C}{\partial X} + \frac{\partial q}{\partial \theta} = 0 \qquad [C]$$

Assume:

1. No external film resistance.

2. No adsorption or chemical reaction.

3. Fickian diffusion as represented by:

$$\frac{\partial q}{\partial \theta} = D_m \left[\frac{\partial^2 q}{\partial r^2} + \frac{1}{r}\frac{\partial q}{\partial r}\right] \qquad [D]$$

in which:

D_m = Molecular diffusion coefficient

SOLUTION OF EQUATION [D]

Assume that diffusion out of the micro-pores can be represented by superposition of solutions of two special boundary conditions considered by Crank (1976):

1. $H_1(r,t)$ is the analytical solution for diffusion into a pore plane having a concentration q_o of zero at time zero, from an exterior surface having a constant concentration of q_s equal to unity.

2. $H_2(r,t)$ is the analytical solution for diffusion out of a pore plane having an initial uniform concentration of q_o of unity, toward an external surface having a constant concentration of q_s equal to zero.

The total rate of change in q can be found by superposition of the two cases since the dispersion equations employed are linear:

$$q = q_s H_1(r,t) + q_o H_2(r,t) \qquad [E]$$

in which q_s and q_o may be assigned constant values other than unity.

The magnitude of q_s will vary with time. The rate of change in q at time t for a q_s input at time λ is:

$$q_s(\lambda) \frac{H_1(r,t-\lambda)}{\partial t}$$

as illustrated in Figure B-2. The total value of q for the q_s term is therefore:

$$\int_o^t q_s(\lambda) \frac{H_1(r,t-\lambda)}{\partial t} d\lambda \qquad [F]$$

which represents the summation of q_s values from time zero to time t.

The value of q_o is assumed constant for the second term on the right hand side of Equation [E]; i.e. q is independent of the radius r at time zero. This assumption will hold if full equilibrium is achieved between the macro- and micro-pores before commencing a column run. If this is not the case, then q_o is a function of r, and a convolution integral similar to Equation [F] would also have to be written in terms of r. Replacing the first term on the right hand

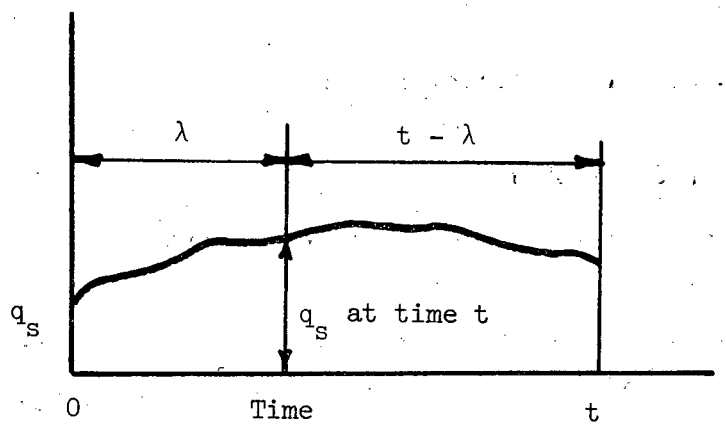

Figure B-2. Definition of convolution time variables.

side of Equation [E] with Equation [F] gives:

$$q = \int_0^t q_s(\lambda) \frac{\partial H_1(r,t-\lambda)}{\partial \theta} d\lambda + q_o H_2(r,t) \qquad [G]$$

Crank presents the solutions for both terms of this equation, (Equations 5.26 and 5.22, respectively of Crank, 1976):

$$q = \frac{2D_m}{b} \sum_1^\infty \frac{\alpha_n J_o(r\alpha_n)}{J_1(b\alpha_n)} \int_0^t q_s(\lambda) \exp\left[-D_m \alpha_n^2 (t-\lambda)\right] d\lambda +$$

$$+ \frac{2q_o}{b} \sum_1^\infty \frac{J_o(r\alpha_n)}{\alpha_n J_1(b\alpha_n)} \exp\left[-D_m \alpha_n^2 t\right] \qquad [H]$$

in which:

J_o, J_1 = Bessel functions of zero and first order.

α_n = [O_n]/ b, in which the [O_n] terms are the zeros of a Bessel function of zero order.

The average concentration q_a of the solute in the micro-pores may now be obtained with Equation [B], by recognizing that:

$$\int_o^{\alpha_n b} u\, J_o(u)\, du = (\alpha_n b)\, J_1(\alpha_n b)$$

in which u is a variable of integration. After manipulation:

average concentration

$$q_a = \frac{4D_m}{b^2} \sum_1^{\infty} \int_o^t q_s(t) \quad \exp\left[-D_m \alpha_n^2 (t - \lambda)\right] d\lambda +$$

$$\frac{4q_o}{b^2} \sum_1^{\infty} \frac{1}{\alpha_n^2} \exp\left[-D_m \alpha_n^2 t\right] \qquad [I]$$

This represents the solution for q in the micro-pores of the cylinders. The expression now has to be coupled in mass balance terms with the macro-pore concentration C.

PLUG FLOW COLUMN OPERATION

The mass continuity equation for packed column operation with assumed plug flow is given by Equation [C]. The relationship between q_s and C at the solid surface must now be established. In this work it was assumed that the resistance to mass transfer in the liquid film on the particle exterior is negligible because the diameters of the particles studied are relatively large, or:

$$q_s = C \qquad [J]$$

The value of C is a function of both θ and the distance X in the column, so q_s now becomes a function of θ and X. Also, Equation [C] shows that the derivative of q_a with respect to θ is required. Equation [I], with the aid of Equations [C] and [J], now becomes:

$$\frac{\partial q_a}{\partial \theta} = \frac{4D_m}{b^2} \sum_1^{\infty} \frac{\partial \int_0^{\theta} C(r,\theta) \exp\left[-D_m \alpha_n^2 (\theta - \lambda)\right] d\lambda}{\partial \theta} -$$

$$\frac{4q_o D_m}{b^2} \sum_1^{\infty} \exp\left[-D_m \alpha_n^2 \theta\right] = -\frac{\partial C}{\partial X} \qquad [K]$$

SOLUTION OF EQUATION [I] BY LAPLACE TRANSFORMS

The Laplace transform of the variable θ ($\theta \rightarrow s$) gives:

$$\frac{dC(X,s)}{dX} + \left[\frac{4D_m}{b^2} \sum_1^{\infty} \frac{s}{s + \alpha_b^2 D_m}\right] C(X,s) =$$

$$4q_o \frac{D_m}{b^2} \sum_1^{\infty} \frac{1}{s + \alpha_n^2 D_m} \qquad [L]$$

The Laplace operation for a convolution integral is used in this transformation:

$$\mathcal{L}\left(\int_0^t f_1(u)\, f_2(t-u)\, du\right) = g_1(s)\, g_2(s)$$

This equation is now an ordinary differential equation which may be solved by commonly used methods. By taking the Laplace transform again for the variable X ($X \rightarrow u$):

$$C(u,s)\left[u + \frac{4D_m}{b^2} \sum_1^{\infty} \frac{s}{s + \alpha_n^2 D_m}\right] =$$

$$C(0,s) + \frac{4q_o D_m}{b^2 Us} \sum_1^{\infty} \frac{s}{s + D_m \alpha_n^2} \qquad [M]$$

in which C(0,s) represents the Laplace transform in terms of θ of the input concentration to the column. This boundary condition must be known before the inverses of the transformed equation can be taken.

If the input concentration is a step function at $\theta = 0$, then:

$$C(0,s) = C_i / s$$

If the input concentration is a unit impulse at time zero then:

$$C(0,s) = 1.0$$

Assuming a step impulse and taking the inverse of Equation [M] for X ($u \rightarrow X$) gives:

$$C(\chi,s) = \frac{q_o}{s} + (C_i - q_o) \left\{\frac{1}{s} \exp[-X\beta(s)]\right\} \qquad [N]$$

in which:

$$\beta(s) = \frac{4D_m s}{b^2} \sum_{1}^{\infty} \frac{1}{s + D_m \alpha_n^2}$$

Taking the inverse for θ ($s \rightarrow \theta$) gives:

$$C(X,\theta) = q_o + (C_i - q_o)\, \mathcal{L}^{-1} \left\{\frac{1}{s} \exp[-X\beta(s)]\right\} \qquad [O]$$

NORMALIZATION OF EQUATION [M]

Equation [O] is not normalized because θ has the dimension of time. A useful normalization is obtained by recognizing that:

$$D_m \alpha_n^2 = D_m [O_n]^2 / b^2$$

and:

$$\beta(as) = \frac{4D_m(as)}{b^2} \sum_1^\infty \frac{1}{(as) + [O_n]^2}$$

in which $a = b^2/D_m$. Using the Laplace transform operation:

$$\mathcal{L}^{-1} g(as) = \frac{1}{a} f\left(\frac{\theta}{a}\right)$$

gives:

$$C\left(\frac{\theta D}{b^2}\right) = q_o + (C_1 - q_o)\, \mathcal{L}^{-1} \left\{\frac{1}{s} \exp[-X\beta(s)]\right\} \qquad [P]$$

in which:

$$X\beta_1(s) = \frac{4D_m Xs}{b^2} \sum_1^\infty \frac{1}{s + [O_n]^2}$$

Equation [P] was solved by numerical inversion with the aid of the LAPINV computer program. Dimensionless parameters $T = \theta D_m / b^2$ and $\alpha X = 4 D_m X / b^2$ were used in the inversion. A copy of the LAPINV program is included in Appendix C.

SPHERES VERSUS CYLINDERS

Letting q_o for pure absorption gives:

$$C\left(\frac{\theta D_m}{b^2}\right) = C_i \mathcal{L}^{-1}\left\{\frac{1}{s}\exp[-X\beta_1(s)]\right\} \qquad [Q]$$

The form of this equation is identical to that given by Rosen (1952, 1954) for absorption in spheres. A comparison of $\beta_1(s)$ terms follows:

$$\beta_1(s) = \frac{4D_m s}{b^2}\sum_1^\infty \frac{1}{s + [O_n]^2} \quad \text{(cylinders)}$$

and

$$\beta_1(s) = \frac{4D_m s}{b^2}\sum_1^\infty \frac{1}{s + [n\pi]^2} \quad \text{(spheres)}$$

In which b represents the radii of the cylinders or the spheres, respectively.

The zeros of the zero order Bessel function $[O_n]$ approximate $n\pi$, with this being especially true as $n \to \infty$: consequently, one might expect that the two particle shapes will yield similar results when $2 / b_{cylinders}$ is set equal to $6 / b_{spheres}$, or:

$$b_{spheres} = 3 / 2\, b_{cylinders}$$

Cylindrical functions were used in this work because: (1) spherical particles cannot be used to fit the obvious geometry of the particles and pore planes, and (2) the deviation between the two solutions became rather significant even when the $b_{spheres}$ were set equal to 3 /2 $b_{cylinders}$ at the shorter values. Commonly, the cylindrical functions tended to yield a more rapid decrease in the concentration C with time θ, and a more pronounced tailing.

INCLUSION OF DISPERSION IN THE STAGE II MODEL DERIVATION

During the final stages of the preparation of this report the advection-dispersion equation, Equation II-1 in the text, containing both dispersive and diffusive terms was solved by Laplace transform techniques. The approach used was similar to that described for the Stage II model solution. The derivation is not included herein because of time constraints. It is useful, however, to discuss the result in general terms for possible application to future studies.

The transformed solution of the augmented model was similar to Equation [O]. Effluent concentration as a function of time and distance was expressed in terms of the same variables used for the Stage II model. The principal difference being that both diffusive and dispersive mechanisms were characterized by coefficients instead of only diffusion as in Equation [O]. When the dispersive coefficient was set to zero, i.e. no dispersion, the equation became identical to Equation [O]. The transformed equation was not inverted by LAPINV but there appeared to be no reason why the inversion would not be possible.

The significance of this derivation is that the effects of both the dispersion and diffusion coefficients upon the effluent concentration may be examined. An approach might be to fix either of the coefficients and then determine a solution set for the transformed equation by the methods used to invert the Stage II model. This would be repeated for other values of the fixed coefficient. Future experimental work could then be directed toward measuring either the dispersion or diffusion coefficient for a particular system thus defining the other coefficient for purposes of modelling the effluent concentration with time and distance.

EXHIBIT C-1. LAPINV COMPUTER PROGRAM

```
LAVERT                    **PROGRAM LAVERT (INPUT,OUTPUT,PUNCH)**

  1.   000000B            PROGRAM LAVERT (INPUT,OUTPUT,PUNCH)
  2.   001544B            DOUBLE PRECISION T,CON(20),G(20),F,U(50,50),TI(50),ALPHA(50)
  3.   001544B            INTEGER  NRUN
  4.   001544B            EXTERNAL F
  5.   001544B            DATA ALPHA/10.D0,5.D0,1.D0,.5D0,.2D0,.1D0,.05D0, .02D0,.01D0/
  6.   001544B            NRUN = 0
  7.   014007B            NMIN=5 $ NMAX=19
  9.   014011B            DO 17 I=2,20
 10.   014013B            READ 100, CON(I)
 11.   014021B            PRINT 22,I,CON(I)
 12.   014027B         17 CONTINUE
 13.   014031B            DO 10 J=1,9
 14.   014033B            CON(1)= ALPHA(J)
 15.   014035B            DO 10  I=1,50    $ T=10.D0**(-I/10.D0)*10.D0
 17.   014054B            TI(I)=T
 18.   014055B            CALL LAPINV (T,F,CON,NMIN,NMAX,G)
 19.   014061B            U(I,J)=1.D0 -G(17)
 20.   014070B         10 CONTINUE
 21.   014077B            PRINT 200
 22.   014102B            PRINT 25, (ALPHA(I), I=1,9) ,(TI(J),(U(J,K), K=1,9) ,J=1,50)
 23.   014132B         22 FORMAT (1X,*   CON(*,I2,*)=*,D18.12)
 24.   014132B         25 FORMAT(*1*,60X,*ALPHA*/4X,*T(I)*,  9F9.4/(1X,E9.2, 9F9.4))
 25.   014132B        100 FORMAT (D18.12)
 26.   014132B        200 FORMAT (1H0)
 27.   014132B            PUNCH 30,NRUN,(ALPHA(I), I=1,9)
 28.   014143B            PUNCH 31,(NRUN, TI(J),(U(J,K),K=1,9),J=1,50)
 29.   014167B         30 FORMAT(I2,9F7.3)
 30.   014167B         31 FORMAT(I2,E9.2,9F6.3)
 31.   014167B            STOP
 32.   014170B            END
```

EXHIBIT C-1. Continued.

```
LAPINV                    ** SUBROUTINE LAPINV(T,F,CON,NMIN,NMAX,G)**

  1.   000000B              SUBROUTINE LAPINV(T,F,CON,NMIN,NMAX,G)
  2.   000000B             DOUBLE PRECISION T,CON(10),G(20),V(40,20),S,A,LN2,FO(40),F
  3.   000000B             DATA ITEST/1/
  4.   000000B             IF(NMIN.LE.0.OR.NMIN.GT.NMAX.OR.NMAX.LE.0.OR.NMAX.GT.20)
                          1GO TO 1000
  5.   003234B             IF(ITEST.EQ.0)GO TO 100
  6.   003236B             CALL CHALT(V)
  7.   003240B             LN2=DLOG(2.D+00)
  8.   003242B             ITEST=0
  9.   003243B        100  A=LN2/T
 10.   003252B             NM2=2*NMAX
 11.   003254B             DO 145 I=1,NM2
 12.   003256B        145  FO(I)=F(I*A,CON)
 13.   003272B             DO 200 I=NMIN,NMAX
 14.   003274B             S=0.
 15.   003274B             LU=2*I
 16.   003276B             DO 150 L=1,LU
 17.   003301B        150  S=S+V(L,I)*FO(L)
 18.   003315B        200  G(I)=A*S
 19.   003325B             RETURN
 20.   003327B       1000  WRITE(6,50)NMIN,NMAX
 21.   003334B         50  FORMAT(/,1X,*SOMETHING WRONG WITH PARAMETERS*,
                          1* NMIN=*,I5,*    NMAX=*,I5,/)
 22.   003334B             RETURN
 23.   003336B             END
```

EXHIBIT C-1. Continued.

```
CHALT                    **SUBROUTINE CHALT(V)**

   1.   000000B          SUBROUTINE CHALT(V)
   2.   000000B          DOUBLE PRECISION V(40,20),G(41),S
   3.   000000B          G(1)=1
   4.   000125B          DO 10 I=2,41
   5.   000130B       10 G(I)=(I-1)*G(I-1)
   6.   000136B          DO 20 K=1,20
   7.   000137B          KK=K+K
   8.   000137B          DO 20 L=1,KK
   9.   000142B          M1=(L+1)/2
  10.   000143B          M2=MINO(L,K)
  11.   000145B          S=0.
  12.   000146B          DO 15 M=M1,M2
  13.   000152B          MM=2*M+1
  14.   000153B       15 S=S+(-1)**(K+L)*FLOAT(M)**(K-1)*(G(MM)/(G(M))**2)/
                        1(G(K+1-M)*G(L+1-M)*G(MM-L))
  15.   000236B       20 V(L,K)=S
  16.   000251B          RETURN
  17.   000253B          END
```

EXHIBIT C-1. Continued.

```
F                          **DOUBLE PRECISION FUNCTION F(P,CON)**

  1.   000000B              DOUBLE PRECISION FUNCTION F(P,CON)
  2.   000000B              DOUBLE PRECISION P,CON(20)
  3.   000000B              F=(1./P)*DEXP(-CON(1) *((P/(P+2.40482560D**2))
                           1+(P/(P+CON(2)**2))
                           2+(P/(P+CON(3)**2))+(P/ (P+CON(4)**2))+(P/(P+CON(5)**2))
                           3+(P/(P+CON(6)**2))+(P/ (P+CON(7)**2))+(P/(P+CON(8)**2))
                           4+(P/(P+CON(9)**2))+(P/(P+CON(10)**2))+   (P/(P+CON(11)**2))
                           5+(P/(P+CON(12)**2))+(P/(P+CON(13)**2))+(P/(P+CON(14)**2))
                           6+(P/(P+CON(15)**2))+(P/(P+CON(16)**2))+(P/(P+CON(17)**2))
                           7+(P/(P+CON(18)**2))+(P/(P+CON(19)**2))+(P/(P+CON(20)**2))))
  4.   000504B              RETURN
  5.   000507B              END

 CON( 2)= .5520078100000D+01
 CON( 3)= .8653727900000D+01
 CON( 4)= .1179153440000D+02
 CON( 5)= .1493091770000D+02
 CON( 6)= .1807106400000D+02
 CON( 7)= .2121163660000D+02
 CON( 8)= .2435247150000D+02
 CON( 9)= .2749347910000D+02
 CON(10)= .3063460650000D+02
 CON(11)= .3377582020000D+02
 CON(12)= .3691709840000D+02
 CON(13)= .4005842580000D+02
 CON(14)= .4319979170000D+02
 CON(15)= .4634118840000D+02
 CON(16)= .4948260990000D+02
 CON(17)= .5262405180000D+02
 CON(18)= .5576551080000D+02
 CON(19)= .5890698390000D+02
 CON(20)= .6204846920000D+02
```

EXHIBIT C-2

SOLUTIONS OF EQUATION IV-9 FOR SELECTED VALUES OF ALPHAX

TIME	ALPHAX 10.0000	5.0000	1.0000	.5000	.2000	.1000	.0500	.0200	.0100
.79E+01	.0000	.0000	.0000	.0000	.0000	.0000	.0000	.0000	.0000
.63E+01	.0001	.0000	.0000	.0000	.0000	.0000	.0000	.0000	.0000
.50E+01	.0042	.0000	.0000	.0000	.0000	.0000	.0000	.0000	.0000
.40E+01	.0408	.0003	.0000	.0000	.0000	.0000	.0000	.0000	.0000
.32E+01	.1768	.0043	.0000	.0000	.0000	.0000	.0000	.0000	.0000
.25E+01	.4273	.0267	.0000	.0000	.0000	.0000	.0000	.0000	.0000
.20E+01	.6924	.0962	.0002	.0000	.0000	.0000	.0000	.0000	.0000
.16E+01	.8730	.2319	.0015	.0003	.0000	.0000	.0000	.0000	.0000
.13E+01	.9593	.4165	.0062	.0013	.0003	.0001	.0000	.0000	.0000
.10E+01	.9898	.6062	.0184	.0045	.0010	.0004	.0002	.0001	.0000
.79E+00	.9980	.7630	.0428	.0121	.0030	.0013	.0006	.0002	.0001
.63E+00	.9997	.8723	.0820	.0261	.0072	.0031	.0014	.0005	.0003
.50E+00	1.0000	.9385	.1357	.0479	.0142	.0063	.0030	.0011	.0006
.40E+00	1.0000	.9739	.2007	.0772	.0245	.0111	.0053	.0020	.0010
.32E+00	1.0000	.9905	.2723	.1127	.0377	.0175	.0094	.0033	.0016
.25E+00	1.0000	.9971	.3465	.1522	.0531	.0250	.0121	.0046	.0024
.20E+00	1.0000	.9993	.4211	.1944	.0701	.0335	.0163	.0064	.0032
.16E+00	1.0000	.9999	.4951	.2385	.0884	.0426	.0209	.0082	.0041
.13E+00	1.0000	1.0000	.5684	.2848	.1078	.0523	.0257	.0102	.0051
.10E+00	1.0000	1.0000	.6399	.3338	.1288	.0628	.0310	.0123	.0061
.79E-01	1.0000	1.0000	.7083	.3855	.1516	.0743	.0367	.0146	.0073
.63E-01	1.0000	1.0000	.7718	.4400	.1766	.0870	.0430	.0171	.0085
.50E-01	1.0000	1.0000	.8285	.4968	.2041	.1010	.0501	.0199	.0099
.40E-01	1.0000	1.0000	.8771	.5553	.2342	.1166	.0579	.0230	.0115
.32E-01	1.0000	1.0000	.9163	.6144	.2670	.1338	.0666	.0265	.0132
.25E-01	1.0000	1.0000	.9462	.6728	.3028	.1529	.0763	.0304	.0152
.20E-01	1.0000	1.0000	.9675	.7291	.3415	.1740	.0871	.0348	.0174
.16E-01	1.0000	1.0000	.9815	.7818	.3830	.1973	.0992	.0397	.0198
.13E-01	1.0000	1.0000	.9902	.8293	.4270	.2229	.1126	.0451	.0226
.10E-01	1.0000	1.0000	.9951	.8706	.4733	.2509	.1274	.0512	.0256
.79E-02	1.0000	1.0000	.9977	.9050	.5212	.2813	.1439	.0580	.0291
.63E-02	1.0000	1.0000	.9989	.9324	.5700	.3142	.1621	.0656	.0329
.50E-02	1.0000	1.0000	.9995	.9533	.6187	.3494	.1821	.0740	.0372
.40E-02	1.0000	1.0000	.9998	.9685	.6663	.3867	.2039	.0834	.0420
.32E-02	1.0000	1.0000	.9999	.9792	.7116	.4257	.2278	.0939	.0473
.25E-02	1.0000	1.0000	1.0000	.9865	.7538	.4658	.2534	.1054	.0533
.20E-02	1.0000	1.0000	1.0000	.9913	.7920	.5065	.2809	.1181	.0599
.16E-02	1.0000	1.0000	1.0000	.9944	.8257	.5470	.3099	.1320	.0672
.13E-02	1.0000	1.0000	1.0000	.9963	.8548	.5863	.3400	.1470	.0752
.10E-02	1.0000	1.0000	1.0000	.9976	.8793	.6237	.3706	.1630	.0839
.79E-03	1.0000	1.0000	1.0000	.9984	.8997	.6585	.4011	.1797	.0932
.63E-03	1.0000	1.0000	1.0000	.9989	.9163	.6902	.4308	.1967	.1027
.50E-03	1.0000	1.0000	1.0000	.9992	.9298	.7185	.4589	.2135	.1122
.40E-03	1.0000	1.0000	1.0000	.9995	.9405	.7433	.4849	.2295	.1215
.32E-03	1.0000	1.0000	1.0000	.9996	.9491	.7646	.5083	.2444	.1302
.25E-03	1.0000	1.0000	1.0000	.9997	.9559	.7828	.5290	.2579	.1381
.20E-03	1.0000	1.0000	1.0000	.9998	.9613	.7980	.5470	.2699	.1452
.16E-03	1.0000	1.0000	1.0000	.9998	.9655	.8106	.5623	.2803	.1514
.13E-03	1.0000	1.0000	1.0000	.9999	.9689	.8211	.5752	.2892	.1567
.10E-03	1.0000	1.0000	1.0000	.9999	.9715	.8296	.5860	.2967	.1613

BIBLIOGRAPHY

Abramowitz, M. and I. Stegun,
Handbook of Mathematical Functions, U.S. Department of Commerce, Applied Mathematical Series, Washington, D.C., 1964.

Amy, G.,
Contamination of Groundwater by Organic Pollutants Leached from from In-Situ Spent Shale, PhD Thesis, Lawrence Berkeley Laboratory- LBL 10526, 1978.

Amy, G., A. Hines, J.Thomas and R. Selleck,
"Groundwater Leaching of Organic Pollutants from In-Situ Retorted Oil Shale, A Mass Transfer Analysis", Environmental Science and Technology, Volume 14, No. 7, July 1980.

Bethea, R, H. Parker, and N. Guven,
Mechanisms of Leaching from In-situ Retorted Oil Shale, Final Report for Grant DE-FG-03-78 ET 13084, Texas Tech, Lubbock, Texas, 1981.

Bird, R., W. Stewart, and E. Lightfoot,
Transport Phenomena, John Wiley and Sons, Inc., N.Y., 1960.

Carley, J. F.,
Dimensions, Exterior Surfaces, Volumes, Densities and Shape Factors for Particles of Crushed Colarado Oil Shale in Two Narrow Sieve Fractions, Lawrence Livermore Laboratory, UCRL Preprint 84583, May 1980.

Colorado School of Mines,
Proceedings of the Oil Shale Symposia, 1964-1981, J. Gary, Ed., Colorado School of Mines Press, Golden, Co.

Crank, J.,
The Mathematics of Diffusion, Clarendon Press, Oxford, 1975.

Farrier, D., J. Fox and R. Poulson,
Intralaboratory, Multimethod Study of an In-Situ Produced Oil Shale Process Water, Lawrence Berkeley Laboratory, LBL 9002, March 1979.

Fox, J.,
Water Related Impacts of In-Situ Oil Shale Processing, Lawrence Berkeley Laboratory, LBL-6300, UC 91, December 1980.

Fox, J., P.Persoff, P. Wagner and E. Peterson,
Retort Abandonment-Issues and Research Needs, Lawrence Berkeley Laboratory, LBL-11197, August 1980.

Fox, J.,
Leaching of Oil Shale Solid Wastes: A Critical Review, A draft

report prepared for the Oil Shale Task Force, University of Colorado, Denver, CO, 1982.

Foust, A., L. Wenzel, C. Clump, L. Maus, and L. Andersen, Principles of Unit Operations, John Wiley and Sons, Inc., 1960.

International Mathematics and Statistical Library (IMSL), "FLINV", IMSL Library, Edition 8, Computer Center, Lawrence Berkeley Laboratory, 1980.

Jackson, L., R, Poulson, T. Spedding, T. Phillips and H. Jensen, "Characteristics and Possible Roles of Various Waters Significant to In-Situ Oil Shale Processing", Colorado School of Mines Quarterly, 70, 105, Golden, Co. 1975.

Jackson, M., Soil Chemical Analysis, Prentice-Hall, 1958.

Kuo, M., W. Park, A. Lindemanis, R. Lumpkin and L. Compton, "Inorganics Leaching of Spent Shale from Modified In-Situ Processing", Twelfth Oil Shale Symposium Proceedings, Colorado School of Mines, Golden, Co. 1979.

Krause, J., W. McLean, E. Dublen, and D. Gann, Mineralogy-Groundwater Quality: A Study of In-situ Retorted Oil Shale, A study submitted to the U.S. Environmental Protection Agency, Ada, Oklahoma, by the Colorado School of Mines, Golden, CO, June 1981.

Krupp, H. and D. Elrack, "Density Effects in Misible Displacement Experiments", Soil Science Volume 107, 1969.

Mandelbaum, J. and U. Bohm, "Mass Transfer in Packed Beds at Low Reynolds Numbers", Chemical Science, Volume 28, 1973.

McWhorter, D., Reconnaissance Study of Leachate from Raw Mined Oil Shale Laboratory Columns, EPA 600/7-80-181, NTIS PB 81 1290 17, 1980.

McWhorter, D. "Laboratory Leaching of Bi-Modal Porous Media", Fourteenth Oil Shale Proceedings, Colorado School of Mines, Golden, Co. 1981.

Merhan, M., T. Narisimhan, P. Fox, Investigation of Dewatering for the In-situ Retorting Process, Piceance Creek Basin, Lawrence Berkeley Laboratory, LBL-11819, 1980.

Ogata, A. and R. Banks, "A Solution of the Differential Equation of Longitudinal Dispersion in Porous Media", Professional Paper 411-4, U.S. Geological Survey, Washington, D.C.

Oil Shale Task Force,
Environmental Research on a Modified In-Situ Oil Shale Process, A Progress ReportFrom the Oil Shale Task Force, DOE/EV-0078, May 1980.

Park, W., A. Lindemanis, G. Rabb,
"Mineral Changes During Oil Shale Retorting", In-situ, Volume B, No. 4, 1979. Reprinted with minor changes in: Proceedings of AIME-TMS Annual Meeting, Feb 27, 1980.

Parker, H., R. Bethea, N. Guven, M. Gazdar, and J. Watts,
"Interactions between Ground Water and In-Situ Retorted Oil Shale", Proceedings of the Second Chemical Engineering Congress, Volume 1, 1977.

Parker, H.,
For report referenced in text as Parker et al. (1981), see Bethea et al. (1981).

Passioura, J.,
"Hydrodynamic Dispersion in Aggregated Media, 1, Theory", Soil Science, Volume III, June 1971.

Passioura, J., and D. Rose,
"Hydrodynamic Dispersion in Aggregated Media, 2, Effects of Velocity and Aggregate Size", Soil Science, Volume III, June 1971.

Perry, R. and C. Chilton,
Chemical Engineers Handbook, McGraw-Hill, N.Y. 1973.

Peterson, E., A. Henicksman and P. Wagner,
Investigation of Occidental Oil Shale, Inc. Retort 3E Spent Shales, Report LA-8792-S, UC-91, Los Alamos Scientific Laboratory, N.M., June 1981.

Ramirez, W.,
Mathematical Modeling and Transport Mechanisms for Leaching of Spent Oil Shale, 1980-1981 Progress Report, University of Colorado, Boulder, Co., 1981.

Rasmuson, A. and J. Neretneiks,
"Migration of Radionuclides in Fissured Rock: The Influence of Micropore Diffusion and Longitudinal Dispersion", Journal of Geophysical Research, Volume 86, May 1981.

Rosen, J.,
"Kinetics of a Fixed Bed System for Solid Diffusion into Spherical Particles", Journal of Chemical Physics, Volume 20, March 1952.

Rosen, J.,
"General Numerical Solution for Solid Diffusion in Fixed Beds", Industrial and Engineering Chemistry, Volume 45, August 1954.

Sherwood, T., R. Pigford and C. Wilke,
Mass Transfer, McGraw-Hill, N.Y., 1975.

Skelland, A.,
Diffusional Mass Transfer John Wiley and Sons, N.Y., 1974.

Standard Methods for Examination of Water and Wastewater,
14th Edition, American Public Health Association, 1975.

Stumm, W. and J. Morgan,
Aquatic Chemistry, John Wiley and Sons, Inc. N.Y., 1981.

Tisot, P.,
"Alterations in Stucture and Physical Properties of Green River Oil Shale by Thermal Treatment", Journal of Chemical and Engineering Data, Volume 12, No. 3, July 1967.

U.S. Environmental Protection Agency,
Methods for Chemical Analysis of Water and Wastes, EPA-600/4-79-020, Cincinnati, Oh., March 1979.

Wildung, R., R. Riley, T. Garland, R. Bean and S. Li,
"Terrestrial Effects of Oil Shale Development", NTIS BNWL-2100, PT2, 1977.

Wildung, R., T. Garland, R. Riley, D. Silviera, J. Rogers, R. Bean and S. Li,
"Terrestrial Effect of Oil Shale Development", NTIS BNWL-2500, PT2, 1978.

Willis, R.,
"LAPINV", Computer Center Library, C3 BKY LAPINV, Lawrence Berkeley Laboratory, 1975.

This report was done with support from the Department of Energy. Any conclusions or opinions expressed in this report represent solely those of the author(s) and not necessarily those of The Regents of the University of California, the Lawrence Berkeley Laboratory or the Department of Energy.

Reference to a company or product name does not imply approval or recommendation of the product by the University of California or the U.S. Department of Energy to the exclusion of others that may be suitable.

TECHNICAL INFORMATION DEPARTMENT
LAWRENCE BERKELEY LABORATORY
UNIVERSITY OF CALIFORNIA
BERKELEY, CALIFORNIA 94720